PB81-186728

Atmospheric Turbulence and Pollutant Dispersion Near Roadways

New York State Dept of Environmental
Conservation, Albany

Prepared for

Environmental Sciences Research Lab
Research Triangle Park, NC

Dec 80

U.S. Department of Commerce
National Technical Information Service
NTIS

PB81-186728

EPA-600/4-80-054
December 1980

ATMOSPHERIC TURBULENCE AND POLLUTANT DISPERSION NEAR ROADWAYS

by

S. Trivikrama Rao, Michael T. Keenan, Gopal Sistla
and
John S. Wilson
New York State Department of Environmental Conservation
50 Wolf Road
Albany, New York 12233

R-806017-01

Project Officer

William B. Petersen
Meteorology and Assessment Division
Environmental Sciences Research Laboratory
Research Triangle Park, N.C. 27711

ENVIRONMENTAL SCIENCES RESEARCH LABORATORY
OFFICE OF RESEARCH AND DEVELOPMENT
U.S. ENVIRONMENTAL PROTECTION AGENCY
RESEARCH TRIANGLE PARK, N.C. 27711

[illegible] OF:
NATIONAL TECHNICAL
INFORMATION SERVICE
U.S. DEPARTMENT OF COMMERCE
SPRINGFIELD, VA. 22161

BIBLIOGRAPHIC INFORMATION

PB81-186728

Atmospheric Turbulence and Pollutant Dispersion Near Roadways,

Dec 80

S. Trivikrama Rao, Michael T. Keenan, Gopal Sistla, and John S. Wilson.

PERFORMER: New York State Dept. of Environmental
Conservation, Albany.
Grant EPA-R-806017-01

SPONSOR: Environmental Sciences Research Lab., Research
Triangle Park, NC.
EPA-600/480-054

The major objectives of this investigation are: (1) to determine the time and space scales of the eddies generated by the traffic, (2) to study the effects of traffic-induced turbulence on the near-field dispersion of pollutants, (3) to evaluate several commonly used highway air pollution dispersion models, and (4) to improve methods of modeling pollutnat dispersion near roadways. To this end, meterological and tracer concentration data from two field experiments, namely, General Motors and New York State, are used.
KEYWORDS: *Air pollution, *Roads, *Exhaust emissions.

Available from the National Technical Information Service,
Springfield, Va. 22161

PRICE CODE: PC A07/MF A01

DISCLAIMER

This report has been reviewed by the Environmental Sciences Research Laboratory, U.S. Environmental Protection Agency, and approved for publication. Approval does not signify that the contents necessarily reflect the views and policies of the U.S. Environmental Protection Agency, nor does mention of trade names or commercial products constitute endorsement or recommendation for use.

ABSTRACT

The major objectives of this investigation are: (i) to determine the time and space scales of the eddies generated by the traffic, (ii) to study the effects of traffic-induced turbulence on the near-field dispersion of pollutants, (iii) to evaluate several commonly used highway air pollution dispersion models, and (iv) to improve methods of modeling pollutant dispersion near roadways. To this end, meteorological and tracer concentration data from two field experiments, namely, General Motors and New York State, are used.

Analysis of the characteristics of turbulence near the roadway during moderate and heavy traffic conditions indicated that the dynamics of air flow are completely dictated by the wake effects due to the traffic flow and that the wake effects play a dominant role in dispersing the pollutants in the near-field. The evaluation of the bulk statistics and spectra allowed the magnitude and extent of wake turbulence in the horizontal and vertical to be identified.

Several commonly used numerical and Gaussian highway dispersion models are chosen for evaluation with the General Motors data set and various statistical techniques are employed to quantify the predictive capability of each of those models. The results revealed that the model with the best performance in accurately predicting the measured concentrations in the General Motors tracer experiment is the GM model followed in order by AIRPOL-4, HIWAY, CALINE-2, DANARD, MROAD2 and ROADS. The GM model is expected to perform well with General Motors tracer data since the model was developed from that data set and, therefore, it is not surprising to see that it ranks high.

The current version of the HIWAY model has unacceptable overprediction of pollutant concentration for parallel wind-road orientation angles and stable ambient atmospheric conditions. This overestimation is due to the fact that the model's dispersion parameters do not properly account for the traffic-generated turbulence near roadways. When the dispersion curves used in the current version of the HIWAY model are replaced by a new set of dispersion curves, applicable for pollutant dispersion estimation near roadways, in conjunction with an empircal vehicle-induced drag flow factor, which in a rough way accounts for the change in

the mean wind field due to the moving vehicles, the model performance is significantly improved.

Various statistical analysis techniques such as scatter plots of observed and predicted concentrations, temporal and spatial regression analysis, regression statistics for various subsets of data, cumulative frequency distributions of observed and predicted concentrations in various concentration intervals, cumulative plots of percent error, model predictability to within a factor of two of the observed concentrations, bivariate frequency distribution of observed versus predicted concentrations in various concentration intervals, distribution of mean fractional error as a function of stability and receptor distance from the source, etc, are included in this study to clearly document the performance characteristics of the original and revised versions of the HIWAY model. The results obtained with the modified HIWAY model are compared to the results obtained with the GM model and the CALINE-3 model. It is found that the modified HIWAY model performs much better than the CALINE-3 model, and the simulation of the modified HIWAY is quite comparable to that of the GM model. Although the modified HIWAY model predictions are significantly improved, a tendency to slightly overestimate concentration still exists which makes the model very useful to the regulatory agencies in their decision-making process.

CONTENTS

Abstract iii
Figures vi
Tables x
Acknowledgments xiii

1. Introduction 1
2. Data Management and Analysis 3
    Mean wind profiles 10
    Skewness and kurtosis 10
    Analysis of the wind field 13
    Characteristics of turbulence 28
    Spectral characteristics 34
    Traffic effects on the dispersion processes 41
3. Verification of Existing Highway Models 45
    Description of the models tested 46
    Model predictions 50
    Regression analysis 51
    Cumulative frequency distributions 64
4. Improvements to the EPA-HIWAY Model 80
    Modifications to the HIWAY Model 80
    Model testing and comparisons 87
    Carbon monoxide data 118
    Calibration of models 118
5. Conclusions 122

References 125

FIGURES

Number		Page
1	Instrument layout in the General Motors dispersion experiment. All units are in meters. Outside the road, horizontal distances are relative to the nearest road edge......	4
2	Specific locations of various instruments in the New York experiment..	5
3	Mean wind profiles upwind and downwind of the roadway for a few selected cases of different wind-road orientation angles........	11
4	Plot of the skewness of the vertical velocity fluctuations as a function of distance from the roadway..........................	12
5	A typical auto-correlegram for the along-wind, u', cross wind, v', and vertical, w' components for (a) a perpendicular wind-road orientation and (b) a parallel wind-road orientation. The primes denote deviation from the mean.......................	14
6	The shape of the averaged wave at the 1.5 m height induced by the traffic having a period of 29 sec. The average shape is found through a superposition of many wave cycles in the record. Δ's indicate the time at which the wave has a positive peak. The dashed line is the observed phase shift as the wave travels downwind. The solid line is the phase shift computed using the cross-road wind speed and the distance between the towers................................	16
7	The behavior of the turbulent energy associated with the 29 sec wave with travel time. X is the downwind distance from the road edge and u is the cross-road component of the wind..	19
8	Plot of the wake turbulent kinetic energy from the theory of Eskridge and Hunt (1979), with the best fit line to the data as given in Figure 7....................................	20
9	Variation of the ratio between the traffic-induced turbulence and the ambient turbulence as a funtion of Richardson number at site 12 for the data of Table 3............................	22
10	The orientation of the perturbation fields at each instrument location for a typical perpendicular wind-road orientation. The vector from the origin denotes the mean wind direction and speed..	24
11	Same as Figure 8 except for a parallel wind-road orientation....	26

Number Page

12 Streamline patterns from the interpolation of observed data of wind flow in the vertical plane for (a) the parellel wind-road orientation and (b) the perpendicular wind-road orientation. $\underline{\Delta}$ indicates the location of observed data......... 27

13 The normalized spectra of the w component at various sites at the 1.5 m level of Run 5.. 35

14 Same as Figure 13 except for Run 13............................ 35

15 Normalized spectra of the v component near (site 12) and away (site 18) from the highway for Run 15.............................. 36

16 Normalized spectra of the w component at the upwind and downwind 4.5 m level sites for Run 13.......................... 36

17 Scatter plot showing the observed versus predicted concentration for the GM model.. 57

18 Same as Figure 17 except for the HIWAY model.................... 58

19 Same as Figure 17 except for the AIRPOL-4 model................. 59

20 Same as Figure 17 except for the CALINE-2 model................. 60

21 Same as Figure 17 except for the DANARD model................... 61

22 Same as Figure 17 except for the MROAD2 model................... 62

23 Same as Figure 17 except for the ROADS model.................... 63

24 Cumulative frequency distribution of the observed concentrations is compared to the predicted concentrations of the Gaussian models. Curves lower (higher) than the dotted curve indicate overprediction (underprediction)................. 65

25 Cumulative frequency distribution of the observed concentrations at the 0.5 m height receptor nearest to the roadway is compared to the distribution of each of the Gaussian model predictions. Curves lower (higher) than the dotted curve indicate overprediction (under-prediction)............................. 66

26 Same as Figure 24 except for the numerical models............... 67

27 Same as Figure 25 except for the numerical models............... 68

28 Cumulative frequency distribution of (O-P)/O where O is the observed concentration and P is the predicted concentration for the HIWAY model.. 70

Number Page

29 Same as Figure 28 except for the GM model 71

30 Same as Figure 28 except for the AIRPOL-4 model 72

31 Same as Figure 28 except for the CALINE-2 model 73

32 Same as Figure 28 except for the MROAD2 model 74

33 Same as Figure 28 except for the ROADS model 75

34 Same as Figure 28 except for the DANARD model 76

35 Comparision between σ_z specified as a function of downwind distance and atmospheric stability according to P-G curves and those computed by solving the Gaussian equation with the observed concentration data in both the GM and NY experiments 84

36 Computed σ_z at the nearest roadside receptor as a function of cross-road wind speed 86

37 Comparison of the new dispersion curves (shaded areas) to the P-G dispersion curves (solid lines) used in the original HIWAY model. The dispersion parameters (σ_y, σ_z) are given as a function of downwind distance for each stability class. The upper bound of the new dispersion curves represents the values used for zero cross-road wind speeds, while the lower bound is for cross-road wind speeds greater than 3.91 m/sec 88

38 Scatter plots showing the observed versus predicted concentrations for HIWAY #1, HIWAY #4, GM and CALINE-3 98

39 Bivariate frequency distributions of the observed versus predicted concentrations for HIWAY #1, HIWAY #4, GM and CALINE-3 99

40 Cumulative frequency distribution of observed concentration is compared to the distribution provided by HIWAY #1, HIWAY #3, HIWAY #4 and the CALINE-3 models 100

41 Same as Figure 28 except for the HIWAY #4 model 102

42 Same as Figure 28 except for the CALINE-3 model 103

43 Cumulative plots of normalized concentrations for $(O_n-P_n)/O_n$ for the original HIWAY model. The observed and predicted concentration at various locations for a given run are divided by their corresponding maximums for that run 104

44 Same as Figure 43 except for the HIWAY #4 model 105

45 Same as Figure 43 except for the GM model 106

Number Page

46 Variation of normalized concentrations ($\chi u/Q$) with horizontal distance and wind-road angle (in degrees) for E-stability as computed from the original HIWAY (HIWAY #1), and observed data; modified HIWAY (HIWAY #3), and the GM model.............................. 117

TABLES

Number Page

1 Summary of the meteorological conditions for the GM tracer runs. The first three digits indicate the Julian day, the next six digits denote time in hours (2 digits), minutes (2 digits), and seconds (last 2 digits). The wind speed and direction are recorded at the 4.5 m height on the upwind side. Friction velocity, u_*, and Monin-Obukhov length, L, were determined by similarity theory (Eskridge et al, 1979b). The standard deviations of the azimuth angle, σ_θ, and elevation angle, σ_ϕ, are for a sampling duration of 30 min with an averaging time of 1 sec at the upwind side. Atmospheric stability in terms of Pasquill classification is obtained from z/L observations and roughness length (z_0) using Golder's (1972) method 7

2 Traffic-induced turbulent kinetic energy (m^2/sec^2), q^T, for perpendicular wind-road conditions at the 1.5 m height, at each downwind location 18

3 Ratio of the turbulent kinetic energy associated with the 29 sec oscillation, q^T, to the total ambient turbulent kinetic energy, Q'_{amb}, at the 1.5 m height, upwind of the highway 18

4 Ratio of the wake turbulent kinetic energy from the theory of Eskridge and Hunt (1979) to the ambient turbulent kinetic energy at the 1.5 m height, upwind (location 3) of the highway 23

5 Parameters in the upwind and downwind regions for the perpendicular wind cases. $\sigma_w(N)$, $\sigma_w(T)$, $\sigma_w(TR)$ are the ambient, total and traffic-generated components of the standard deviation of the vertical wind fluctuations, respectively 29

6 Parameters of the undisturbed and traffic affected flow regions for the parallel wind cases. $\sigma_v(N)$, $\sigma_v(T)$, $\sigma_v(TR)$ are the ambient, total and traffic-generated components of the lateral wind fluctuations, respectively 32

7 Time and length scales of the dominant eddies; the ambient, traffic-generated and total vertical diffusivities (K) and their ratios; and the dispersion parameters (σ) in the perpendicular wind cases 39

8 Time and space scales of the dominant eddies; the ambient, traffic-generated and total vertical diffusivities and their ratios at the nearest tower site with the wind against the traffic flow in the parallel wind cases 40

Number **Page**

9 Ensemble regression statistics for the models as a function of wind-road orientation. Explained portion of the variance (r^2), slope (b), intercept (a), standard error of estimate ($S_{o/p}$) between observed (o, dependent variable) and predicted (p, independent variable), and sample size (N) for each data subset are included in the table. In the case of the Caline-2 model, wind speeds less than 1 m/sec are excluded since the model cannot handle these situations.................. 52

10 Same as Table 9 except the data are segregated according to wind speed class.. 53

11 Same as Table 9 except the data are segregated according to stability class.. 55

12 Same as Table 9 except the data are segregated according to source-receptor location.................................... 56

13 Summary of the (O-P)/O where O is the observed and P is the predicted concentrations to within a factor of two of the observed are compared.................................... 77

14 Same as Table 13 except only data greater than half maximum observed per each sampling run is presented............ 79

15 Same as Table 9 except the models compared here are GM, HIWAY #1, HIWAY #2, HIWAY #3, HIWAY #4 and CALINE-3. One additional parameter, R, is the ratio of the mean observed concentration to the mean predicted concentration for that data subset. Here again, the data are segregated according to wind-road orientation angle........................ 90

16 Same as Table 15 except the data are segregated according to stability class.................................... 91

17 Same as Table 15 except the data are segregated according to wind speed class.. 92

18 Same as Table 15 except the data are segregated according to source-receptor location................................ 94

19 Distribution of Fractional Error by stability and distance for GM data, when the wind speed was greater than 1 m/sec, for HIWAY #1 and HIWAY #4...................................... 95

20 Distribution of Standard Deviation of Fractional Errors presented in Table 19.. 95

21 Number of data points for each category used in analyses of Tables 19, 20, and 21...................................... 96

Number Page

22 Distribution of Absolute Fractional Error by stability and distance for GM data, when wind speed is greater than 1 m/sec, for GM, HIWAY #1, HIWAY #4, and CALINE-3 models......... 96

23 Regression statistics between normalized observed and normalized predicted values for the original HIWAY, HIWAY #3, and HIWAY #4, CALINE-3 and the GM model for the GM data set. The regression analysis here shows how well the models predict the concentration profile........... 108

24 Ensemble regression statistics for the original HIWAY, HIWAY #4, CALINE-3 and the GM model for the New York data set.. 109

25 Quantitative evaluation of the dispersion models tested. Here, the model's ability to predict concentrations to within a factor of two of the observed are compared............. 110

26 Regression summary of all models by stability classification for GM data when wind speed was greater than 1 m/sec.. 111

27 Summary of (O-P)/O for stable case data used in Table 26........ 112

28 Summary of (O-P)/O for unstable case data used in Table 26...... 112

29 Same as Table 25 except only data greater than half maximum observed per each run is presented...................... 114

30 Summary of (O-P)/O for the upper half (50th through 100th percentile) of the observed GM data cumulative frequency distribution.. 115

31 Same as Table 30, except only data when the wind speed was greater than 1m/sec is presented............................ 116

32 Ensemble regression statistics for the Carbon Monoxide data collected in the NY experiment. The HIWAY #1, HIWAY #4 and GM models are presented for ground-level and all sampling points concentrations, as well as for the normalized values.. 119

33 Ensemble regression statistics for GM data sub-sets using HIWAY #4.. 119

34 Ensemble regression statistics for NY CO data sub-sets using HIWAY #4.. 121

35 Same as Table 34, but for ground level measurements only........ 121

ACKNOWLEDGMENTS

The authors are grateful to Robert Eskridge, William Petersen, and Bruce Turner of the EPA's Meteorology Laboratory for giving us an opportunity to discuss the results of this project with them. Their constructive criticism and helpful comments have been extremely valuable in the preparation of this report. Thanks are extended to Perry Samson and Leon Sedefian for their help in the analysis of data. The cooperation of Ulrich Czapski of the State University of New York at Albany is gratefully acknowledged.

The diagrams were skillfully drafted by Carol Clas and Gary Lanphear. The authors would also like to thank Catherine Cassidy, Patricia Craig, Doris Neiman, and Linda Stuart for their help in the preparation of both this report and related items. Last but not least, the authors appreciate the support of the Division of Air in pursuing this research project.

SECTION 1

INTRODUCTION

In response to the Clean Air Act, the United States Environmental Protection Agency (USEPA) has developed National Ambient Air Quality Standards (NAAQS) and oversees the State enforcement of these standards. Before a permit is issued to construct a new highway or make major modifications to an existing highway, an air quality assessment must be made to ensure that the resulting vehicle emissions will not cause a violation of the NAAQS. Mathematical dispersion models are currently being used to predict the concentrations of carbon monoxide and particulate species in the vicinity of highways. While there have been several models proposed to predict the concentration for different atmospheric conditions and highway configurations, there have been only a few experimental validation studies. The models developed to predict air pollutant concentrations near roadways vary in complexity; namely from a simple Gaussian line source approach to a numerical solution of fluid dynamic equations. However, the reliability and accuracy of various models have not been documented well due to the lack of sufficient field data. Two recent studies, conducted by General Motors (GM) and the New York State Department of Environmental Conservation (NY) have collected sufficiently detailed pollutant, traffic and meteorological data that are useful for model validation. Both the studies were conducted on at-grade roadways in relatively flat terrain. Whereas the NY experiment (Rao et al, 1978) was carried out along a major highway with average daily traffic in excess of 100,000 vehicles, the GM study (Cadle et al 1976) was a controlled experiment on a test track. Of great value in these studies is the inclusion of special tracer gas release experiments.

The major objectives of this investigation are: (i) to evaluate several commonly used highway air pollution dispersion models using the tracer gas data base developed in the GM experiment, (ii) to study the characteristics of traffic-induced turbulence and its effects on near-field dispersion, and (iii) to improve methods of modeling pollutant dispersion near roadways.

This report describes the data management and analysis of atmospheric turbulence in Section 2. Evaluation of various existing mathematical dispersion models and the relative simulation capability of each of these models is presented in Section 3. In Section 4, the weaknesses of the EPA-HIWAY model are assessed and suggestions for its improvement are made. The results from the revised EPA-HIWAY model are compared to the General Motors model and the third-generation California line source model in Section 4. Also, the revised model is evaluated with an independent data base. The findings of this research are summarized in Section 5.

SECTION 2

DATA MANAGEMENT AND ANALYSIS

The aerometric data were collected at the proving ground in Milford, Michigan, by the General Motors (GM) Corporation during October 1975. A fleet of 352 cars, divided into 32 packs consisting of 11 cars in each pack, was driven around a 10 km narrow oval track. Sixteen packs of cars were assembled in each of the outer lanes of the north-south straightway. At sampling locations, near the mid point of the oval, the track cross section simulated a four-lane road with a median. Eight pickup trucks were equipped to release sulfur hexafluoride, SF_6, as a tracer and were distributed evenly in the vehicle fleet with four trucks in each lane. The SF_6 was sampled at 20 locations in the vicinity of the test track with SF_6 samplers located on towers 1 through 6 at heights of 0.5, 3.5 and 9.5 m. Samplers were also located on stands 7 and 8 at the 0.5 m height. A total of 20 Gill UVW anemometers were located 1 m above each SF_6 sampling point. The orientation of the test track and perpendicular distances of the meteorological towers from the center of the test track are shown schematically in Figure 1. Further descriptions of the experiment can be found in Cadle et al (1977).

The other data set used in this study was collected by the New York State Department of Environmental Conservation in a similar experiment on the Long Island Expressway. The specific locations of various instruments in the New York experiment (NY) are shown in Figure 2. The experimental details of the New York Study can be found in Rao et al (1978).

DATA PROCESSING

A total of 61 tracer runs from the GM experiment and 23 tracer runs of the NY experiment are used in this study. All the tracer concentrations and corresponding meteorological data were stored on the UNIVAC 1110 computer

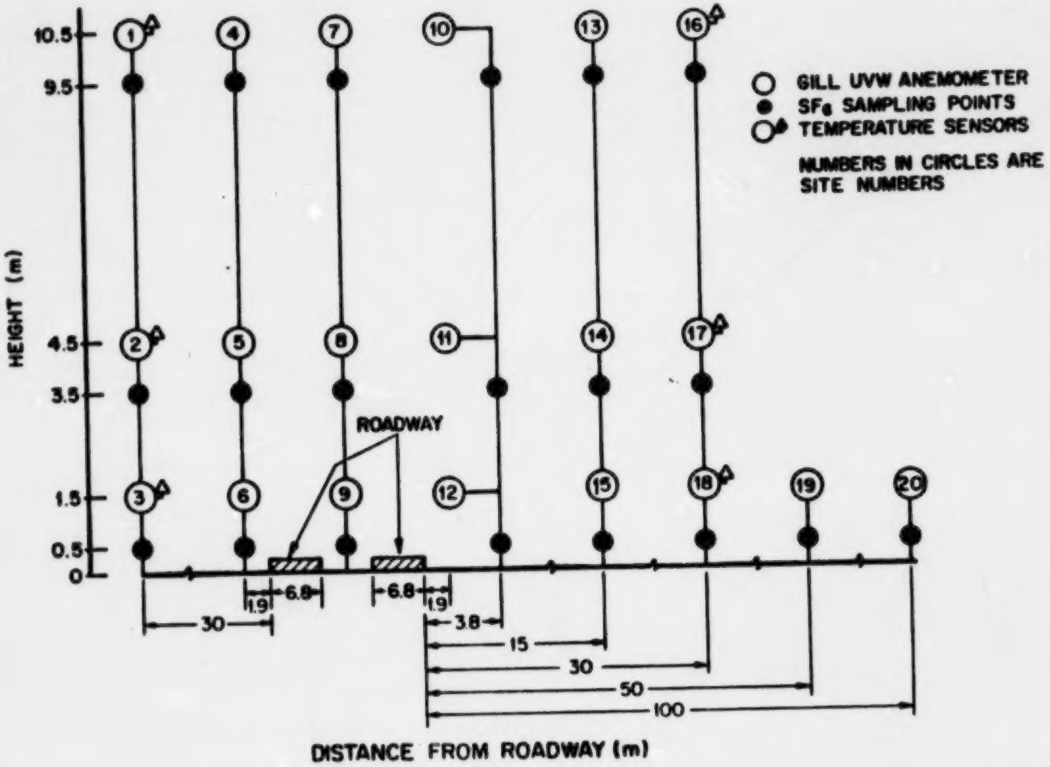

Figure 1: Instrument layout in the General Motors dispersion experiment. All units are in meters. Outside the road, horizontal distances are relative to the nearest road edge.

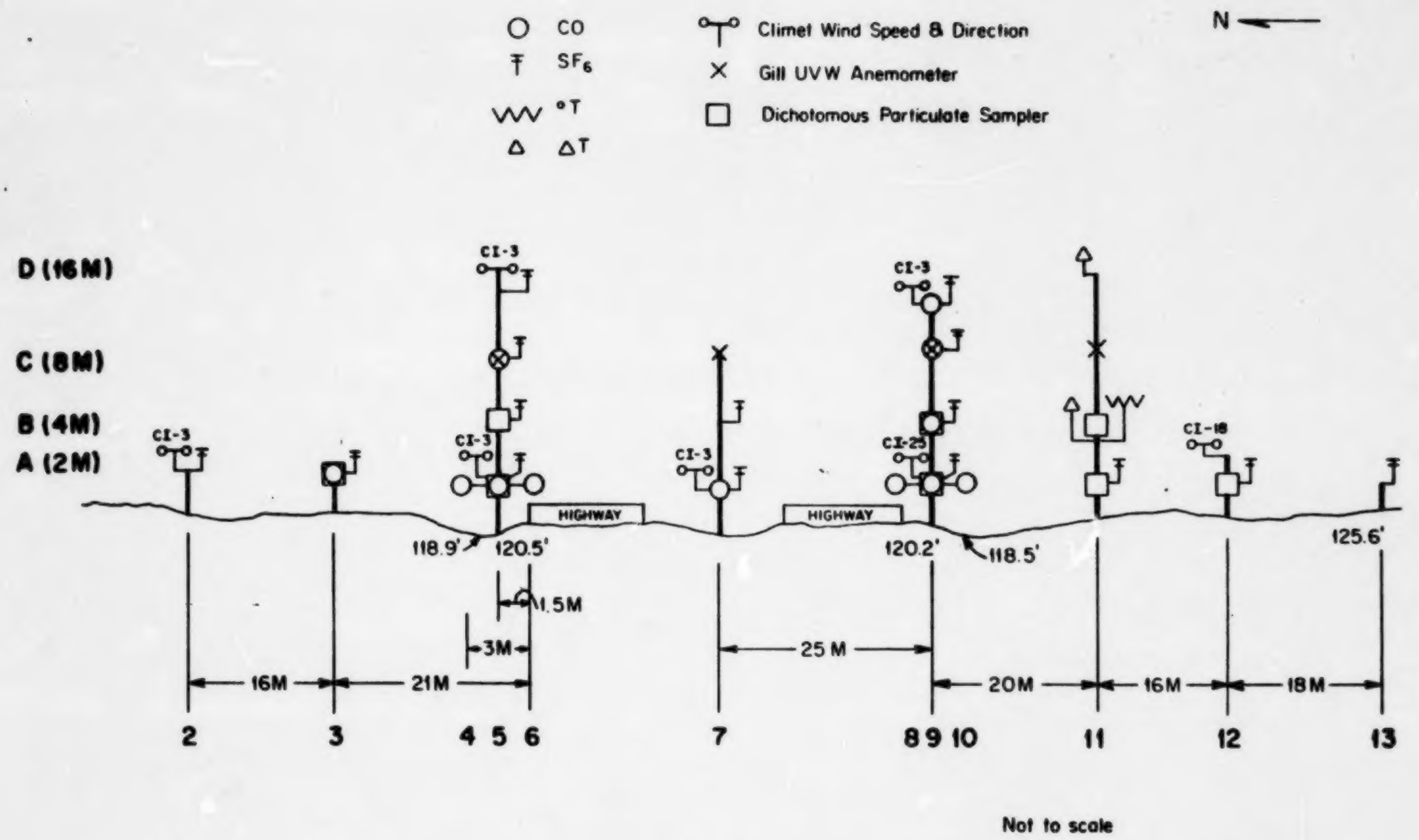

Figure 2: Specific locations of various instruments in the New York experiment.

system. Of all the tracer experiments available, the GM study was a well-controlled experiment and has the largest data base. Therefore, emphasis is placed on the analysis of the GM experimental data. A computer program was written to read the meteorological data from the tape and compute several statistical parameters and wind fluctuation statistics. For each GM tracer run period (½ hour), the one-second Gill UVW data is transposed into along-wind, cross-wind and vertical components at each measurement location. The fluctuations of along-wind (u'), cross-wind (v'), and vertical wind (w') were then computed and these one-second data were used to calculate the following variables at each location:

(i) standard deviations of all wind components (σ_u, σ_v and σ_w)

(ii) skewness and kurtosis of each wind component (S_u, S_v, S_w, K_u, K_v and K_w)

(iii) momentum fluxes ($\overline{u'w'}$, $\overline{v'w'}$ and $\overline{u'v'}$)

(iv) standard deviations of momentum fluxes ($\sigma_{u'w'}$, $\sigma_{v'w'}$)

(v) friction velocity (u_*) and momentum transfer efficiency funtion ($\sigma_{u'v'}/u_*^2$)

(vi) intensities of turbulence along each direction (i_x, i_y, and i_z)

(vii) total mean and turbulent kinetic energy

(viii) cross correlations ($R_{u'w'}$, $R_{v'w'}$ and $R_{u'v'}$)

(ix) standard deviations of azimuth angle (σ_θ) and elevation angle (σ_ϕ) for a sampling period of 30 min with averaging times of 1,5,10,15, 20,25 and 30 sec.

(x) auto-correlation funtions ($R_{u'}(t)$, $R_{v'}(t)$ and $R_{w'}(t)$) for lag times 1 to 60 sec.

In addition, power spectra at each location were computed using a fast Fourier transform technique.

A summary of all the GM tracer experiments used in this study is provided in Table 1. The wind speed and direction in the table correspond to the values observed at the 4.5 m height and 30 m distance from the roadway in the upwind direction. The atmospheric stability for each tracer run period was

Table 1

Perpendicular Wind-Road Summary
($60^\circ \leq \theta < 90^\circ$)

Run No.	Wind Speed (m/sec)	Wind Direction From True North (DEG)	Emission Strength (ul/m/sec)		Richardson No.	U_* (m/sec)	L (m)	σ_θ (DEG)	σ_ϕ (DEG)	Ambient Atmospheric Stability Golder's Technique Using z_0 and L		Airport Data
			Outer Lanes (1&4)	Inner Lanes (2&3)						Pasquill Type	Turner Type	Turner Class
274140958	2.87	291.1	3.166	2.941	-0.15	0.30	-13.4	15.5	8.0	B	B	D
274143957	2.56	292.1	3.166	2.941	-0.53	0.28	-7.7	18.3	8.6	A	A	D
274150957	2.81	290.9	3.166	2.941	-0.33	0.30	-11.7	18.9	8.6	B	B	D
274153956	2.98	291.7	3.166	2.941	-0.25	0.30	-17.4	18.3	8.6	B	B	D
279080959	1.00	251.1	2.282	3.150	0.41	0.03	2.6	12.0	5.2	F	G	C
279084000	0.97	246.7	2.282	3.150	0.33	0.05	7.3	12.6	5.7	F	G	C
279090959	1.45	253.2	2.282	3.150	-0.31	0.14	-30.5	15.5	8.0	C	C	C
279093959	1.82	250.1	2.282	3.150	-0.35	0.18	-23.2	15.5	8.6	B	C	C
281090504	0.94	77.7	3.150	3.166	0.34	0.06	12.0	43.5	12.0	F	G	C
281093504	2.05	94.2	3.150	3.166	0.02	0.18	193.0	14.9	6.9	D	D	C
283081959	1.24	254.4	3.150	2.394	0.02	0.10	58.8	16.6	6.3	E	F	C
283085000	0.95	263.2	3.150	2.394	-0.18	0.09	-146.4	14.9	6.9	D	D	C
283092000	1.12	241.6	3.150	2.394	-0.43	0.11	-18.7	24.1	6.9	B	B	B
290080958	2.17	68.0	3.214	2.411	0.13	0.17	44.3	13.8	6.9	E	F	D
290090958	2.17	61.7	3.214	2.411	0.07	0.18	72.9	16.0	7.5	E	F	D
293103458	2.00	272.3	3.214	3.182	-0.07	0.18	-133.3	13.2	7.5	D	D	D
293110458	2.10	271.3	3.214	3.182	-0.11	0.20	-78.8	16.0	9.2	B	C	D
295083958	0.62	75.1	3.166	2.394	1.06	0.00	0.01	30.4	14.9	F	G	E

Table 1: Summary of the meteorological conditions for the GM tracer runs. The first three digits indicate the Julian day, the next six digits denote time in hours (2 digits), minutes (2 digits), and seconds (last 2 digits). The wind speed and direction are recorded at the 4.5 m height on the upwind side. Friction velocity, u_*, and Monin-Obukhov length, L, were determined by similarity theory (Eskridge et al, 1979b). The standard deviations of the azimuth angle, σ_θ, and elevation angle, σ_ϕ, are for a sampling duration of 30 min with an averaging time of 1 sec at the upwind side. Atmospheric stability in terms of Pasquill classification is obtained from z/L observations and roughness length (z_0) using Golder's (1972) method.

Table 1 (cont.)

Oblique Wind-Road Summary
($30^{\circ} \leq \theta < 60^{\circ}$)

			Emission Strength (ul/m/sec)							Ambient Atmospheric Stability Golder's Technique Using z_0 and L		Airport Data
Run No.	Wind Speed (m/sec)	Wind Direction From True North (DEG)	Outer Lanes (1&4)	Inner Lanes (2&3)	Richardson No.	U_* (m/sec)	L (m)	σ_θ (DEG)	σ_ϕ (DEG)	Pasquill Type	Turner Type	Turner Class
275080959	1.07	321.3	3.085	2.362	-0.18	0.12	-9.4	22.4	11.5	C	A	C
276084459	2.15	213.6	3.053	3.085	-0.21	0.21	-29.5	12.6	7.5	C	C	D
276091459	2.65	227.4	3.053	3.085	-0.39	0.27	-15.4	13.2	7.5	B	B	C
276094459	3.07	236.5	3.053	3.085	-0.42	0.32	-15.0	13.2	8.0	B	B	C
281080504	1.82	35.7	3.150	3.166	0.14	0.13	19.3	11.5	7.5	F	G	D
283095000	1.29	220.3	3.150	2.394	-0.58	0.13	-13.1	25.2	8.6	B	B	B
290083958	2.13	58.5	3.214	2.411	0.12	0.17	42.7	13.8	7.5	E	F	D
290093957	2.46	56.0	3.214	2.411	0.02	0.21	183.3	16.0	7.5	D	E	D
294080502	1.59	229.7	3.198	3.166	0.20	0.10	12.6	13.2	6.9	F	G	C
294083502	1.52	234.7	3.198	3.166	0.22	0.11	17.8	16.0	7.5	F	E	C
294093501	1.38	219.2	3.198	3.166	-0.58	0.15	-9.0	16.6	8.6	A	A	B
295080958	0.45	51.4	3.166	2.394	3.96	0.00	0.0	85.9	30.9	F	G	F
295090958	0.62	48.9	3.166	2.394	0.34	0.02	2.3	37.2	21.77	F	G	D
303080957	0.91	320.6	3.134	3.134	0.14	0.06	13.8	22.9	10.3	F	G	E

Table 1 (cont.)

Parallel Wind-Road Summary
($0° \leq \theta < 30°$)

			Emission Strength (ul/m/sec)							Ambient Atmospheric Stability		
										Golder's Technique Using z_0 and L		Airport Data
Run No.	Wind Speed (m/sec)	Wind Direction From True North (DEG)	Outer Lanes (1&4)	Inner Lanes (2&3)	Richardson No.	U_* (m/sec)	L (m)	σ_θ (DEG)	σ_ϕ (DEG)	Pasquill Type	Turner Type	Turner Class
275083959	1.56	335.4	3.085	2.362	-0.40	0.18	-4.8	21.2	13.2	A	A	C
275090959	2.18	341.0	3.085	2.362	-0.26	0.23	-9.7	20.6	10.9	B	A	C
275093958	2.44	345.3	3.085	2.362	-0.38	0.26	-9.8	17.8	10.9	B	A	C
276081459	2.31	209.3	3.053	3.085	-0.05	0.21	-222.5	9.7	6.3	D	D	D
281083504	1.21	29.4	3.150	3.166	0.26	0.08	14.7	25.2	10.9	F	G	C
286081501	2.29	187.1	3.182	2.378	0.11	0.19	62.3	12.6	6.9	E	F	D
286084501	2.44	195.4	3.182	2.378	0.04	0.21	102.2	12.6	7.5	E	E	D
286091501	2.65	201.8	3.182	2.378	0.01	0.23	219.8	10.3	6.3	D	D	C
286094501	2.86	202.3	3.182	2.378	-0.11	0.27	-78.9	12.0	6.3	C	D	C
294090501	1.13	209.8	3.198	3.166	-0.14	0.10	-210.6	16.6	8.0	D	D	B
295093958	0.35	7.8	3.166	2.394	7.53	0.00	0.2	92.3	20.6	F	G	D
296080500	2.92	181.4	3.166	3.166	0.10	0.24	62.3	8.6	5.2	E	F	F
296083459	2.99	182.8	3.166	3.166	0.08	0.26	98.9	9.7	6.3	E	F	E
296090459	3.01	184.3	3.166	3.166	0.02	0.27	282.1	11.5	6.3	D	D	D
296093458	2.50	186.8	3.166	3.166	-0.03	0.23	-134.3	12.0	6.9	D	D	D
297080458	2.49	182.2	2.378	3.166	0.14	0.20	44.1	9.7	6.3	E	F	E
297083458	2.24	183.3	2.378	3.166	0.13	0.18	40.2	11.5	7.5	E	F	D
297090458	3.04	177.1	2.378	3.166	0.05	0.26	92.5	10.9	6.3	E	F	D
300080000	1.77	194.4	3.166	3.150	0.17	0.14	29.4	11.5	6.9	E	F	D
300083000	2.33	203.3	3.166	3.150	-0.06	0.22	-86.9	9.2	5.7	C	D	D
300090000	2.38	199.5	3.166	3.150	-0.18	0.23	-35.9	12.0	6.9	C	C	D
300093000	2.23	201.4	3.166	3.150	-0.39	0.23	-17.7	16.6	8.0	B	B	C
302080456	1.83	345.7	3.053	3.037	0.07	0.15	47.9	12.0	7.5	E	F	E
302083456	2.57	351.7	3.053	3.037	-0.02	0.23	-30.0	12.6	7.5	C	C	D
302090457	2.89	351.8	3.053	3.037	-0.05	0.27	-104.7	13.2	6.9	C	D	D
302093457	3.12	354.3	3.053	3.037	-0.07	0.28	-123.7	14.3	6.9	D	D	D
303083957	0.99	351.3	3.134	3.134	-1.19	0.11	-9.3	16.6	9.7	B	A	D
303090957	1.47	10.5	3.134	3.134	-0.56	0.14	-35.0	17.8	8.0	C	C	C
303093956	1.76	17.3	3.134	3.134	-0.57	0.18	-18.6	21.2	9.2	B	B	B

determined from the nearest airport data using the Turner (1964) method. In addition, both Pasquill and Turner type stability classifications were determined from the roughness length (z_o) and Monin-Obukhov length (L), estimated using the on-site meteorological data, according to the method outlined by Golder (1972). From this table, one can readily see that there is a considerable difference between the stability classifications determined from the airport data and local stabilities obtained from micrometeorological measurements. This is extremely important in the model evaluation studies. It is observed that the model predictions based on the local stability estimated from z_o and L are in better agreement with the measurements than those based on stability estimated from the airport data.

Mean Wind Profiles

The mean wind profiles upwind and downwind of the roadway under different wind-road orientation angles are shown in Figure 3 for a few selected runs. Under low ambient wind speeds, the wind speed decreases with height due to a pronounced increase of wind in the lowest 4.5 m. This observation is consistent with the results of Rao et al (1979). The vehicle-induced drag is significant under low ambient wind speeds resulting in a larger mean wind immediately downwind of the highway.

Skewness and Kurtosis

If the atmospheric fluctuations are Gaussian, the skewness should be zero and kurtosis is 3.0. The skewness of the vertical velocity fluctuation at each height as a function of distance from the roadway for a very stable atmospheric case is plotted in Figure 4. Here the mean wind direction is from the east and is perpendicular to the roadway. Also, included in the diagram is the momentum flux $\overline{u'w'}$. The atmosphere is very stable with a mean wind speed of 0.675 m/sec at the 4.5 m height on the upwind side. It is interesting to note that the momentum flux is close to zero up to 20 m from the eastern edge of the highway. This is representative of ambient conditions where the atmospheric stability inhibits vertical transport of momentum. The traffic on the roadway increases the momentum flux immediately close to the roadway. A bi-modal distribution of $u'w'$ is also evident at the 1.5 m height. It

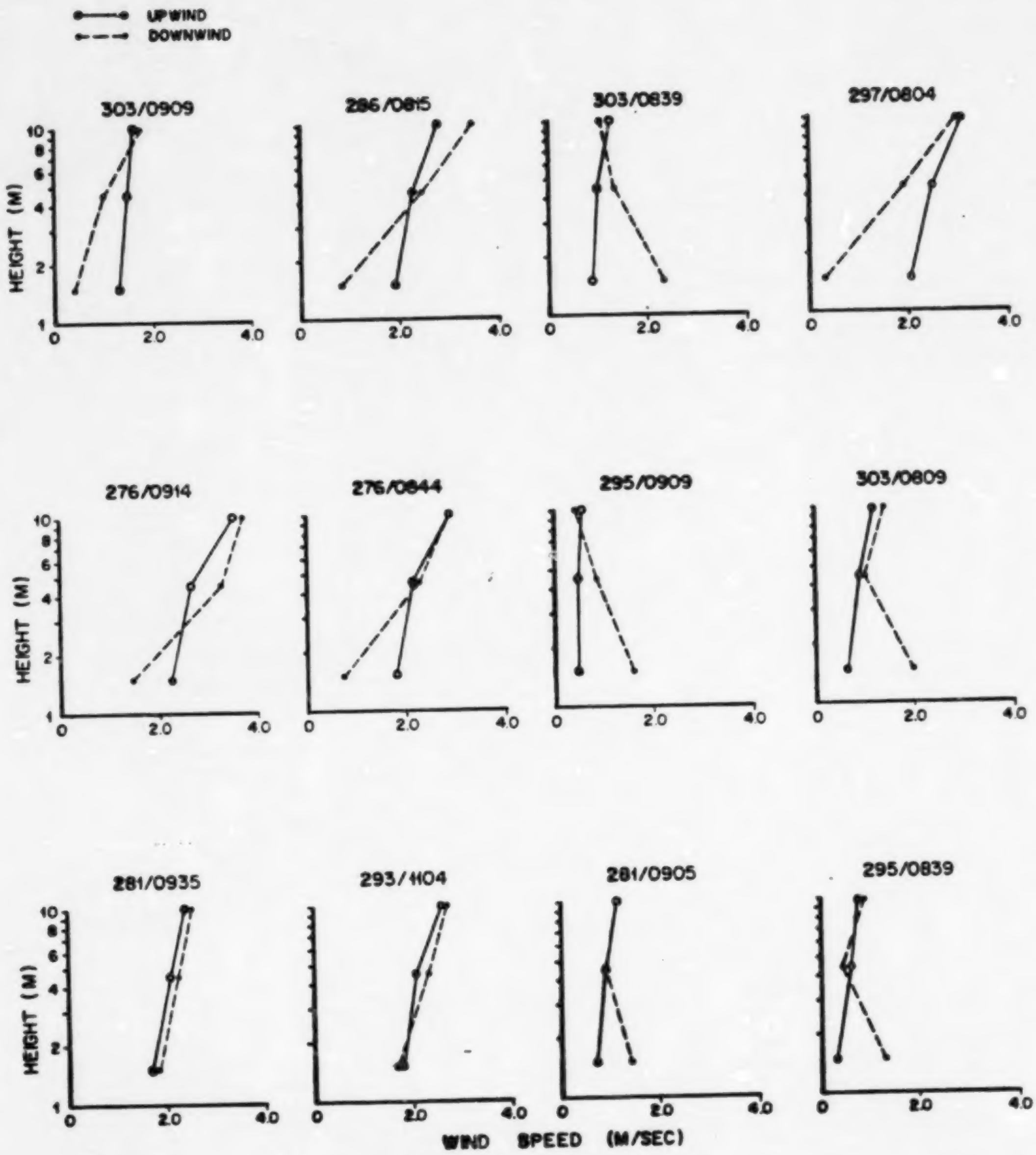

Figure 3: Mean wind profiles upwind and downwind of the roadway for a few selected cases of different wind-road orientation angles.

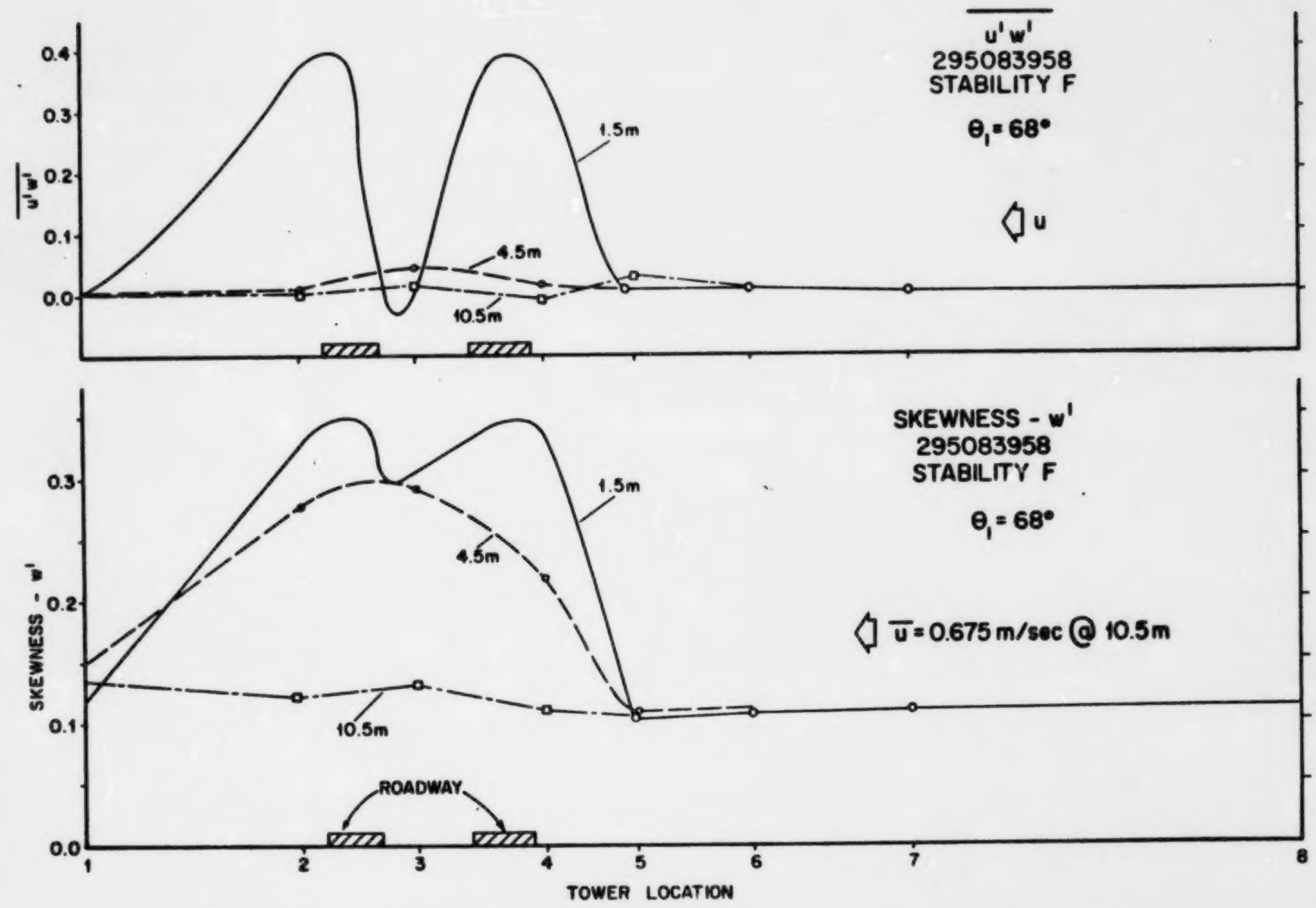

Figure 4: Plot of the skewness of the vertical velocity fluctuations as a function of distance from the roadway.

should be noted that the momentum flux reaches a minimum in the median and is of opposite direction to what is observed on either side of the roadway. There is a slight increase of momentum flux near the roadway at the 4.5 m height and the increase at 10.5 m is negligible. Since the vertical wind component is non-Gaussian near the roadway, the pollutant spread in the vertical might also be non-Gaussian. A detailed account of the effects of locally generated turbulence on the pollutant dispersion is provided in the following sections.

Analysis of the Wind Field

The perturbations of the wind components are used to compute the auto-correlagrams at the downwind edge of the highway for RUN 293/110458 (Figure 5a) with near perpendicular wind and RUN 296/080500 (Figure 5b) with near parallel wind to the roadway. From these diagrams, it is apparent that the scale of turbulence (i.e., the lag at which the auto-correlation reaches a 1/e value from the maximum) is about 4 sec. The auto-correlation approaches zero in about 8 to 10 sec, and then depicts a sinusoidal oscillation with a characteristic period of 29 sec. In the GM experiments, vehicles were driven in packs of eleven cars each through a vertical plane of meteorological sensors at relatively precise intervals of 29 sec. This exactness in the field experiment resulted in a distinct forcing in the perturbation components of the wind. This periodic type disturbance is evident in all cases where vehicles were being driven, and the above two runs are presented as typical cases. It is the use of this forcing function which allows a more exact description of the characteristics of turbulence generated on the roadway.

The values of u', v', and w' are then re-examined by averaging at consecutive seconds over the 29 sec period in a manner described by

$$A(i) = \frac{1}{N(i)} \sum_{m=1}^{M} A[i + (m-1)J] \quad \text{for } i=1....J \qquad (1)$$

where i is the 1 sec increment of the oscillation varying between 1 and J (29 sec in this case). The value M is the total number of data points over the 30

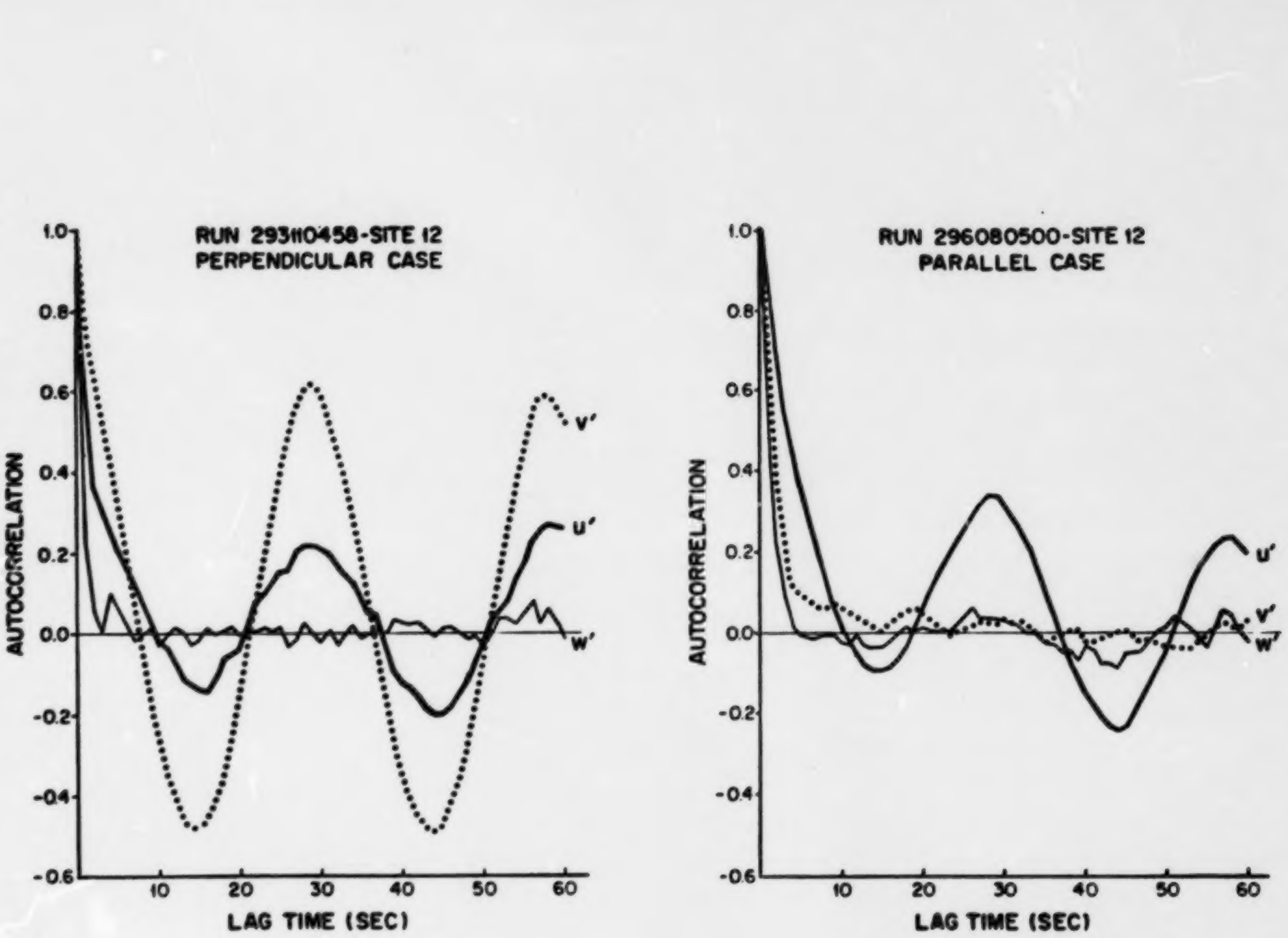

Figure 5a

Figure 5b

Figure 5: A typical auto-correlegram for the along-wind, u', cross wind, v', and vertical, w' components for (a) a perpendicular wind-road orientation and (b) a parallel wind-road orientation. The primes denote deviation from the mean.

min study period, N (i) is the specific number of data points in each 29 sec data block, and A is the amplitude. This procedure yields the shape of the averaged wave having a period of 29 sec. This constant-phase or harmonic lock representation has been used previously by Rao and Ketchum (1975) to study the characteristics of baroclinic waves in a rotating annulus, and by Rao et al (1977) to identify the characteristics of internal waves in large lakes. It should be indicated here that the averaged wave of a 29 sec period in this particular situation does not really represent the average size of the traffic-induced eddy or that there exists an eddy of this scale. However, in the time scale of this forcing function, all the traffic-generated eddies are included so that one-half of the square of the amplitude of this 29 sec oscillation is indicative of the integrated total energy contributed by various smaller scale eddies generated by the moving traffic on the roadway. In theory, one should find the energy associated with the wake from each vehicle and integrate it over all the multiple wakes generated by the traffic. In real-world situations, although traffic seems to flow in packs, the vehicle spacing and speed of each vehicle are quite variable, and, hence, it is not possible to derive the traffic-generated energy from the type of analysis presented here. Since the GM study is a controlled experiment, it is possible to take advantage of the constant vehicle speed and spacing on the roadway by treating this 29 sec oscillation as a marker for the traffic effects.

RUN 293110458 was a half-hour run where the wind was nearly perpendicular to the highway. The wind direction recorded at six towers at the 4.5 m height ranged between 262° to 272° (the highway orientation is north-south). Figure 6 shows a plot of A(i) at the 1.5 m height for u', v', and w' for this run. The amplitude of the 29 sec wave is greater for v' than u' near the highway and downwind of the highway. The w' plot did not show any significant trends on this time scale across the highway reflecting the lack of autocorrelation shown in Figure 5a.

The translation of this forcing function away from the highway is evident in Figure 6. The dashed line in the v' component of Figure 6 connects the points at which the amplitude of the oscillation in the crosswind component is maximum for each location downwind of the highway. This line represents the observed phase shift between each downwind location. The solid line shows the

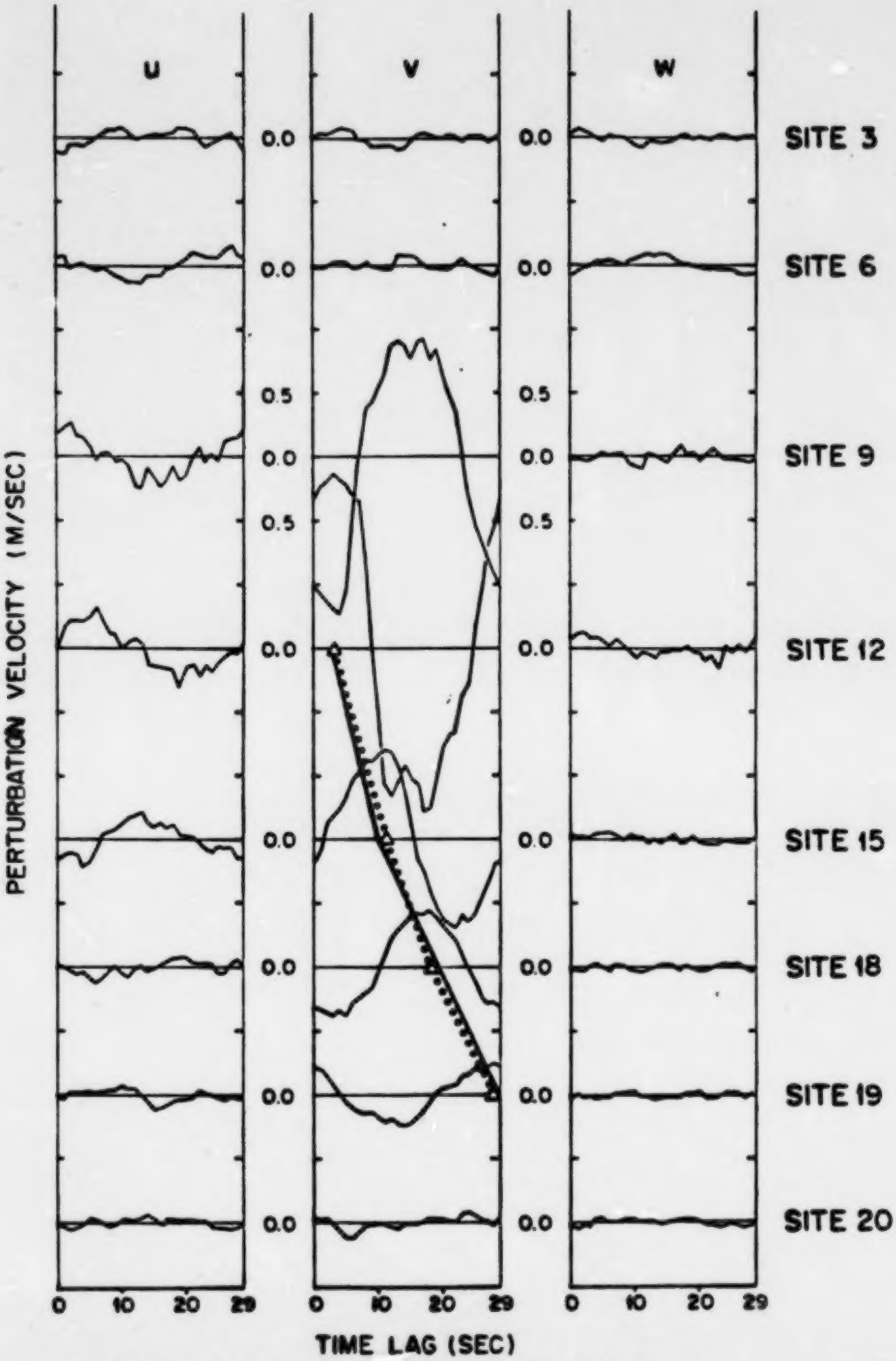

Figure 6: The shape of the averaged wave at the 1.5 m height induced by the traffic having a period of 29 sec. The average shape is found through a superposition of many wave cycles in the record. Δ's indicate the time at which the wave has a positive peak. The dashed line is the observed phase shift as the wave travels downwind. The solid line is the phase shift computed using the cross-road wind speed and the distance between the towers.

phase shift of the oscillation computed from the cross-highway wind speed at the height using winds averaged between towers ($t = x/U$). The good agreement between these two lines indicates that the disturbance is frozen into the flow and is advected past the tower line.

The turbulent kinetic energy associated with the 29 sec oscillation, q^T, is computed as

$$q^T = \tfrac{1}{2}(\bar{A}^2_{u',max} + \bar{A}^2_{v',max} + \bar{A}^2_{w',max}) \qquad (2)$$

where $A_{u',max}$ is the maximum amplitude of the 29 sec oscillation for the u' perturbations. For the thirteen tracer gas runs when the wind was perpendicular to the roadway from the west ($240^o < \theta < 300^o$) the turbulent kinetic energy of the 29 sec oscillation is computed as a function of downwind location at the 1.5 m height level. These results are presented in Table 2. The variations in q^T from run to run can be accounted for by plotting these values as a function of travel time from the highway defined as the distance from the downwind edge of the highway to the sampling site divided by the mean wind speed at that level over that distance. These results are shown in Figure 7. The decay of traffic-induced turbulent energy with travel time is best fit to a power law ($r = 0.88$). This relationship is also shown in Figure 8 . This equation will not describe the behavior of turbulence as $t \to 0$, and is, thus, restricted to travel times greater than or equal to 2 sec. The turbulence decays to about 1/10th of its site 12 value in about 15 sec of travel time. Figure 8 shows the distributions of wake kinetic energy according to the model predictions of Eskridge and Hunt (1979) at various distances downwind of the roadway. The theoretical results differ from the analyzed results by decreasing faster, with the wake kinetic energy going to zero by 12 sec. The observed kinetic energy of the wake is approximately 15-20% greater than the theoretical values. The difference between the theoretical value of the wake turbulent kinetic energy and the observed value may be due to the method used in determining the energy in the 29 sec peak and/or approximations made in the theory.

A measure of the influence of the highway-generated turbulence on the naturally occurring turbulence can be obtained by considering the ratio of the

Table 2

Site Run No.	12	15	18	19	20
274140958	1.039	0.261	0.100	0.051	0.017
274143957	0.883	0.189	0.070	0.041	0.012
274150957	1.127	0.384	0.093	0.081	0.017
274153956	1.089	0.301	0.127	0.064	0.034
279080959	0.762	0.089	0.014	0.003	0.001
279084000	0.818	0.099	0.029	0.007	0.001
279090959	0.895	0.179	0.038	0.007	0.002
279093959	1.039	0.220	0.078	0.022	0.008
283081959	0.988	0.167	0.030	0.007	0.003
283085000	0.857	0.096	0.013	0.002	0.001
283092000	0.947	0.112	0.022	0.006	0.002
293103458	0.923	0.295	0.109	0.040	0.016
293110458	0.928	0.266	0.087	0.036	0.008

Table 2: Traffic-induced turbulent kinetic energy (m^2/sec^2), q^T, for perpendicular wind-road conditions at the 1.5 m height, at each downwind location.

Table 3

Site Run No.	12	15	18	19	20
274140958	1.45	0.36	0.14	0.07	0.02
274143957	1.18	0.25	0.09	0.05	0.02
274150957	1.32	0.45	0.11	0.09	0.02
274153956	1.28	0.35	0.15	0.07	0.04
279080959	21.17	2.47	0.39	0.08	0.03
279084000	15.73	1.90	0.56	0.13	0.02
279090959	4.86	0.97	0.21	0.04	0.01
279093959	3.82	0.81	0.29	0.08	0.03
283081959	8.67	1.46	0.26	0.06	0.03
283085000	10.99	1.23	0.17	0.03	0.01
283092000	4.14	0.50	0.10	0.02	0.00
293103458	3.46	1.10	0.40	0.16	0.06
293110458	2.74	0.78	0.26	0.10	0.02

Table 3: Ratio of the turbulent kinetic energy associated with the 29 sec oscillation, q^T, to the total ambient turbulent kinetic energy, Q'_{amb}, at the 1.5 m height, upwind of the highway.

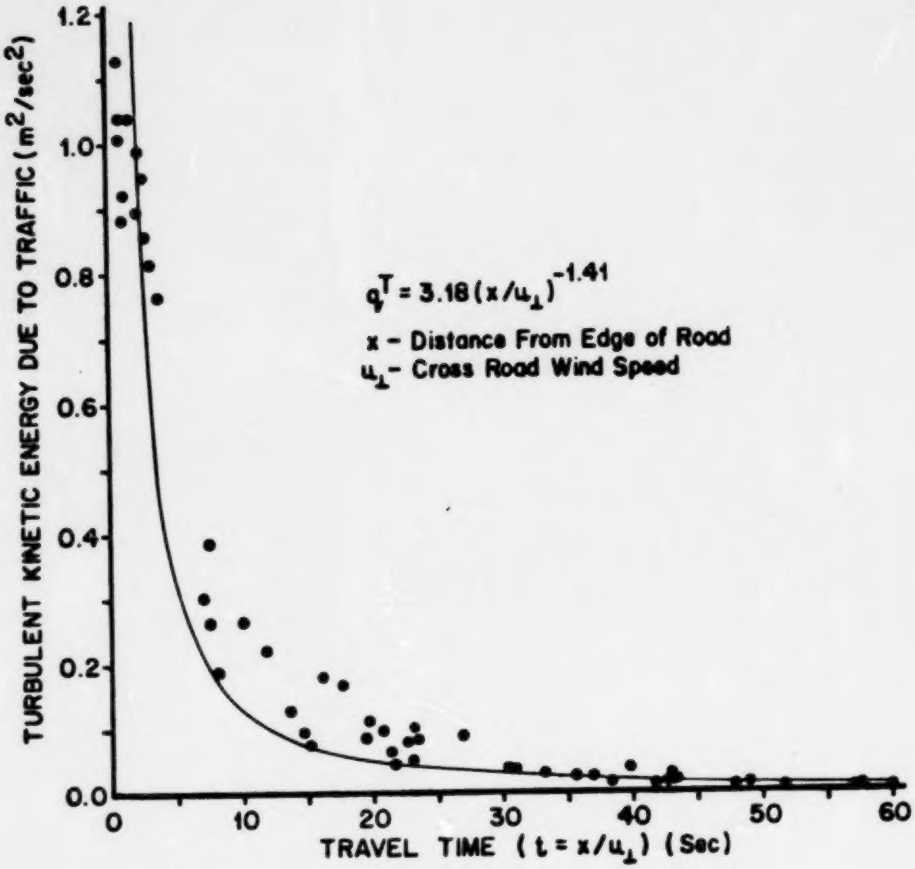

Figure 7: The behavior of the turbulent energy associated with the 29 sec wave with travel time. X is the downwind distance from the road edge and u is the cross-road component of the wind.

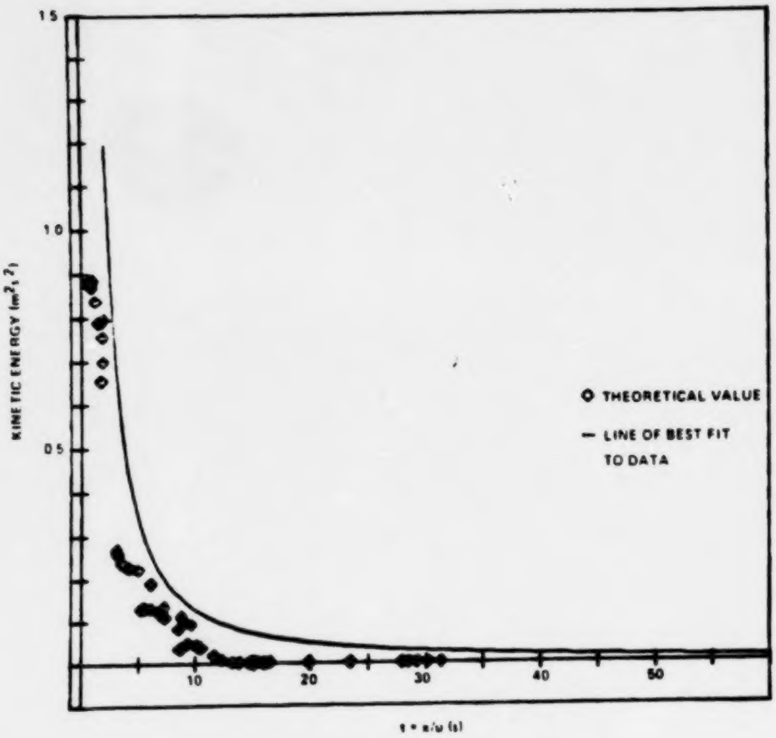

Figure 8: Plot of the wake turbulent kinetic energy from the theory of Eskridge and Hunt (1979), with the best fit line to the data as given in Figure 7.

turbulent kinetic energy associated with the 29 sec oscillation, q^T, to the total ambient turbulent kinetic energy, $Q_{amb} = \frac{1}{2}(\overline{u'^2} + \overline{v'^2} + \overline{w'^2})$, over the period. This ratio is tabulated for perpendicular cases in Table 3. This table shows that the traffic-induced turbulence is between 118% to 2100% of the naturally occurring turbulence at the roads edge with exponential decay away from the highway. The variation of this ratio is due to differences in both travel time, as indicated before, and ambient atmospheric stability. It is seen that the ratio of locally generated turbulence to naturally occurring turbulence is small under unstable ambient conditions. It is presumed that q^T is independent of atmospheric stability; thus, the ratio q^T/Q'_{amb} will be large when Q'_{amb} is small under stable conditions. The variation of the ratio between the traffic-induced turbulence and the ambient turbulence as a function of atmospheric stability is shown in Figure 9. It is evident from this diagram that as the atmosphere becomes more stable, the ratio q^T/Q'_{amb} increases. This suggests that the traffic effects become dominant as the atmospheric stability increases. The ratio of the model (Eskridge and Hunt, 1979) predicted turbulent kinetic energy to the ambient turbulent kinetic energy for each run is shown in Table 4. The ratios, according to the theory, vary from 0 to 18.5 with the maximum value occurring near the roadway.

The primary manifestation of the 29 sec forcing function is in the horizontal plane. To understand the perturbations generated by the traffic, plots were made of $A_{u'}(i)$ and $A_{v'}(i)$, i = 1, 29 sec at each anemometer for selected runs. Figure 10 shows this plot for a typical perpendicular situation along with vectors indicating the relative magnitude and direction of the mean wind over the study period. The vertical axes (north-south component of wind) drawn at each location are scaled to represent perturbations of $\pm$ 0.5 m/sec and mean wind speeds of 2.0 m/sec. The horizontal axes (east-west component of wind) denote a perturbation of $\pm$ 0.25 m/sec and a mean wind of 1.0 m/sec. The orientation of the 29 sec oscillation in time is depicted by the arrow heads with a common time, zero, marked by a triangle. Each vector represents a time interval of one second duration. Traffic passes between Towers 2 and 3 traveling from south to north. This causes a turning of the mean wind flow in the median (Tower 3) towards the direction of the traffic flow. The opposite flow between Towers 3 and 4 produces the opposite effect. The southerly component of the mean wind produced by this north to south

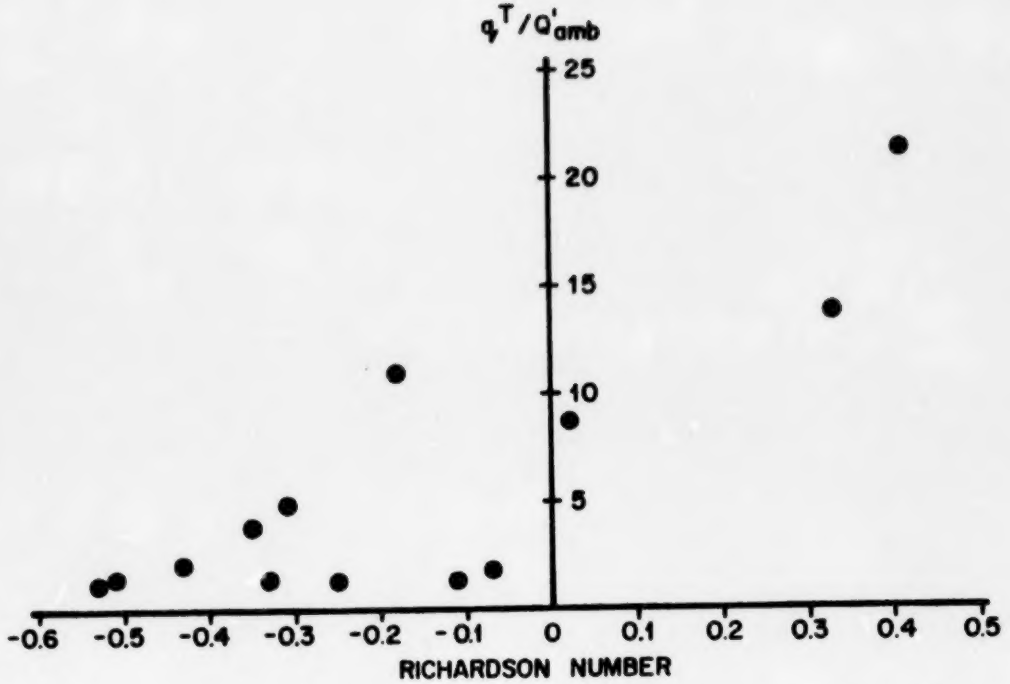

Figure 9: Variation of the ratio between the traffic-induced turbulence and the ambient turbulence as a funtion of Richardson number at site 12 for the data of Table 3.

Table 4

Site Run No.	12	15	18	19	20	Q'_{amb} (m^2 sec^{-2})
274140958	1.23	0.18	0.05	0.0	0.0	0.72
274143957	1.16	0.17	0.02	0.0	0.0	0.75
274150957	1.04	0.15	0.04	0.0	0.0	0.85
274153956	1.04	0.15	0.05	0.0	0.0	0.85
279080959	18.46	0.0	0.0	0.0	0.0	0.04
279084000	13.56	0.0	0.0	0.0	0.0	0.05
279090959	4.55	0.20	0.0	0.0	0.0	0.19
279093959	3.27	0.30	0.0	0.0	0.0	0.27
283081959	6.88	0.06	0.0	0.0	0.0	0.12
283085000	9.70	0.02	0.0	0.0	0.0	0.08
283092000	3.45	0.01	0.0	0.0	0.0	0.23
293103458	2.99	0.0	0.0	0.0	0.0	0.27
293110458	2.57	0.32	0.0	0.0	0.0	0.34

Table 4: Ratio of the wake turbulent kinetic energy from the theory of Eskridge and Hunt (1979) to the ambient turbulent kinetic energy at the 1.5 m height, upwind (location 3) of the highway.

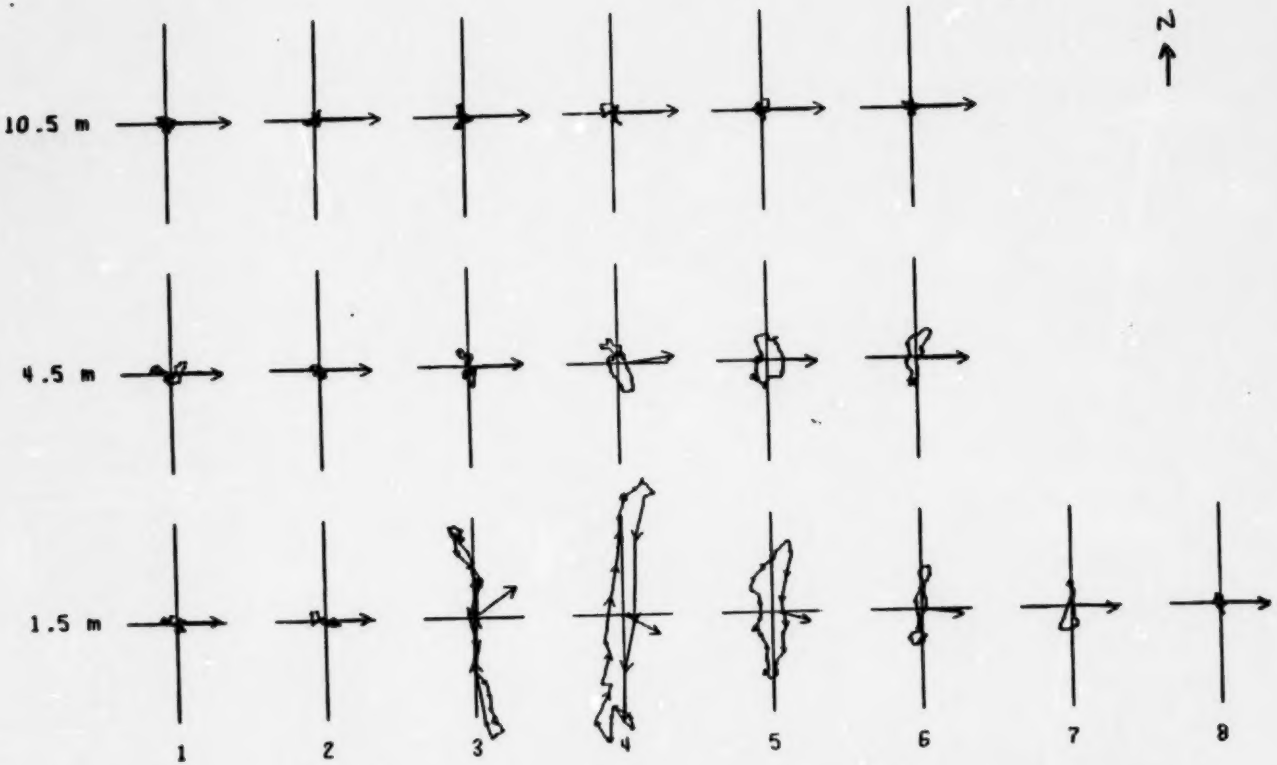

Figure 10: The orientation of the perturbation fields at each instrument location for a typical perpendicular wind-road orientation. The vector from the origin denotes the mean wind direction and speed.

traveling traffic is damped slowly with distance from the highway, returning to upwind conditions be tween 50 to 100 m downwind of the highway. In some cases a change in the mean wind flow is also evident at the 4.5 m level. Changes at that height, however, are limited to Towers 3 and 4 with an apparent return to ambient conditions within 15 m of the highway. There appears to be little effect on the mean wind flow at the 10.5 m level. The primary component of the perturbations, as mentioned before, is elongated parallel to the highway. This orientation is maintained as the disturbance is translated away from the highway. Again, little, if any organized motion can be discerned at the 10.5 m level. At the 4.5 m level, a discernible oscillation becomes apparent at Tower 3 and can be followed downwind, loosing its amplitude at a lesser rate than at the 1.5 m level. This is due to the diffusion of turbulence from below over this range and the increased distance from the surface.

Since the energy of the perturbation has been shown to drop off as a function of travel time, it follows that the decrease in amplitude with distance will be much greater for the near parallel case compared to the perpendicular situation. The extent of discernible perturbations is limited to the volume very near the highway under parallel wind conditions (see Figure 11). An organized pattern can be seen at the 4.5 m height over the highway but is barely visible 15 m from the highway at the 1.5 m height. The orientation of the perturbation ellipse is again oriented along the highway with the largest perturbations on the east side of the highway. This pattern recurred for all parallel cases with southerly wind direction. The symmetry is destroyed probably due to the opposition of traffic to the wind on this side of the highway versus the travel with the wind in the western lanes. The mean wind is increased at 1.5 m on the western edge of the highway by the traffic but reduced on the eastern edge because of the opposition between the wind and the vehicle. This observation suggests that models which incorporate turbulent wake effects should be sensitive to the wind-vehicle orientation in the parallel wind situation.

This interaction between vehicle and wind can also be observed in the mean cross-sectional wind pattern in the parallel case. Figure 12a shows the streamline of tangential flow as analyzed from observed wind components for

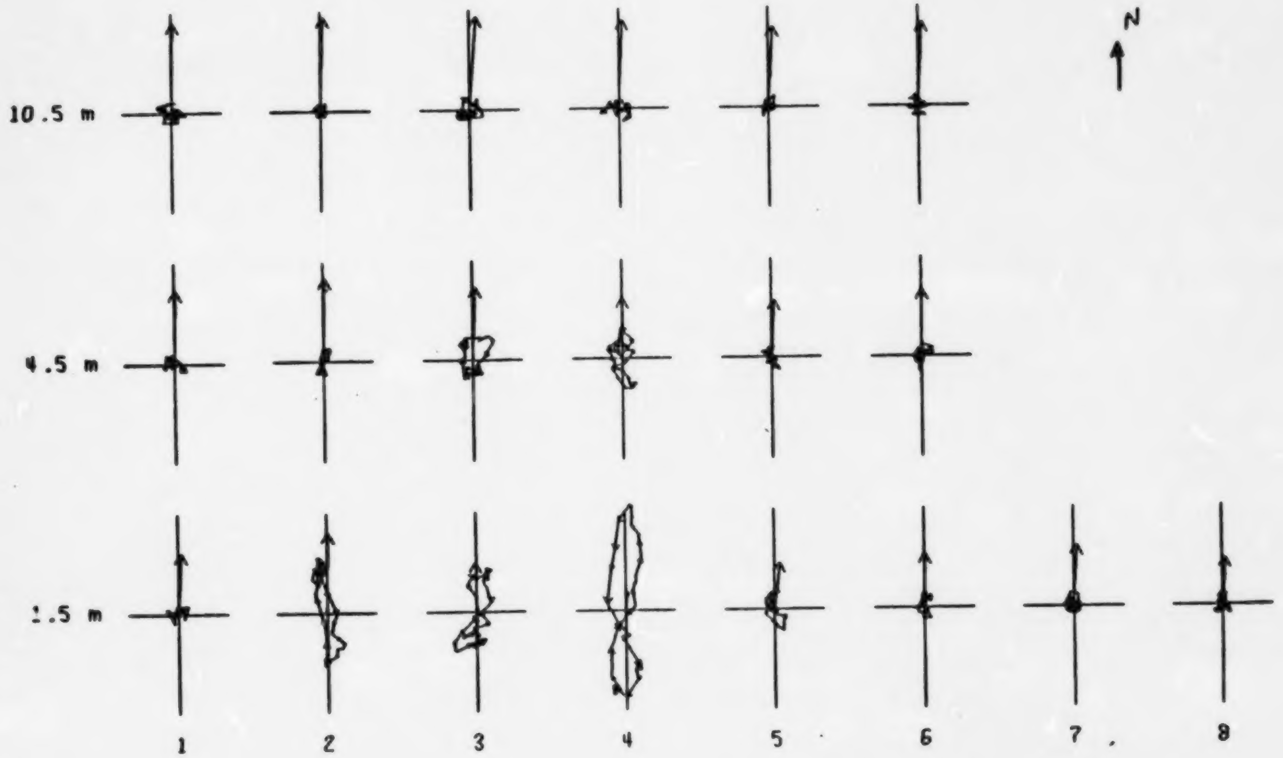

Figure 11: Same as Figure 8 except for a parallel wind-road orientation.

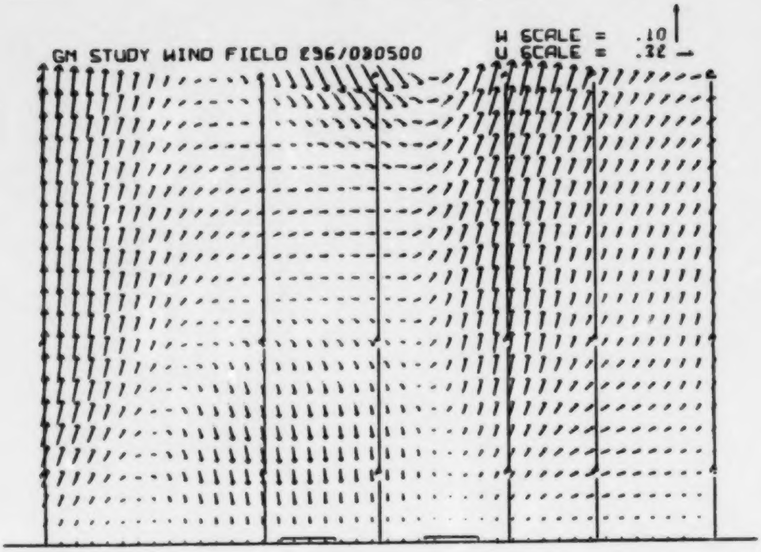

Figure 12a

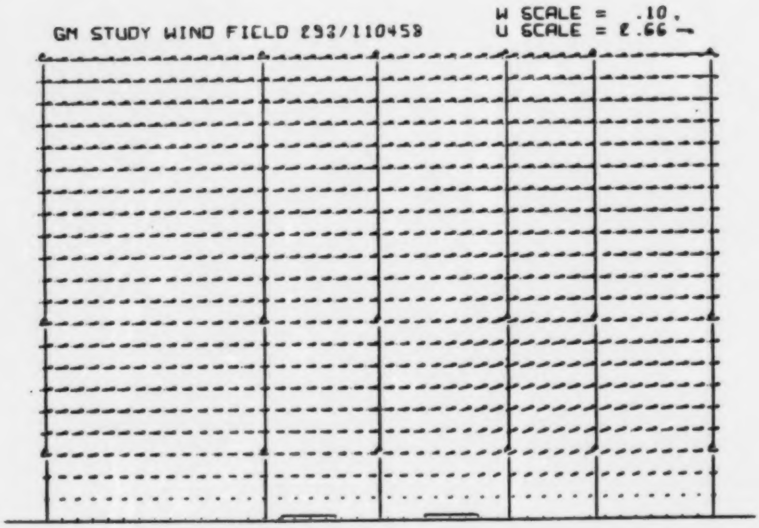

Figure 12b

Figure 12: Streamline patterns from the interpolation of observed data of wind flow in the vertical plane for (a) the parellel wind-road orientation and (b) the perpendicular wind-road orientation. $\underline{\Delta}$ indicates the location of observed data.

the parallel wind situation discussed above. This analysis suggests the opposition of wind and traffic produce a mean upward motion on the eastern edge of the highway and a mean downward motion on the eastern lane where traffic and wind are in the same direction. In the perpendicular case, Figure 12b, there is much less organized vertical motions over the highway. Here advective terms dominate and vertical motions become less important in the transport across the highway. It should be indicated here that the streamline patterns are generated without using the continuity equation and hence, these depict trends only.

Characteristics of Turbulence

The role of the traffic-generated turbulence on the naturally occurring turbulence adjacent to the roadway are assessed through bulk turbulence statistics and spectral analysis. Because of fundamental differences between effects with winds parallel or perpendicular to the traffic flow some of the results are presented separately.

Bulk Statistics--

(i) Perpendicular Winds--

Of the eighteen perpendicular wind cases, 13 had wind directions from the west and, thus, yield more information in the downwind direction. In these cases, site 3 (see Figure 1) represents upwind or ambient conditions. Table 5 gives the mean wind speed, u, the standard deviation of the vertical wind component, σ_w (N), and the Richardson number (Ri) for the 1.5 m level at the upwind site 3. Also, presented in Table 5 are the standard deviations of the vertical wind σ_w (T) values measured at various downwind distances at the 1.5 m level, and at the 4.5 m level of the nearest tower. More emphasis is placed on the data at the 1.5 m height since these should more readily show the traffic effects.

Close to the ground, where turbulent energy is of mechanical origin, σ_w depends mainly on surface roughness and wind speed. Chock (1977) had already

Table 5

		Site 3			$\sigma_w(T)$ at sites (m/s)				$\sigma_w(TR)$ at sites (m/s)				$\sigma_w(TR)$ ratios		$\sigma_w(T)/\sigma_w(N)$ at sites	
Run No.	GM Run No.	U(m/s)	$\sigma_w(N)$ (m/s)	Ri	12	15	18	11	12	15	18	11	15/12	18/12	12	15
1	274140958	2.42	.28	-.42	.38	.30	.28	.41	.25	.09	0	.11	.36	0	1.33	1.07
2	274143957	2.11	.27	-.53	.37	.29	.30	.39	.25	.08	.09	.14	.32	.36	1.35	1.07
3	274150957	2.29	.30	-.33	.37	.28	.30	.41	.21	0*	0	0	0	0	1.22	.93
4	274153956	2.44	.31	-.25	.37	.32	.31	.42	.21	.08	0	.06	.38	0	1.21	1.03
5	279080959	0.65	.06	.41	.35	.19	.13	.29	.34	.15	.11	.28	.44	.32	5.68	3.17
6	279084000	0.71	.08	.33	.37	.18	.13	.27	.36	.16	.11	.25	.44	.31	4.63	2.25
7	279090959	1.24	.15	-.31	.36	.20	.17	.26	.33	.14	.08	.16	.42	.24	2.41	1.33
8	279093959	1.56	.20	-.35	.37	.22	.20	.28	.31	.11	0	.10	.35	0	1.84	1.10
9	283081959	0.98	.10	.02	.35	.19	.14	.26	.33	.16	.10	.22	.48	.30	3.63	1.90
10	283085000	0.80	.08	-.18	.34	.17	.12	.25	.33	.15	.09	.23	.45	.27	4.25	2.13
11	283092000	0.95	.10	-.43	.36	.19	.14	.29	.34	.16	.10	.26	.47	.29	3.60	1.90
12	293103458	1.66	.19	-.07	.33	.21	.19	.25	.27	.09	0	0	.33	0	1.74	1.11
13	293110458	1.76	.20	-.11	.34	.22	.20	.26	.28	.09	0	0	.32	0	1.70	1.10

*A value of 0 indicates a difference of $\leq$ 0.

Table 5: Parameters in the upwind and downwind regions for the perpendicular wind cases. $\sigma_w(N)$, $\sigma_w(T)$, $\sigma_w(TR)$ are the ambient, total and traffic-generated components of the standard deviation of the vertical wind fluctuations, respectively.

noted the linear dependence of the σ_w on u at the upwind sites of the GM data. In addition, a plot of σ_w/u_* versus Ri, not presented here, indicates that σ_w/u_* is independent of stability at least at the 1.5 m level. An interesting feature (see Table 5) is the rather constant value of σ_w (T) at the first tower downwind (site 12), implying independence on wind speed or stability. If the traffic-generated turbulence can be represented as (see Rao et al, 1979 and Eskridge and Hunt, 1979)

$$\sigma_w^2(TR) = \sigma_w^2(T)-\sigma_w^2(N) \tag{3}$$

then σ_w (TR) should be inversely proportional to the wind speed. Table 5 gives σ_w (TR) values calculated from equation (3) at three downwind distances. At site 12, σ_w (TR) is proportional to $u^{-\alpha}$ where α is approximately - 1/3, with a 0.95 correlation coefficient. An inverse relationship between σ_w (TR) and u is also found at other downwind distances. It should be noted that the exponent of the power law will be influenced by errors in small differences in σ_w (T) and σ_w (N), limitations of the Gills to sense the high frequency eddies, and the validity of equation (3).

Table 5 shows that σ_w (TR) decays faster with distance from the roadway with increasing wind speed. This can be clearly seen from the ratios of σ_w (TR) at sites 15 and 18 to σ_w (TR) at the nearest site 12. Furthermore, this difference becomes more distinct when one notes that the effective travel time of the traffic-generated eddies is large for the lower wind speeds.

The vertical extent of the traffic influence on σ_w (T) is found to be large under lower wind speeds as can be seen from Table 5 values of σ_w (TR) at site 11 (4.5 m) of the nearest tower. These σ_w (TR) values were calculated using σ_w at site 2 as representative of the ambient conditions. A comparison of σ_w at the 10.5 m level sites, on both sides of the roadway, indicated that the traffic influence is not of any noticeable importance at this elevation.

From the above results, a picture emerges in which traffic-generated turbulence and mean wind advection are complementary. When wind speeds are high, dissipation of the traffic turbulence is fast ($\varepsilon \alpha u^3$) but is transported to greater horizontal distances per unit time. When wind speeds are low, traffic-generated turbulence is not only dissipated less, but also can spread to higher elevations. The compensatory effect of advection and wake turbulence can explain the observed constancy of σ_w (T) at the 1.5 m level immediately downwind of the roadway.

The additional contribution from the traffic turbulence to σ_w affects the vertical dispersion of pollutants because of the direct relationship between these two parameters. The amount of enhancement in the spread of pollutants can be seen from the ratios of σ_w (T) to σ_w (N) given in Table 5. It is clear that the enhancement of turbulent dispersion is considerable for the low wind speed cases. For example, near the roadway the ratio is 5.68 for the lowest wind speed case compared to 1.21 for the highest wind speed case. At the next downwind distance of 15 m the enhancement is almost nil for the higher wind speed but is still 300% for the lowest wind speed case. The incorporation of this dispersion enhancement into the Gaussian and numerical models should alleviate some of the problems found in near-field dispersion modeling studies.

It should be noted that the lateral component of turbulence, σ_v, need not be considered for perpendicular wind cases since the models assume a uniform distribution of pollutants in the direction of the roadway. Also, an analysis along the above lines showed no systematic variations of σ_w (T) at site 9 of the median tower where the mean flow and the turbulence characteristics are complicated by the influence of the two lanes of traffic equidistant from both sides of the tower.

(ii) Parallel Winds --

The set of runs which are representative of parallel wind cases is given in Table 6 along with the ambient flow parameters. As in the perpendicular wind cases, σ_w (N) is dependent on wind speed and not on stability while the lateral component, σ_v(N), does not seem to depend on either parameter in any systematic way. The effects of traffic were found to be considerably different for the nearest site to the roadway where the wind direction was with the

Table 6

Run No.	GM Run No.	Ambient Parameters Wind dir. (degrees)	U(m/s)	Ri	$\sigma_w(N)$ (m/s)	$\sigma_v(N)$ (m/s)	Along Traffic flow sites(1.5m) U	$\sigma_w(T)$	$\sigma_v(T)$	$\sigma_w(TR)$	$\sigma_v(TR)$	Against Traffic flow sites(1.5m) U	$\sigma_w(T)$	$\sigma_v(T)$	$\sigma_w(TR)$	$\sigma_v(TR)$	Against Traffic flow sites(4.5m) $\sigma_w(T)$	$\sigma_w(TR)$
14	296080500	181	2.14	.10	.21	.46	3.2	.25	.45	.14	0	.75	.44	.71	.39	.54	.37	.24
15	296090459	191	2.56	.02	.25	.53	3.2	.25	.55	0	.15	1.40	.49	.78	.42	.57	.36	.24
16	296093458	193	2.48	-.03	.25	.54	3.0	.25	.53	0	0	1.00	.47	.78	.40	.57	.35	.24
17	297080458	183	2.00	.14	.25	.46	2.87	.27	.45	.14	0	.28	.45	.89	.39	.76	.38	.22
18	303083957	1	1.00	-1.2	.13	.30	2.37	.30	.54	.27	.45	1.12	.31	.54	.28	.45	.29	.24
19	303090957	11	1.72	-.56	.16	.56	2.52	.30	.53	.25	0	.40	.39	.77	.36	.53	.33	.25
20	303093956	17	1.54	-.57	.18	.64	2.24	.26	.76	.19	.41	.62	.40	1.27	.36	1.10	.32	.20

Table 6: Parameters of the undisturbed and traffic affected flow regions for the parallel wind cases. $\sigma_v(N)$, $\sigma_v(T)$, $\sigma_v(TR)$ are the ambient, total and traffic-generated components of the lateral wind fluctuations, respectively.

traffic flow as compared to the site where the winds opposed the traffic flow. Therefore, the various parameters for the two situations are given separately in Table 6 for the 1.5 m level of the nearest sites. For runs 14 to 17 these sites are 6 and 12 for winds along and opposite to the traffic flow, respectively, while for runs 18 to 20 these sites are reversed.

Clearly, at the sites with the winds along the traffic flow, there is a noticeable acceleration of the wind due to the drag of the cars on the flow field. There is no increase of the vertical or lateral components of turbulence except under low wind speeds. On the other hand, at the sites where the wind opposes the traffic flow there is considerable deceleration of the flow as well as a large increase of σ_w and σ_v. Here, the σ_w (T) values are directly related to the corresponding ambient mean wind speeds. This is also true of the traffic-generated turbulence, σ_w (TR), as determined by equation (3). These characteristics can be attributed to the interaction of the ambient flow field with the opposing traffic, resulting in a larger wake turbulence under high ambient wind speeds. These effects are noticeable in this experiment because of the controlled traffic flow structure.

The horizontal advection of the traffic-generated turbulence away from the roadway is controlled by the resultant wind speed perpendicular to the roadway, which is considerably influenced by the vehicle drag. Not surprisingly, the effects of traffic are limited to a considerably shorter distance away from the roadway under parallel wind cases as compared to the perpendicular cases. However, at the nearest site to the roadway the maximum value of σ_w (TR) is higher for the parallel winds. Traffic effects are also noticeable at the 4.5 m level, (but not at the 10 m level) as can be seen from σ_w (TR) values of Table 6 for the sites with the winds against the traffic flow.

For wind directions parallel to the roadway, the lateral component of turbulence is an important parameter in the dispersion models. Calculated σ_v (TR) values for the sites with the wind against the traffic flow are presented in Table 6. These show no systematic dependence on wind speed or stability. A possible explanation for this follows.

Spectral Characteristics

In order to determine the size of the eddies generated by the traffic and to support the results of the previous section, spectral analysis of the u, v and w components of the wind fluctuation was performed by the fast Fourier transform technique as described by Rao and Ketchum (1975). Although we were able to identify the wake turbulence effects by this technique in our previous study (Rao et al, 1979), we could not determine its relative magnitude due to limitations in that data set.

Figures 13 and 14 present the normalized spectra of the w component at various sites at the 1.5 m height for perpendicular runs 5 and 13, respectively. Here ϕ is the spectral energy in the frequency internal n to n+dn, and f is the normalized frequency defined as $f = nz/U$. It is evident that, for f greater than about 0.1, the energy at the higher frequencies (smaller scale eddies) is increased considerably at the nearest downwind site 12 as compared to the upwind site 3. This increase in spectral energy for f greater than 0.1 is due to the presence of traffic-generated eddies. This was confirmed by identical spectra obtained at the two sites during runs with no traffic on the roadway. The figures also show an assimilation of the curve towards the upwind spectra as downwind distance increases. In general, this is seen to occur faster for the higher wind speed cases consistent with the results of the previous section. Also, the largest decrease of traffic influence occurs within the first 15 m from the road. Similar results are noted in the u and v spectra in the perpendicular wind cases, and in the u, v and w spectra of the parallel wind cases, although for the latter the traffic effects are only seen at the nearest sites on both sides of the roadway. An additional feature in the u and v spectra, as previously noted, is a distinct peak at frequencies corresponding to a period of 29 sec, which is the time interval of the passage of the packs of cars past the tower line (See Figure 15). This forcing is not present in the w component; it is imposed primarily on the horizontal flow field. A comparison of the v spectra for the parallel wind cases revealed that the magnitude of the peak of the 29 sec oscillation varied considerably from run to run. Interestingly, the v spectra for run 18 did not have a significant peak while run 20 did have a large peak. This might partially explain the lack of systematic variation in the σ_v (T) values of

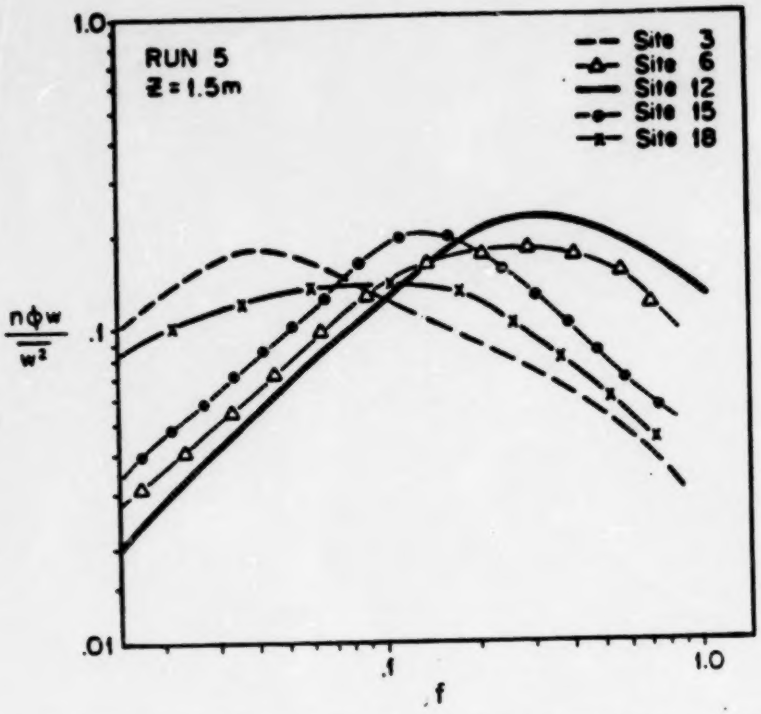

Figure 13: The normalized spectra of the w component at various sites at the 1.5 m level of Run 5.

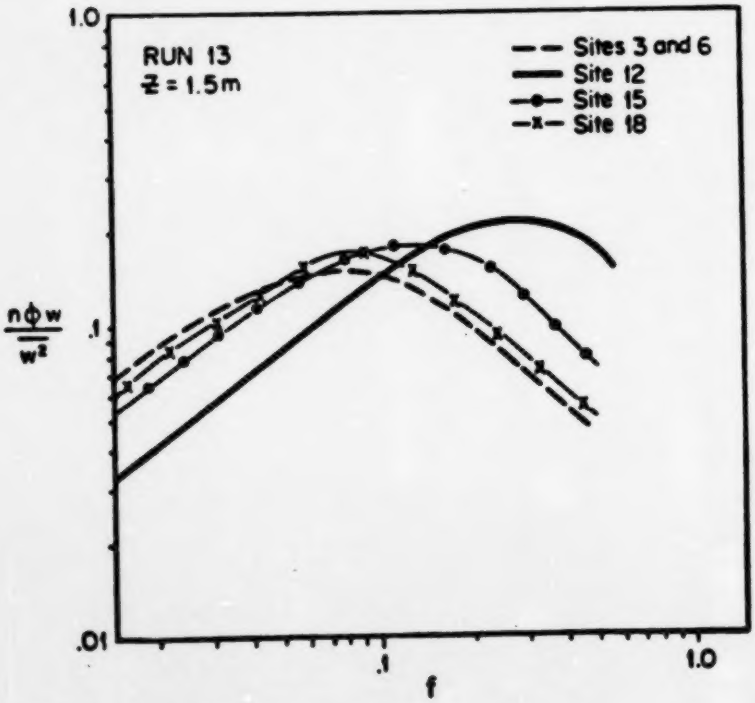

Figure 14: Same as Figure 13 except for Run 13.

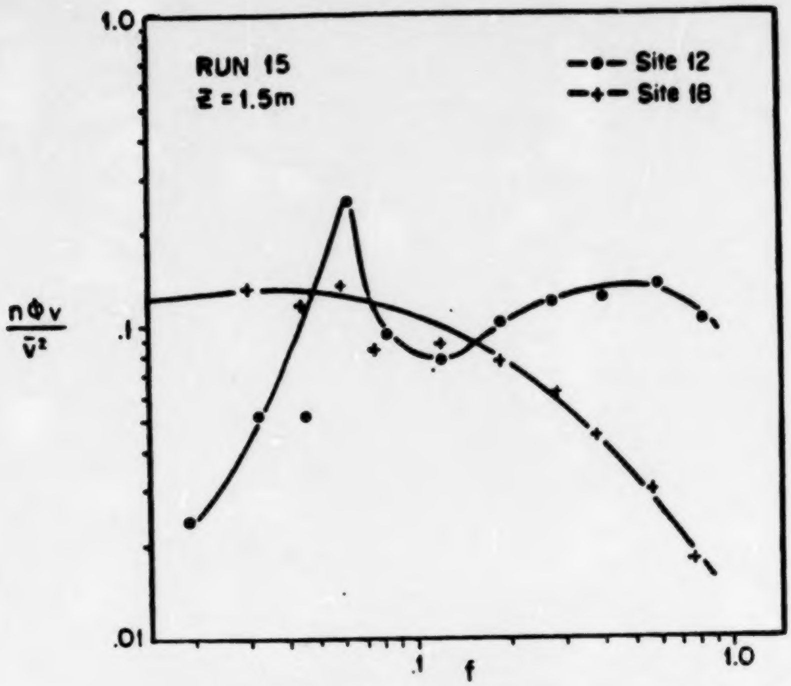

Figure 15: Normalized spectra of the v component near (site 12) and away (site 18) from the highway for Run 15.

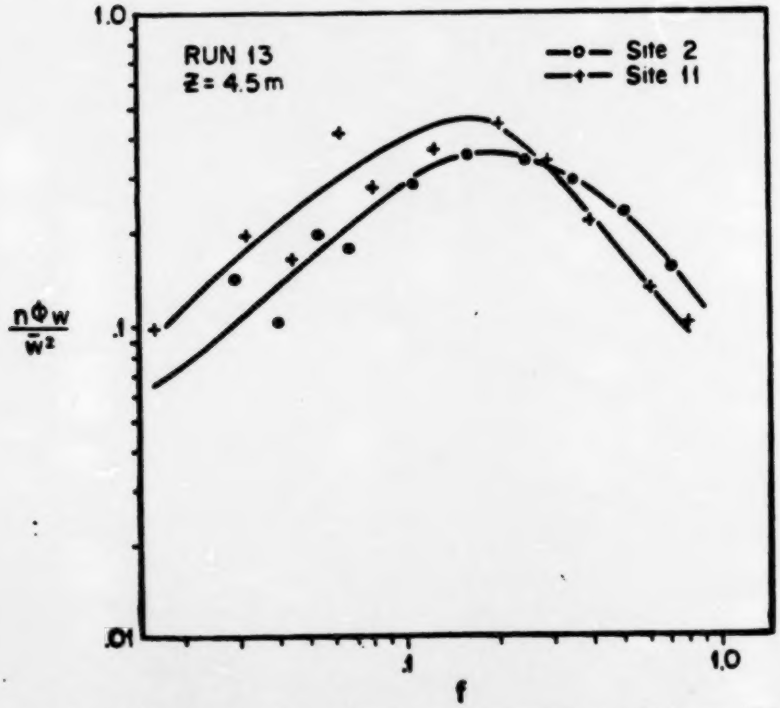

Figure 16: Normalized spectra of the w component at the upwind and downwind 4.5 m level sites for Run 13.

Table 6, and, thus, implies that σ_v (TR) values calculated from equation (3) do not truly represent wake turbulence in that the effects of the 29 sec oscillation have been included.

An approximation to the energy of the wake turbulence can be obtained from the spectral estimates as

$$\sigma^2 (TR) = \int_{n_1}^{\infty} (\phi_T - \phi_N)\, dn \tag{4}$$

where n_1 is the frequency above which the spectral energy at the downwind site exceeds that of the upwind site and ϕ_T and ϕ_N are the energies per frequency interval at the downwind and upwind sites, respectively. The upper limit of integration is actually dictated by the cut-off frequency imposed by the response of the instruments and the sampling rate of 1 reading/sec. The traffic-generated eddies have frequencies mainly below the cut-off frequency (see Figures 13 and 14), and this minimizes the underestimation of σ_w (TR) values from equation (4). This is particularly true at the nearest site where σ_w (TR) thus estimated are close to the values given in Tables 5 and 6. However, in some cases σ_w (TR) and σ_v (TR) are considerably underestimated at the site nearest to the roadway as well as at further downwind sites. This can be attributed to the errors in the estimation of ϕ_T and ϕ_N, and errors introduced by the cut off of high frequency eddies. Energy transfer due to nonlinear interactions might also play an increasingly important role away from the roadway and further limit the applicability of equation (3). Thus, σ_v (TR) calculations by equation (4) might not be superior to the values given in Table 6.

From detailed inspections of the spectra and spectral differences for the various runs, the following results become apparent:

(i) The traffic effects are less dominant at the 4.5 m level compared to the 1.5 m level sites of the nearest tower. This can be seen from a comparison of Figures 16 and 14 which show upwind and downwind spectra for two different levels for run 13. In addition, the upwind and downwind spectra did not show any noticeable differences at the 10 m level sites.

(ii) For perpendicular cases, the spectral differences appear to be large for the low wind speed cases at both the 1.5 and 4.5 m heights of the nearest tower.

(iii) For parallel cases, where the wind direction is against the traffic flow, the traffic effects are larger than for perpendicular cases except for runs with ambient wind speeds less than 1 m/sec.

In order to be able to incorporate the wake contributions to the total diffusivities or dispersion coefficients used in diffusion models, an estimate of char acteristic length scale of the traffic eddies is made from the spectra. The time scale associated with dominant traffic eddies is given by $t_w=1/2\pi n_w$ where n_w is the frequency at which the maximum spectral energy occurs in the high frequency region of the spectra at the 1.5 m level site of the nearest downwind tower. These time scales, in turn, can be used to calculate the dominant eddy size from the relation

$$l_{w,v} = t_{w,v}\sigma_{w,v}(TR) \qquad (5)$$

where $t_{w,v}$ is the vertical or lateral eddy time scale and $\sigma_{w,v}(TR)$ is taken to represent the corresponding eddy velocity. Table 7 gives the calculated values of t_w and l_w for the perpendicular wind cases, while Table 8 gives both the time, and vertical and lateral length scales of the dominant eddies for the parallel cases. It is seen that the average length scales of these eddies range from 0.5 to 3.0 m for the perpendicular wind cases with the higher values occurring under low wind speeds. For the parallel cases, the average length scales are 2.5 to 5.0 m. It is to be noted that for the calculation of the lateral length scale, $\sigma_v(TR)$ values of Table 6 were used and this explains the unrealistically high value of l_v for run 20.

The estimates of l_w and l_v give approximate values of the average size of the eddies generated by the traffic. Estimates of the dominant eddy sizes at

Table 7

Run No.	Site 12 t_w (sec)	Site 12 l_w (m)	Site 3 K_N	Site 12 K_{TR} (m^2/s)	Site 12 K_T	Site 12 K_T/K_N	Site 12 K_{TR}/K_T	Site 15 K_{TR} (m^2/s)	Site 15 K_T	Site 15 K_T/K_N	Site 15 K_{TR}/K_T	$\sigma_z(T)$ at sites 12	$\sigma_z(T)$ at sites 15	$\sigma_z(TR)$ at sites 12	$\sigma_z(TR)$ at sites 15
1	5	1.3	.15	.33	.48	3.2	.69	.01	.16	1.1	.01	2.5	3.9	2.5	3.5
2	5	1.3	.13	.33	.46	3.5	.72	.01	.14	1.1	.01	2.1	3.8	2.0	3.3
3	3	.6	.14	.13	.27	1.9	.48	0	.14	1.0	0	2.6	4.2	2.6	3.7
4	3	.6	.15	.13	.28	1.9	.46	.01	.16	1.1	.01	2.2	3.4	2.2	2.9
5	8	2.7	.04	.98	1.02	25.5	.96	.16	.20	5.0	.80	2.9	6.2	2.9	6.1
6	6	2.2	.04	.79	.83	20.8	.95	.14	.18	3.5	.78	2.4	5.3	2.4	5.1
7	5	1.7	.08	.56	.64	8.0	.88	.06	.14	1.8	.43	3.7	5.4	3.7	5.1
8	5	1.6	.10	.50	.60	6.0	.83	.04	.14	1.4	.29	3.5	5.3	3.5	5.0
9	5	1.7	.06	.56	.62	10.3	.90	.08	.14	2.3	.57	4.0	6.4	4.0	6.3
10	5	1.7	.05	.56	.61	12.2	.92	.07	.12	2.4	.58	3.1	6.1	3.1	5.9
11	5	1.7	.06	.58	.64	10.7	.91	.08	.14	2.3	.57	4.9	6.9	4.9	6.8
12	3	.8	.10	.23	.33	3.3	.90	.01	.11	1.1	.09	3.9	4.8	3.9	4.5
13	3	.8	.11	.22	.33	3.0	.67	.01	.12	1.1	.08	3.6	5.7	3.6	5.5

Table 7: Time and length scales of the dominant eddies; the ambient, traffic-generated and total vertical diffusivities (K) and their ratios; and the dispersion parameters (σ) in the perpendicular wind cases.

Table 8

Run No.	t_w (sec)	l_w (m)	t_v (sec)	l_v (m)	K_N	K_{TR}	K_T	K_T/K_N	K_{TR}/K_T
						(m^2/s)			
14	7	2.7	7	3.7	.13	1.2	1.3	10.0	.92
15	5	2.1	7	4.0	.16	1.0	1.2	7.5	.83
16	7	2.8	10	5.7	.15	1.3	1.5	10.0	.87
17	7	2.7	7	5.3	.12	1.2	1.3	10.8	.92
18	6	1.8	10	4.5	.06	0.6	0.66	11.0	.91
19	7	2.5	10	5.3	.11	1.0	1.1	10.0	.91
20	5	1.8	10	11.0	.09	0.7	0.8	8.9	.88

Table 8: Time and space scales of the dominant eddies; the ambient, traffic-generated and total vertical diffusivities and their ratios at the nearest tower site with the wind against the traffic flow in the parallel wind cases.

the other downwind sites cannot be readily obtained from the spectral maxima since the locations of the maxima revert to larger eddies (see Figure 13). However, a method of approximating the effects of the eddy sizes at downwind distances farther than site 12 is discussed next in the context of estimating the traffic eddy diffusivities.

Traffic Effects on the Dispersion Processes

For ground-level release and short downwind distances the gradient transfer or K-theory is the basis for most numerical models used for highway situations. Numerical models such as Danard (1972) use a large K_z value to simulate the enhanced diffusion due to the traffic. A more representative value for vertical diffusivity due to traffic-induced turbulence can be determined from

$$K_{TR} = \sigma_w(TR) l_w \qquad (6)$$

which is along the lines of the mixing-length concept and assumes that the transfer of pollutants is controlled by the scales and velocities of the traffic-generated eddies. The formulation in equation (6) was chosen over that represented by the ratio of vertical turbulent energy flux to its gradient because of the large values of flux divergence of the vertical energy, and due to the reversal of the sign of energy gradient under low wind speeds, which would then imply a negative K_{TR}.

To determine the contribution of K_{TR} to the total vertical diffusivity (K_T), the background diffusivity was calculated from

$$K_N = ku_* z = k^2 uz/\ln(z/z_o) \qquad (7)$$

where it is assumed that diabatic effects on K_N are small at the 1.5 m height as was the case for $\sigma_w(N)$ values in Tables 5 and 6.

The friction velocity, u_*, was replaced by the wind speed due to possible underestimation of the former parameter. The surface roughness length, z_o, was taken as 3 cm (Chock, 1977).

Tables 7 and 8 give the K_{TR} and K_N values at the 1.5 m level sites, for the perpendicular and parallel cases, respectively. For the parallel cases, K_{TR} represents the traffic diffusivities at the 1.5 m sites nearest the highway with the wind against the traffic flow. The estimates of K_{TR} are very close to the values obtained by Eskridge et al (1979) from their numerical model but are an order of magnitude less than the value of 20 m^2/sec suggested by Danard (1972). Tables 7 and 8 also show that the total diffusivity, as given by

$$K_T = K_{TR} + K_N \tag{8}$$

is about ten times as large as the background diffusivity (K_T/K_N ratios) and is almost totally due to the traffic effects (see K_{TR}/K_T values at the 1.5 m sites) for the parallel cases. For the perpendicular cases, the K_T/K_N ratio ranges from 2 to 25 as the wind speed decreases from 2.44 to .65 m/sec for runs 4 and 5, respectively. In addition, the corresponding traffic contribution to the total diffusivity (K_{TR}/K_T) increases from 46 to 96 percent at this nearest site.

The contribution of the traffic-induced turbulence to the total diffusivity at higher elevations and at further downwind distances should be less than the above values because of the decrease of K_{TR} at these sites as well as the generally larger K_N at higher elevations. For example, for Run 1 the K_{TR} value at the 4.5 m level of the nearest downwind tower is 0.14 m^2/sec while K_N upwind is 0.41 m^2/sec. This leads to a K_{TR}/K_T ratio of 0.25 and a K_T/K_N ratio of only 1.34. These further imply that, for run 1 the traffic effect on the diffusivity has decreased by 60% from 1.5 m to 4.5 m. For parallel wind cases, the traffic effects are confined to the nearest tower sites, and, therefore, can be incorporated by the K_{TR} values given in Table 8. At further downwind distances, the K_{TR} values can be assumed to be zero, and thus, K_T can be represented by K_N.

Since it was not possible to determine the length scales associated with the dominant traffic eddies at downwind distances farther than site 12 for perpendicular wind cases, K_{TR} values at these sites cannot be determined by equation (6). For these cases, one can assume that K_{TR} decreases with distance at the same rate as $\sigma_w(TR)$ by taking l_w (of site 12) independent of the downwind distance. An alternative approach is to compare the frequencies of maximum spectral power at the various sites downwind to the upwind frequency (see Figure 13). By assigning a value of unity to the difference between the peak frequency at the nearest downwind site and at the upwind site, the decrease of this frequency difference with distance from the roadway is taken as a measure of the decrease of K_{TR} with downwind distance. Of course, the accuracy of this approximation is dependent on the resolution of the frequencies of the maximum spectral power in the w spectra which are somewhat flat. Diffusivities determined in this way (see Table 7) indicate that traffic-induced diffusivities are considerably smaller at site 15 than at site 12 and are almost non-existent under high wind speeds. The traffic effects persist further downwind under low wind speed cases as is obvious from the K_{TR}/K_T ratios. These show that while for high wind speeds the total diffusivity is mostly due to the upwind components, the contribution of K_{TR} to K_T is greater than 50% under the lower wind speeds. Calculations of K_{TR} at 30 m downwind (site 18) indicate that the maximum traffic effect, for the lowest wind speed case (run 5), is at most 50% of the total diffusivity. It should be noted that the values of K_{TR} at site 15 compare favorably with those calculated by Eskridge et al (1979).

A different approach was used for the calculation of the traffic effects on the vertical dispersion parameter, σ_z, used in Gaussian models. For these, the contribution of the traffic, $\sigma_z(TR)$, was determined from

$$\sigma_z^2(TR) = \sigma_z^2(T) - \sigma_z^2(N) \tag{9}$$

where $\sigma_z(T)$ and $\sigma_z(N)$ are the total and ambient components, respectively. The latter represents the dispersion that would occur in the absence of the traffic and was calculated from Taylor's equation assuming an exponential form for the autocorrelation function (Draxler, 1976)

$$\sigma_z(N) = \sigma_w T_s[2(t_L/T_s)^2(\exp(-T_s/t_L) + T_s/t_L - 1)]^{1/2} \tag{10}$$

where T_s is the travel time and the Lagrangian integral time scale, t_L, was calculated from

$$t_L = 0.44ut_E/\sigma_w \tag{11}$$

as given by Wandel and Koefoed-Hansen (1962). The Eulerian integral time scale, t_E, was determined from the auto-correlation function of the vertical component of the wind. It should be noted that the assumptions inherent in the derivation of the above formulations are not critical at small downwind distances such as the 3.8 m distance of site 12 from the roadway.

The SF_6 tracer data were used to calculate the $\sigma_z(T)$ values from observed concentration (C) by the approximate formula

$$C = 0.8Q/u\sigma_z(T) \tag{12}$$

where Q is the emission strength. The calculations were made for the perpendicular wind cases only since equation (12) is then applicable.

The calculated $\sigma_z(N)$ values average .5, 1.5 and 3 m at sites 12, 15 and 18 respectively. Table 3 gives the $\sigma_z(T)$ and $\sigma_z(TR)$ for the perpendicular wind cases at sites 12 and 15. The previously observed larger effect of the traffic under lower wind speeds cannot be deduced from the $\sigma_z(TR)$ values. It is also noted that, unlike K_{TR}, $\sigma_z(TR)$ values increase with downwind distance. This is because K is associated with the flow structure while σ_z is related to the vertical dimension of the plume at a given downwind distance and, thus, can only increase with downwind distance. The actual values of $\sigma_z(TR)$ might differ from those given in Table 3 due to errors in the measurements of SF_6, its observed non-Gaussian vertical distribution, and the validity of equation (12) for all downwind distances but these should represent fair estimates. The incorporation of the traffic effects in Gaussian models can be accomplished by a simple enhancement of the dispersion parameters by an amount represented by $\sigma_z(TR)$ of Table 7. As an approximation, the $\sigma_z(TR)$ determined at site 12 can be included as initial traffic dispersion parameters. For the parallel wind cases, one can use the $\sigma_z(TR)$ values of Table 7 as representative of traffic effects while the σ_y (TR) values can be taken to be twice these vertical parameters. The latter follows from the observed average ratio of the traffic eddy length scales in the lateral and vertical directions (l_v, l_w), as given in Table 8.

SECTION 3

VERIFICATION OF EXISTING HIGHWAY MODELS

In this investigation several commonly used highway air pollution dispersion models are evaluated using the tracer data base developed in the General Motors Sulfate Dispersion Experiment. Five Gaussian models; GM (Chock,1977), HIWAY (Zimmerman and Thompson, 1975), CALINE-2 (Ward, Ranzieri and Shirley, 1977), CALINE-3 (Benson, 1979), and AIRPOL-4 (Carpenter and Clemaña, 1975), and three numerical models; DANARD (Danard, 1972), MROAD2 (Kirsch and Mason, 1975), and ROADS (Pitter, 1976) are tested, and various statistical parameters that quantify the ability of a model to predict air pollutant concentrations are developed. The relative performances of the models are compared and the levels of accuracy and precision that can be expected of the above models are determined. These analyses will be of use to the regulatory agencies in selecting and using highway dispersion models with confidence in the results that can be expected of these models.

The atmospheric stability during the GM tracer experiments was determined from the nearest airport data by the EPA staff (W. Petersen, personal communication) according to the method suggested by Turner (1964). In addition, the stability near the site was determined using the boundary layer parameters, roughness lenth (z_o) and Monin-Obukhov length (L) estimated from the similarity theory (R. Eskridge of EPA, personal communication), according to the method outlined by Golder (1972). Both Pasquill and Turner type classifications were determined from the Golder technique. A comparison of the stabilities derived from the airport data and from the Pasquill and Turner classifications based on z_o and L, revealed that there is a great difference among them for a given experimental run. For example, when the stability determined from the airport data suggests a 'C' category, Pasquill type from z_o and L indicates a 'F' category, and the Turner method using the same z_o and L yields a 'G' category (See Table 1). It is extremely important to accurately determine the atmospheric stability since the predictions are very sensitive to the stability condition used in the model.

Since the objective of this study is to compare the performances of several models, the results would be valid provided the same atmospheric stability is used in all the model simulations. In order to provide meaningful results for a given model, it is felt that the stability determined from z_o and L, estimated using the on-site data, is more representative of conditions existing at the site during an experimental run than the stability determined from the airport data. Therefore, Pasquill type classification based on Golder's method for atmospheric stability; and wind speed and direction, measured at the 4.5 m height on the upwind side, either tower 1 or tower 6 depending upon the wind direction, are used in all the models.

DESCRIPTION OF THE MODELS TESTED

A brief description of the Gaussian and numerical models evaluated in this study is included here. For a complete description, the reader is referred to the papers/reports published by the authors of these models.

(i) GM Model

This model was developed by Chock (1977) based on the experimental data obtained in the General Motors dispersion study on a test track. The model avoids the point source assumption but uses an infinite line source approach, and specifies one dispersion parameter as a function of wind-road orientation angle and distance from the source. Further, the model considers plume rise over the roadway under very stable and light wind conditions. Pollutant concentrations are computed from the equation

$$C = \frac{q}{2\pi U\sigma_z} \{\exp[-\tfrac{1}{2}((z + H_o)/\sigma_z)^2] + \exp[-\tfrac{1}{2}((z-H_o)/\sigma_z)^2]\} \quad (13)$$

where q is the emission rate per unit length, U, is the sum of the effective crossroad wind speed and the wind speed correction factor, H_o is the plume height. The effect of lateral and vertical dispersion on the distribution of concentration is incorporated by specifying σ_z as

$$\sigma_z = (A+BFX)^C \qquad (14)$$

Here, X is the distance from the lane center to the receptor, and $F = 1 + \beta\ |(\theta-90)/90|^\gamma$ where θ is the wind angle relative to the road. A, B, C, β and γ are the empirical parameters determined according to the stability conditions from the data base. The plume height H_o is determined from the relation

$$H_o = [(RG(\rho_o-\rho))/\alpha\rho_o u^2]^{\frac{1}{2}} x \qquad (15)$$

where R is the width of the plume, G is the gravitational acceleration, ρ_o and ρ are the densities of the ambient air and the plume respectively, α is the entrainment coefficient, u is the crossline wind speed, and x is the distance from the road.

(ii) HIWAY Model

This is basically a Gaussian dispersion model developed by the U.S. Environmental Protection Agency (Zimmerman and Thompson, 1975). For an "at-grade" roadway configuration, highway emissions are considered to be equivalent to a series of finite line sources. Each lane of traffic is modeled as if it were a straight, continuous, finite line source with a uniform emission rate. A highway is simulated with an increasing number of point sources with the total contribution of all points computed by a trapezoidal integration of the Gaussian point source equation over a finite length until the solution converges. The concentration from a line source is given by

$$C = q/u \int_0^D f\ dl \qquad (16)$$

where q is the emission rate per unit length, u is the wind speed, D is the length of the line source, and f is the point source dispersion function. The dispersion parameters σ_y and σ_z in the Gaussian plume equation are specified at each downwind distance as a function of atmospheric stability. Mechanical mixing over the highway is simulated by specifying a set of initial dispersion values.

(iii) CALINE-2 Model

This model, based on the Gaussian plume theory together with concepts of a box model, is described by Ward et al (1977) It uses a separate equation for computing pollutant concentrations under cross-wind and parallel-wind to the highway configuration. The model assumes that the pollutants are well mixed over the roadway up to a fixed height. This region is referred to as the "mixing cell". The downwind concentrations from the roadway are determined by using both continuous line source and continuous point source equations. The model uses Pasquill dispersion parameter curves which are modified to handle downwind distances of less than 100 m from the source.

(iv) CALINE-3 Model

CALINE-3 (Benson, 1979) is a third generation line source air quality model developed by the California Department of Transportation. As with its predecessors, this model is also based on the Gaussian diffusion equation and employs a mixing zone concept to characterize pollutant dispersion over the roadway. This model employs a new set of dispersion curves which take into account the turbulence enhancement near the roadway. It is not designed to handle low-wind speed situations ((personal communication from E. Shirley.)

(v) AIRPOL-4 Model

Carpenter and Clemaña (1975) developed this model based on the technique of segmentation in conjunction with an appropriate numerical scheme to evaluate the Gaussian integral. The roadway coordinate system is translated onto a receptor coordinate system. The advantage of using two coordinate systems and this transformation is that they permit the Gaussian equation to be directly applied to each roadway point to determine the contribution of that point source to the pollution at the receptor. The model is capable of predicting concentrations both upwind and downwind of a roadway at any desired sampling interval.

(vi) DANARD Model

This is a two-dimensional Eulerian model which solves the mass conservation equation according to the numerical scheme outlined by Dufort and Frankel (1953). The grid is fixed in the horizontal, extending from -150 m to +150 m from the center of the roadway. The vertical grid is confined to 10 cells between the surface (assumed flat) and the mixing height. The pollutants are assumed to be mixed uniformly within the lowest 3 m layer above the roadway, but the user can specify the diffusivity value desired over the roadway (Danard (1972) suggests a value of 20 m^2/sec). The user must also specify the diffusivities (K_x, K_z) at the 10 m height. If the mixing height is greater than 10 m, the model requires additional wind measurements at higher levels.

(vii) MROAD2 Model

This is a two-dimensional grid model (See Kirsch and Mason, 1975) which uses an Eulerian code to numerically solve the mass conservation equation. The size of the grid can be specified by the user and the model allows the existence of several line sources (all assumed to be perpendicular to the plane of the model), including elevated roadways. There is a provision to include topography adjacent to the roadway. Mixing of pollutants is assumed to be uniform to 3.3 m above each road bed. Wind profiles are described as a function of atmospheric stability, but can be specified by the user. The model can accept wind direction and speed for up to eight locations. The final wind field is based on the solution of a potential field and is fitted to the measured wind velocities via a least-squares fit.

(viii) ROADS Model

This is a two-dimensional conservation of mass model and is described by Pitter (1976). The model determines the steady state concentrations of pollutants by numerically solving the equation governing atmospheric advection and diffusion, and chemical reactions. In each time step, the pollutants are first advected and diffused horizontally, then advected and diffused vertically, and finally allowed to react to modify the pollutant mix. A Lax-Wendroff finite-difference scheme is used to solve the advection-diffusion equation numerically.

MODEL PREDICTIONS

All the above models were run with the General Motors tracer data. The results of the CALINE-3 model are discussed in the next section. The model predictions are compared to the measurements, and various statistical tests that quantify the simulation capability of each model are performed. In this regard, the following tests have been applied:

a) Regression analysis providing the explained portion of variance (square of the correlation coefficient, r^2), slope (b), intercept (a), and standard error of estimate ($S_{o/p}$) between observed (dependent variable) and predicted (independent variable).

b) Spatial variation of explained variance.

c) Cumulative frequency distributions of observed and predicted concentrations.

d) Cumulative frequency plots showing the distribution of (O-P)/O, where O is the observed and P is the predicted concentration.

All the data are divided into various subsets and regression analysis is performed on each data subset. The data are classified according to:

a) Wind-road orientation angle (θ) - grouped as perpendicular ($60^\circ \leq \theta \leq 90^\circ$), oblique ($30^\circ \leq \theta < 60^\circ$), parallel ($0^\circ \leq \theta < 30^\circ$).

b) Stability classes-grouped as unstable (A to C), neutral (D), and stable (E and F).

c) Wind speed classes-grouped as $U<1$ m/sec, $1<U<2.5$ m/sec, $U\geq 2.5$ m/sec, and all data with $U>1$ m/sec.

d) Predictions at the nearest roadside receptor (maximum concentrations).

e) Predictions at all downwind ground level receptors and

f) All the data combined.

The results of these types of analysis on the above mathematical models are presented below:

Regression Analysis

The ensemble regression statistics for the four Gaussian and three numerical models segregated according to wind-road orientation angle are presented in Table 9. All these models have correlation coefficients that are statistically significant at the 99% confidence level which reflects the trivial result that all models predict decreasing concentrations away from the highway as the observations indicate. A comparison of explained variance from model to model, however, illustrates the relative ability of each model to reproduce the observed concentration field. One has to exercise caution in comparing the explained portion of variance between data subsets since the sample size varies. For a given data subset, the number of data points are the same, and hence, it is possible to compare the performance of one model with another model. A slope of unity indicates on average that the predicted concentrations are equal to the measured concentrations when the intercept is zero. For the analysis presented here, a slope of less than unity corresponds to overpredictions and a slope of greater than unity corresponds to underpredictions of the observed concentrations. It should be indicated here that it is not advisable to apply these calibration factors (i.e., a and b) to predictions from models such as the models evaluated in this study (See Section on Calibration of Models).

For the perpendicular wind-road orientation, GM followed by AIRPOL-4 and HIWAY models have the highest explained variance. For the oblique and parallel wind cases, again GM and AIRPOL-4 have better correlations than the other models. When all the data are combined, it is evident that the GM model has the best correlation and a slope near unity compared to all the other models. This is not surprising since the GM model's parameters were developed based on this set of data and as such the GM model is expected to perform well. The numerical models in general, performed no better than the Gaussian models.

When the data are segregated according to the wind speed class (see Table 10), all models, except GM, performed very poorly for wind speeds less than 1 m/sec. In the case of CALINE-2, when the input wind speed is less than 1 m/sec, the model automatically assumes a wind speed of 1 m/sec, and hence, no evaluations of this model for this wind speed class are possible. Even though

TABLE 9

Data Subset	Statistical Parameter	GM	HIWAY	AIRPOL-4	CALINE-2	DANARD	MROAD 2	ROADS
Perpendicular $60^\circ \le \theta \le 90^\circ$	r^2	0.92	0.65	0.75	0.40	0.62	0.50	0.48
	b	0.99	0.41	1.50	1.14	0.84	0.26	0.10
	a	0.12	0.37	0.10	0.09	0.18	0.59	0.58
	$S_{o/p}$	0.19	0.39	0.33	0.42	0.40	0.47	0.48
	N	173	173	173	128	173	173	173
Oblique $30^\circ \le \theta < 60^\circ$	r^2	0.77	0.37	0.49	0.16	0.36	0.33	0.24
	b	0.97	0.22	0.96	0.19	0.49	0.13	0.05
	a	0.25	0.65	0.37	0.68	0.47	0.80	0.82
	$S_{o/p}$	0.36	0.60	0.53	0.65	0.60	0.61	0.65
	N	128	128	128	105	128	128	128
Parallel $0 \le \theta < 30^\circ$	r^2	0.83	0.24	0.58	0.26	0.13	0.14	0.17
	b	0.94	0.08	1.58	0.26	0.10	0.07	0.03
	a	0.03	0.80	0.31	0.58	0.71	0.94	0.90
	$S_{o/p}$	0.32	0.67	0.50	0.65	0.72	0.71	0.70
	N	293	293	293	276	293	293	293
All Data Combined	r^2	0.83	0.26	0.49	0.24	0.14	0.20	0.20
	b	0.94	0.11	0.61	0.26	0.12	0.09	0.04
	a	0.12	0.75	0.42	0.58	0.72	0.85	0.83
	$S_{o/p}$	0.30	0.64	0.53	0.62	0.68	0.66	0.66
	N	594	594	594	509	594	594	594

Table 9: Ensemble regression statistics for the models as a function of wind-road orientation. Explained portion of the variance (r^2), slope (b), intercept (a), standard error of estimate ($S_{o/p}$) between observed (o, dependent variable) and predicted (p, independent variable), and sample size (N) for each data subset are included in the table. In the case of the Caline-2 model, wind speeds less than 1 m/sec are excluded since the model cannot handle these situations.

TABLE 10

Data Subset	Statistical Parameter	GM	HIWAY	AIRPOL-4	CALINE-2	DANARD	MROAD 2	ROADS
U < 1 m/sec	r^2	0.82	0.24	0.32		0.10	0.37	0.20
	b	0.78	0.05	0.38		0.08	0.06	0.02
	a	0.26	1.03	0.87		1.03	0.99	1.09
	S_o/p	0.36	0.74	0.70		0.80	0.67	0.75
	N	85	85	85		85	85	85
1 ≤ U < 2.5 m/sec	r^2	0.87	0.65	0.54	0.22	0.19	0.46	0.52
	b	1.10	0.40	0.73	0.22	0.22	0.41	0.13
	a	0.02	0.30	0.34	0.62	0.62	0.62	0.59
	S_o/p	0.26	0.43	0.49	0.64	0.65	0.54	0.50
	N	339	339	339	339	339	339	339
U ≥ 2.5 m/sec	r^2	0.82	0.69	0.67	0.46	0.26	0.72	0.61
	b	0.86	0.41	0.69	0.61	0.55	1.15	0.18
	a	0.12	0.24	0.22	0.29	0.45	0.46	0.41
	S_o/p	0.29	0.37	0.39	0.49	0.58	0.36	0.42
	N	170	170	170	170	170	170	170
All Data with U ≥ 1 m/sec	r^2	0.84	0.66	0.57	0.24	0.19	0.45	0.54
	b	1.00	0.41	0.71	0.26	0.23	0.46	0.14
	a	0.07	0.28	0.30	0.58	0.62	0.62	0.54
	S_o/p	0.28	0.41	0.47	0.62	0.64	0.53	0.48
	N	509	509	509	509	509	509	509

Table 10: Same as Table 9 except the data are segregated according to wind speed class.

the AIRPOL-4 model is designed to handle very low wind speeds through a wind speed correction function, its simulation is rather poor. It should be borne in mind that the assumptions in the Gaussian model are violated in these situations and as such these models cannot be expected to perform well. It is interesting to note that under very low wind speeds, in spite of high correlation, the GM model has a slope of 0.78. In the range 1 to 2.5 m/sec, GM and HIWAY have better correlations than the other models. It should be noted that GM provides a better simulation in this wind speed class. Most GM experiments were conducted under these conditions, and hence, the GM model parameters are tuned to this range. This could be the reason why the GM model performs so well in this range compared to other wind speed classes. When all cases with wind speeds greater than 1 m/sec are combined, next to the GM model, HIWAY has a better correlation compared to the other models. However, the slope of AIRPOL-4 is consistently better than HIWAY.

The predictive capability of the models according to stability class is shown in Table 11. Except for CALINE-2, all the other Gaussian models perform well for unstable and neutral stability conditions. In the stable situations, however, the GM model provides by far a better simulation than any of the models tested here. Large overpredictions with models other than the GM model occurred under the stable conditions. When only ground level (0.5 m height) receptors are considered, again GM and AIRPOL-4 have better correlations than the other models.

The spatial variability of the regression statistics is presented in Table 12. Ideally, the model should have the same correlation coefficient and as such the predictions are independent of the location of the receptor with respect to the source. In general, all the models seem to predict well close to the source and the correlations decrease with increasing distance from the source. Further, the models tend to overestimate pollutant concentrations a great deal more as the distance between source and receptor increases.

The scatter plots showing the observed and predicted concentrations for each model are presented in figures 17 to 23. A one-to-one correspondence line (observed = predicted) is also indicated in the diagram to facilitate comparison of observed versus predicted.

TABLE 11

Data Subset	Statistical Parameter	GM	HIWAY	AIRPOL-4	CALINE-2	DANARD	MROAD 2	ROADS
UNSTABLE (A to C)	r^2	0.91	0.61	0.69	0.28	0.15	0.68	0.50
	b	1.18	0.54	1.51	0.95	0.21	1.64	0.24
	a	0.04	0.22	0.00	2.31	0.53	0.34	0.41
	S_o/p	0.18	0.37	0.33	0.50	0.55	0.34	0.42
	N	276	276	276	265	276	276	276
NEUTRAL (D)	r^2	0.80	0.69	0.61	0.41	0.17	0.67	0.61
	b	1.01	0.45	0.88	0.58	0.26	0.99	0.18
	a	0.05	0.18	0.13	0.24	0.52	0.38	0.48
	S_o/p	0.31	0.39	0.43	0.54	0.63	0.40	0.43
	N	100	100	100	89	100	100	100
STABLE (E to F)	r^2	0.82	0.23	0.46	0.28	0.10	0.25	0.20
	b	0.90	0.08	0.51	0.25	0.08	0.08	0.03
	a	0.07	0.93	0.51	0.49	0.94	0.99	1.01
	S_o/p	0.36	0.75	0.63	0.71	0.81	0.74	0.76
	N	218	218	218	155	218	218	218
DOWNWIND GROUND LEVEL (0.5m) RECEPTORS ONLY.	r^2	0.84	0.21	0.44	0.37	0.05	0.19	0.18
	b	0.99	0.09	0.62	0.36	0.09	0.08	0.03
	a	0.12	1.0	0.55	0.75	1.03	1.11	1.05
	S_o/p	0.35	0.78	0.66	0.67	0.85	0.79	0.79
	N	260	260	260	225	260	260	260

Table 11: Same as Table 9 except the data are segregated according to stability class.

TABLE 12

Data Subset	Statistical Parameter	GM	HIWAY	AIRPOL-4	CALINE-2	DANARD	MROAD 2	ROADS
TOWERS 2 & 4 (2 meters from Highway)	r^2	0.85	0.69	0.54	0.16	0.31	0.20	0.24
	b	0.92	0.38	0.65	0.21	0.23	0.08	0.04
	a	0.22	0.53	0.66	0.93	0.93	1.22	1.21
	$S_{o/p}$	0.39	0.56	0.70	0.92	0.86	0.92	0.90
	N	182	179	182	152	182	182	182
TOWER 5 (15 meters from Highway)	r^2	0.75	0.55	0.48	0.25	0.24	0.28	0.39
	b	0.89	0.30	0.54	0.23	0.13	0.27	0.09
	a	0.18	0.50	0.51	0.65	0.75	0.81	0.76
	$S_{o/p}$	0.27	0.36	0.39	0.46	0.47	0.46	0.43
	N	137	137	137	122	137	137	137
TOWERS 1 & 6 (30 meters from Highway)	r^2	0.56	0.25	0.29	0.21	0.11	0.16	0.10
	b	0.73	0.13	0.30	0.16	0.05	0.06	0.01
	a	0.19	0.54	0.50	0.51	0.64	0.67	0.69
	$S_{o/p}$	0.23	0.30	0.30	0.28	0.33	0.32	0.34
	N	183	180	183	153	183	183	183

Table 12: Same as Table 9 except the data are segregated according to source-receptor location.

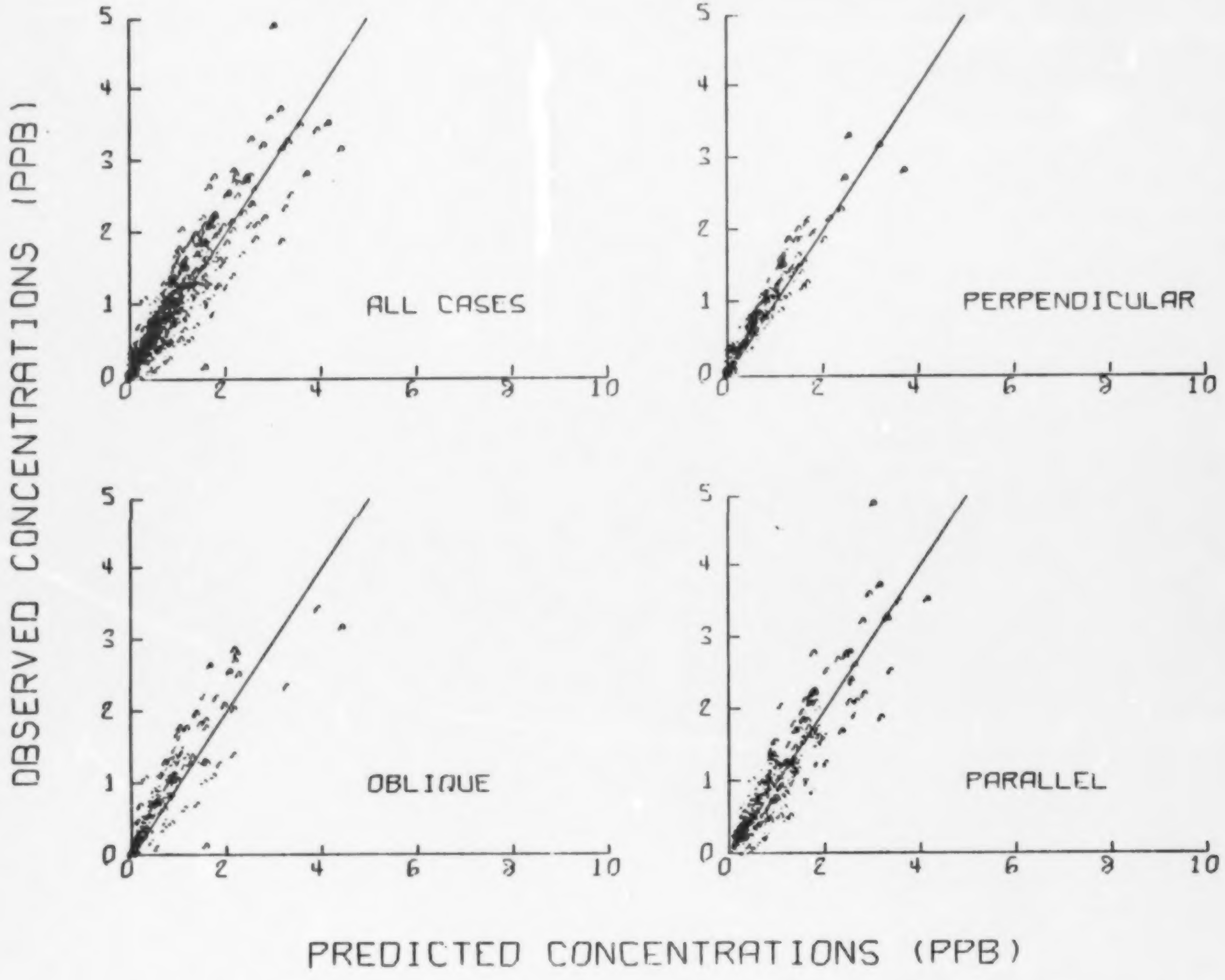

Figure 17: Scatter plot showing the observed versus predicted concentration for the GM model.

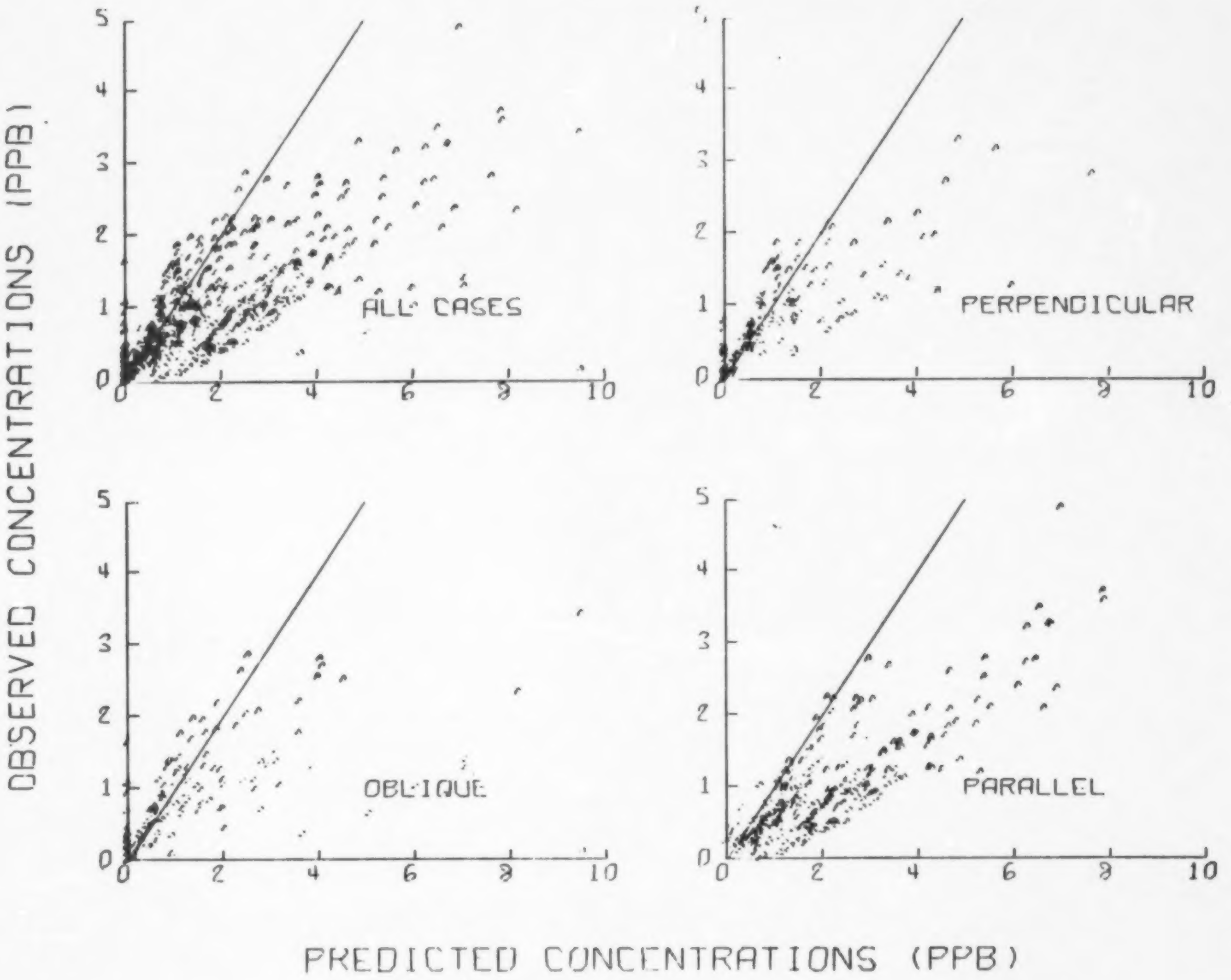

Figure 18: Same as Figure 17 except for the HIWAY model.

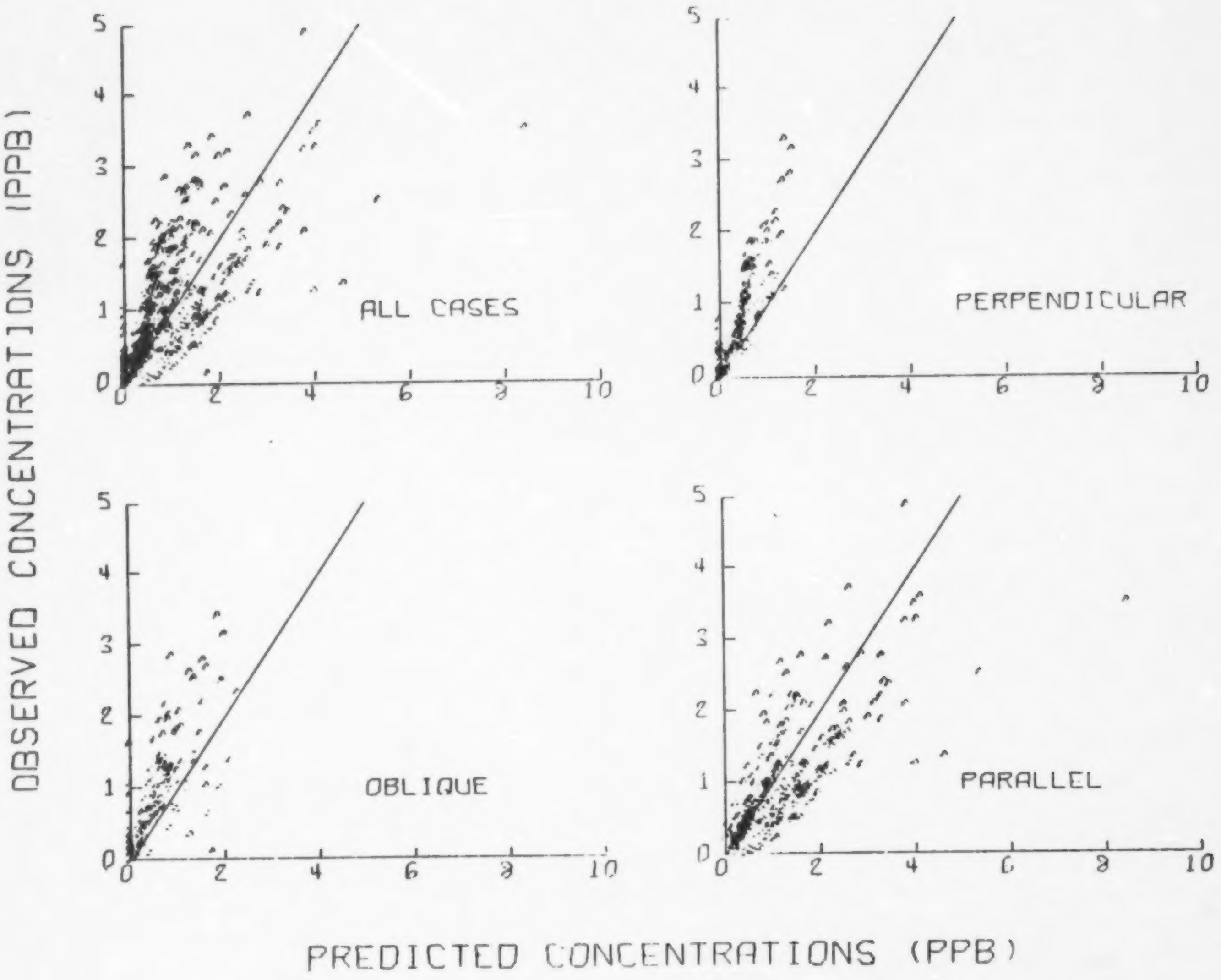

Figure 19: Same as Figure 17 except for the AIRPOL-4 model.

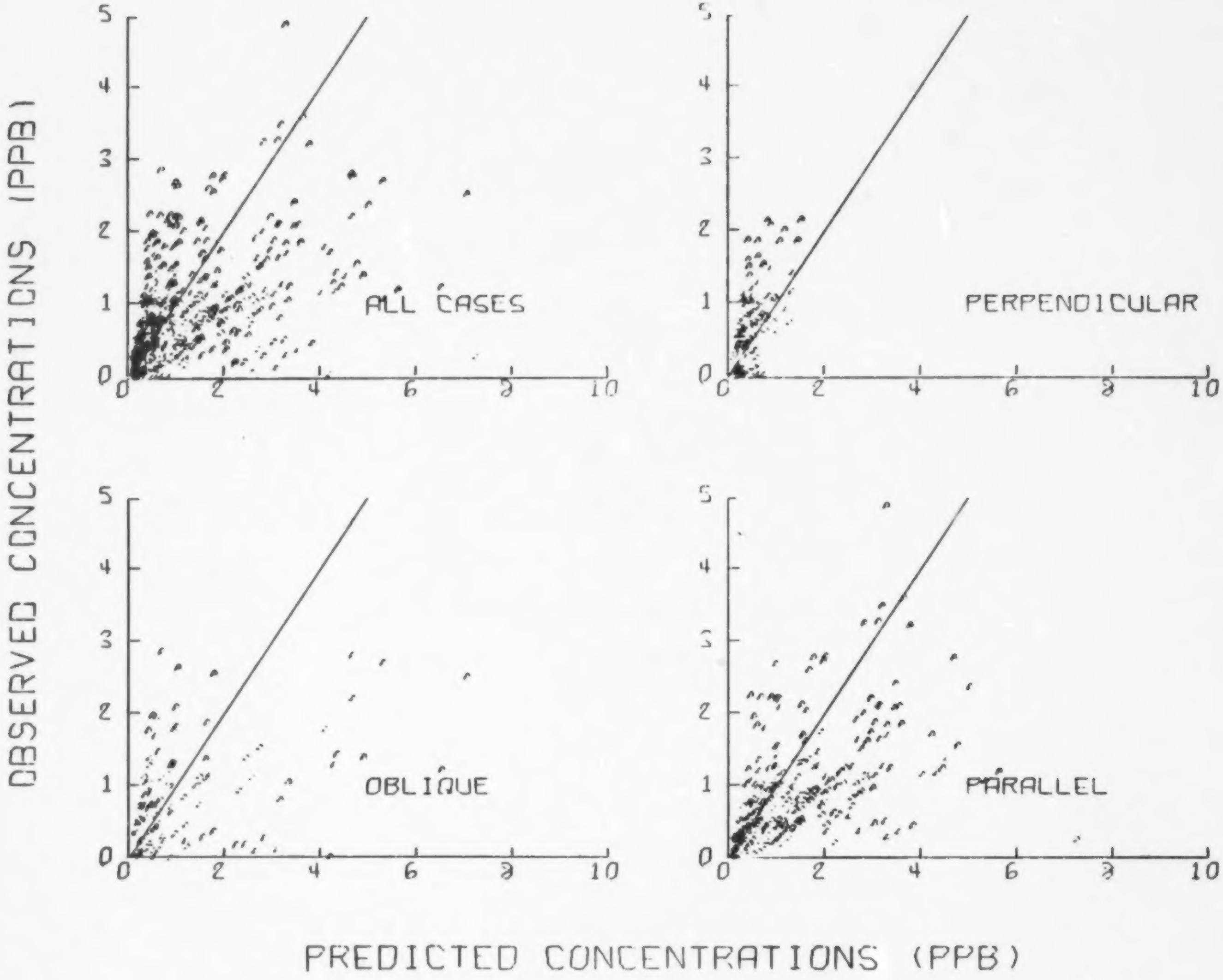

Figure 20: Same as Figure 17 except for the CALINE-2 model.

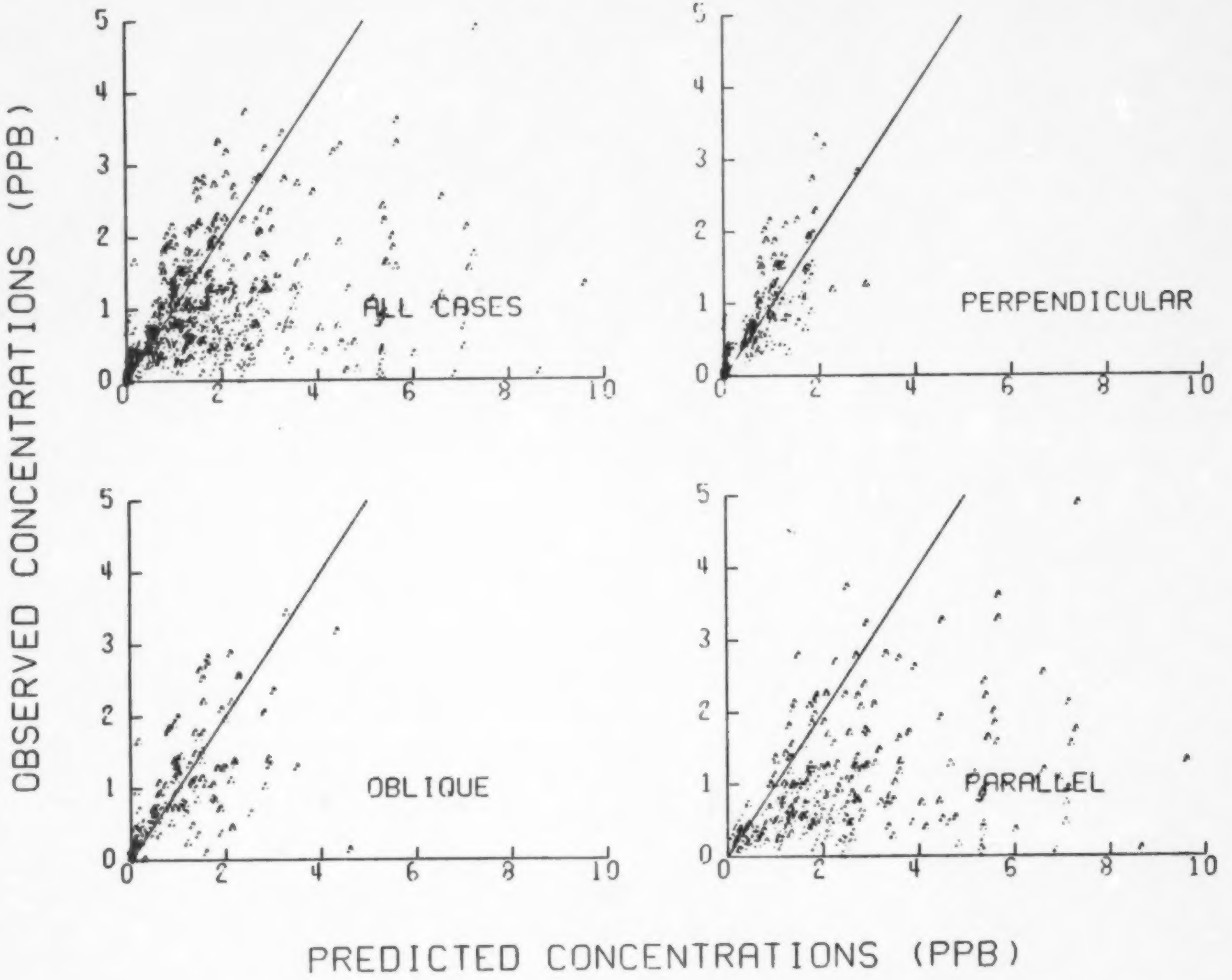

Figure 21: Same as Figure 17 except for the DANARD model.

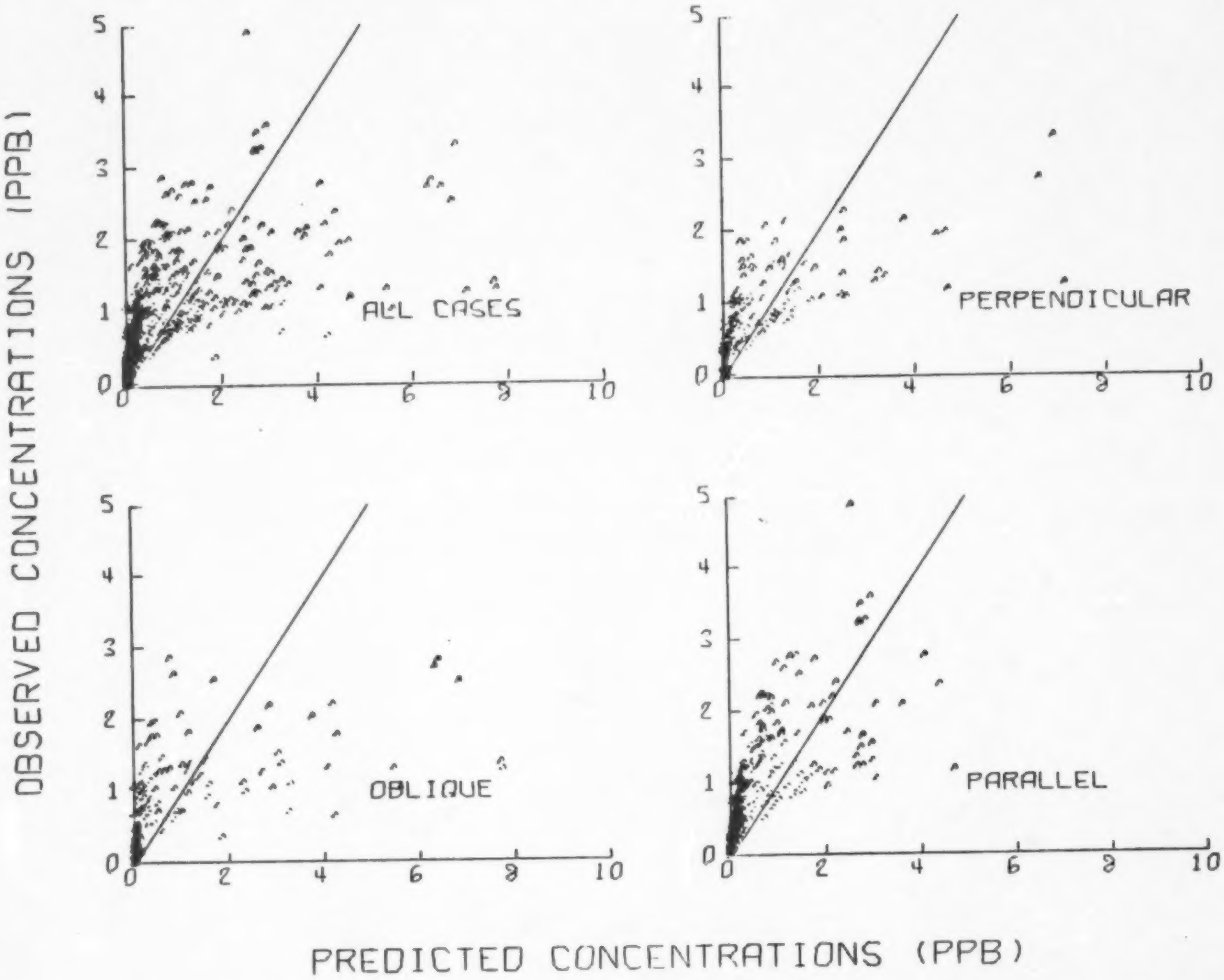

Figure 22: Same as Figure 17 except for the MROAD2 model.

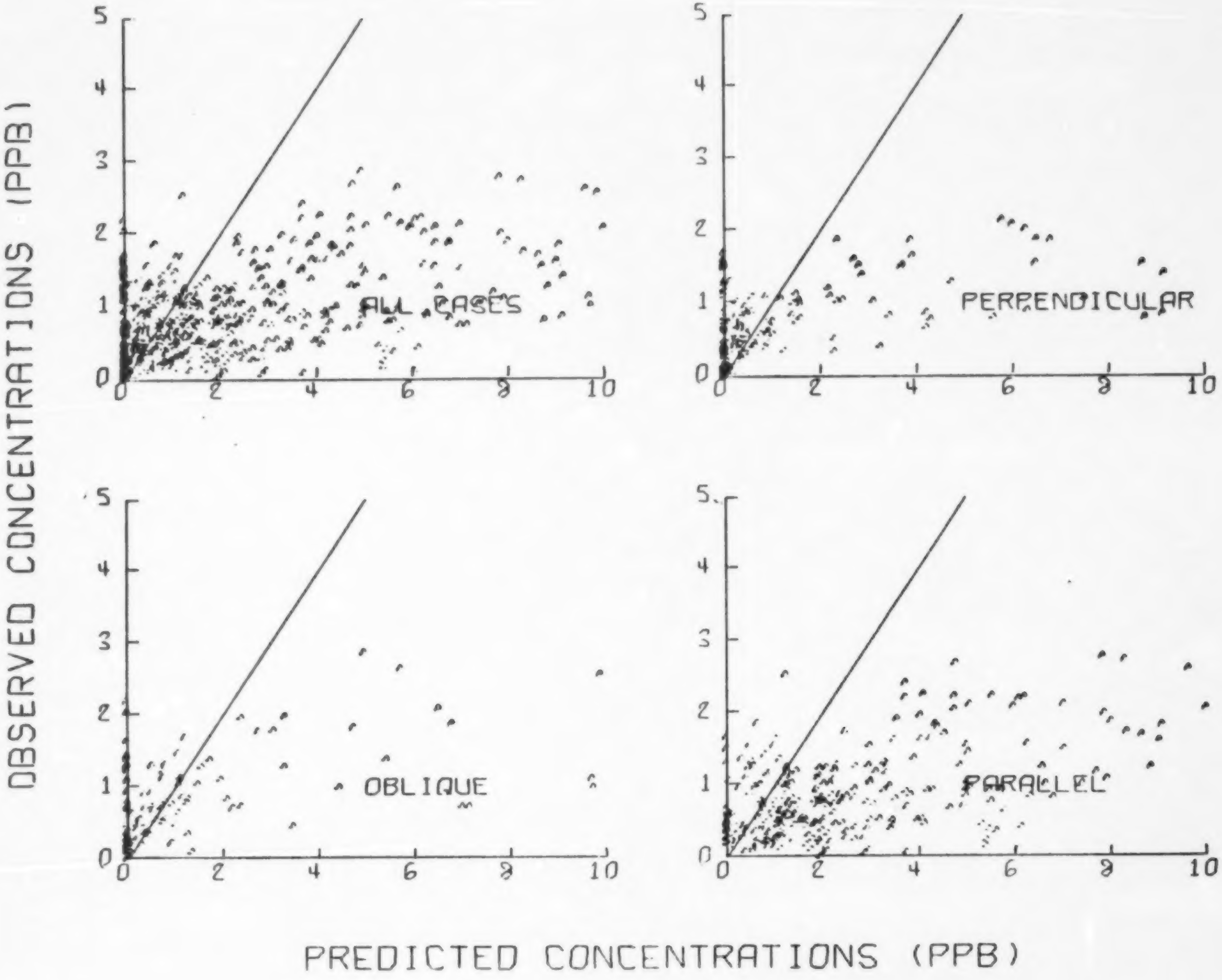

Figure 23: Same as Figure 17 except for the ROADS model.

Cumulative Frequency Distributions

The cumulative frequency distribution for the observed data is compared to those from the Gaussian models in Figure 24. While the distribution of predictions of AIRPOL-4 and GM are very close to the observed frequency distribution, the predictions of the CALINE-2 and HIWAY models deviate significantly from the observed. As indicated before, the HIWAY model consistently overpredicts concentrations. When only the ground level receptor close to the roadway (where maximum concentrations occur) is considered, the cumulative plot, shown in Figure 25, indicates that except for HIWAY, all the other Gaussian models predict the maximum concentration reasonably well in the concentration interval 3.0 to 4.0 ppb. When the observed concentration is below 2.5 ppb (55% of the time), CALINE-2, GM, and AIRPOL-4 underpredict the maximum.

One should bear in mind that, although the observed and predicted cumulative distributions are close to each other, there is no one-to-one correspondence, both temporally and spatially, between a predicted value and its corresponding observed value. However, for comparisons between maxima predicted and maxima observed, the cumulative plots are better than the straightforward regression analysis. This is because most of the points fall in a cluster offset far enough from the origin to make the regression line not accurately reflect the best correspondence between the two variables.

The cumulative frequency distributions for the three numerical models are shown in Figure 26. MROAD2 appears to underpredict concentrations in the range 0 to 1.5 ppb and overpredict in the range of concentrations greater than 1.5 ppb. The ROADS model consistently overpredicts the concentrations compared to the DANARD model. DANARD and MROAD2 models underpredict maximum concentrations (see Figure 27) in the interval 0 to 2.5 ppb and overpredict in the range 2.5 to 5.0 ppb. Again, the ROADS model overpredicts maximum concentrations all the time.

Cumulative Frequency Plots of Percent Error

These plots depict the distribution of (O-P)/O, where O is the observed and P is the predicted concentration. This type of analysis provides a better

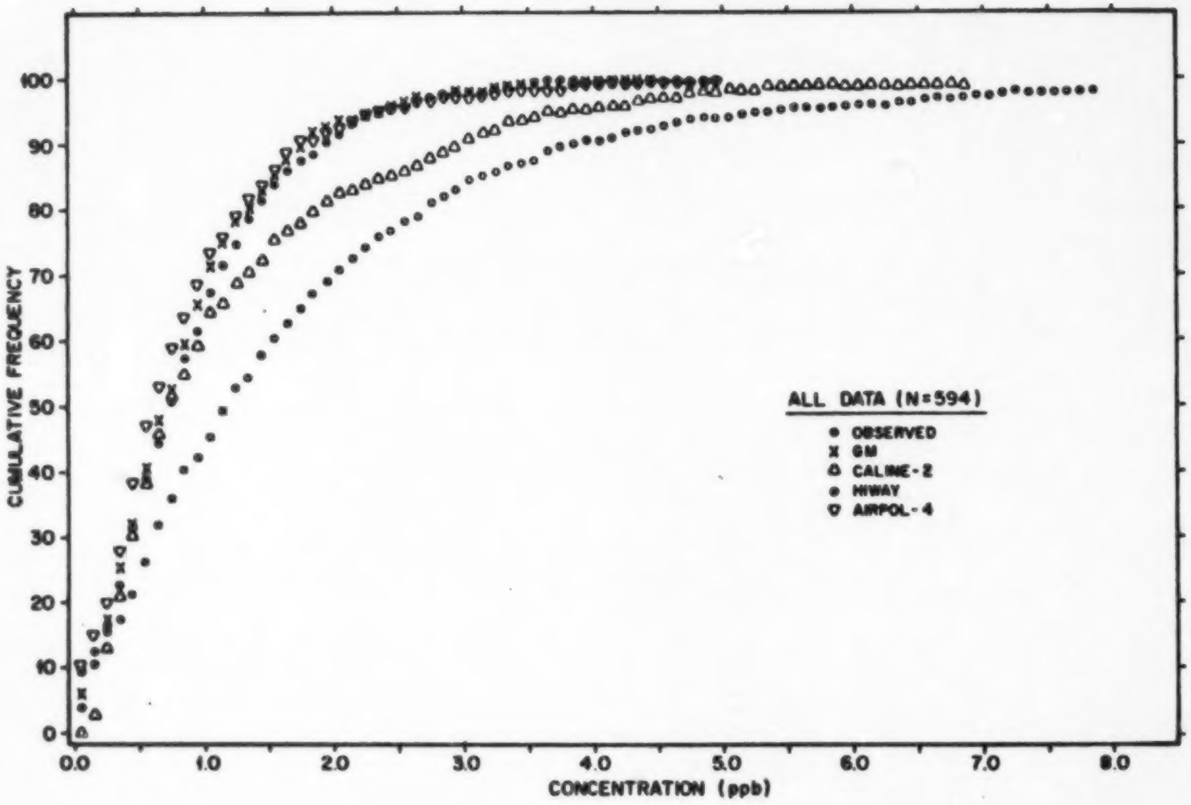

Figure 24: Cumulative frequency distribution of the observed concentrations is compared to the predicted concentrations of the Gaussian models. Curves lower (higher) than the dotted curve indicate overprediction (underprediction).

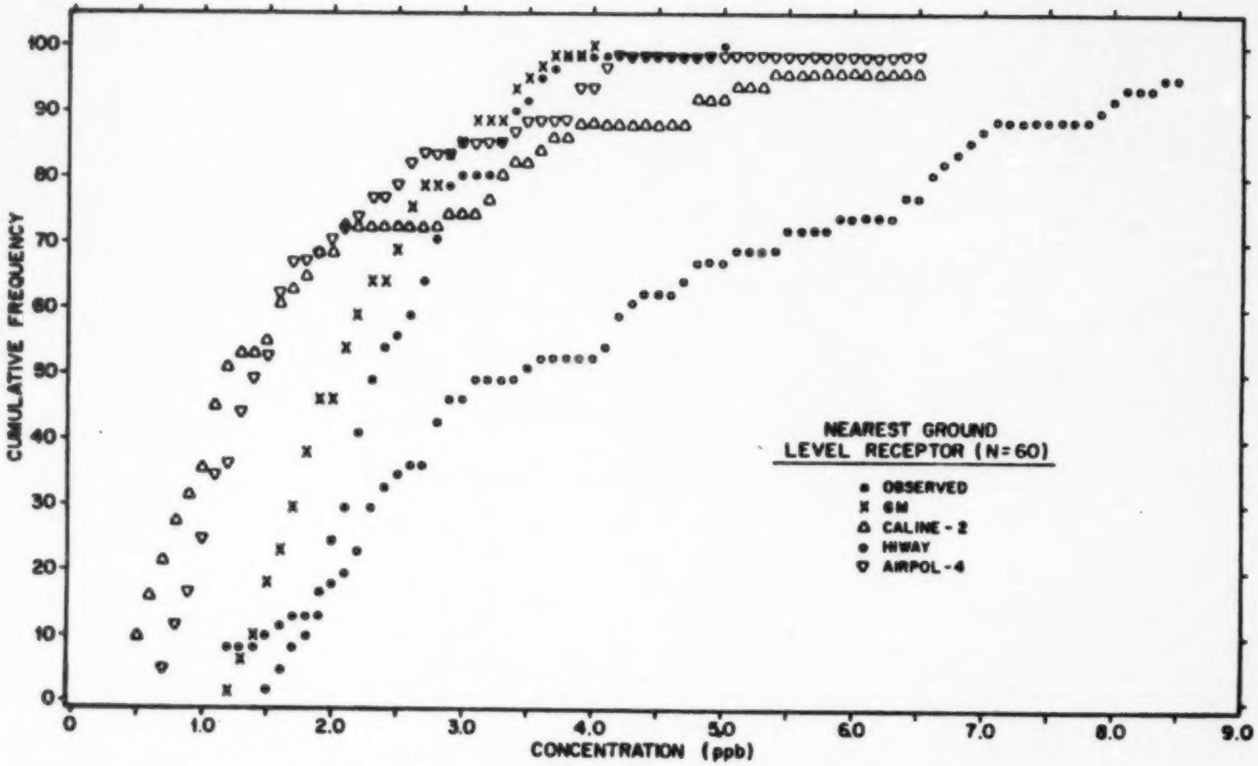

Figure 25: Cumulative frequency distribution of the observed concentrations at the 0.5 m height receptor nearest to the roadway is compared to the distribution of each of the Gaussian model predictions. Curves lower (higher) than the dotted curve indicate overprediction (underprediction).

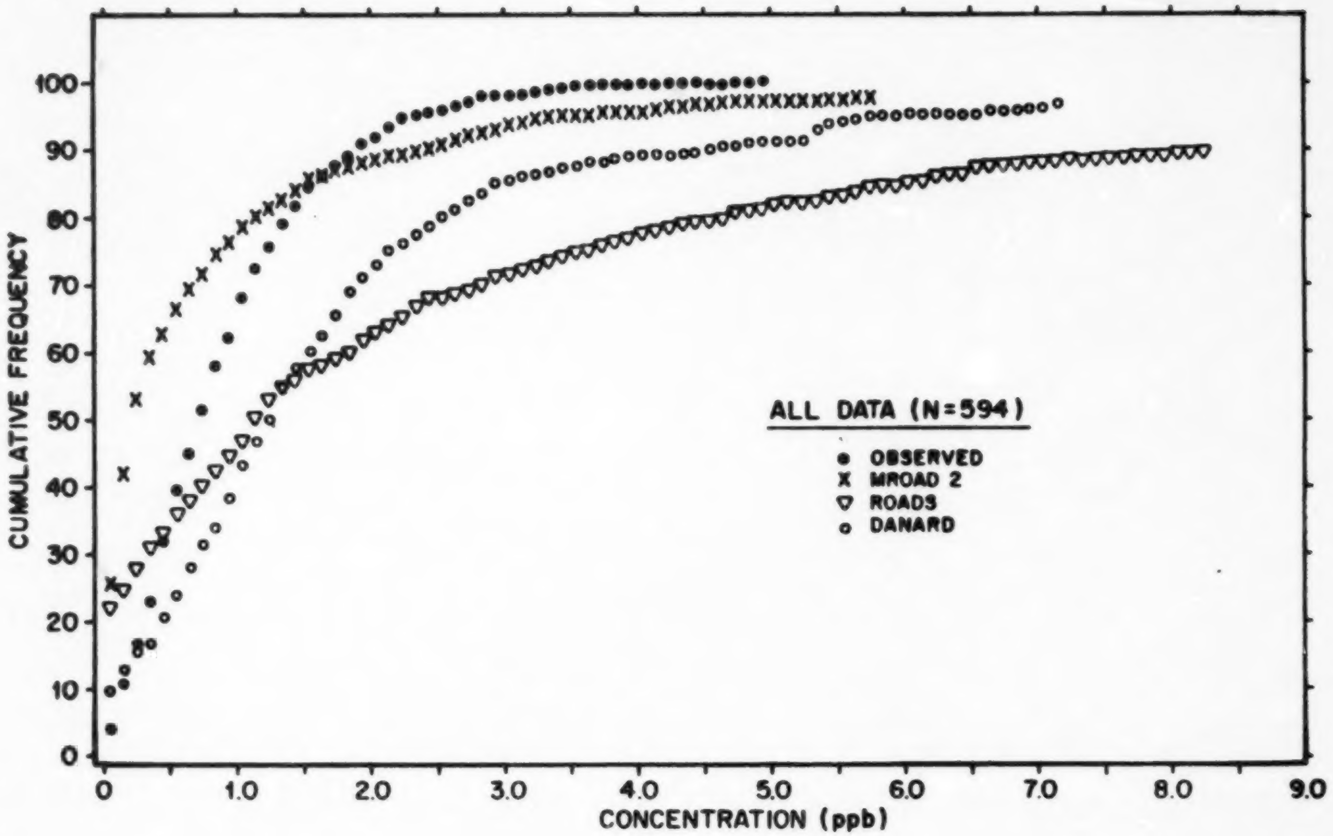

Figure 26: Same as Figure 24 except for the numerical models.

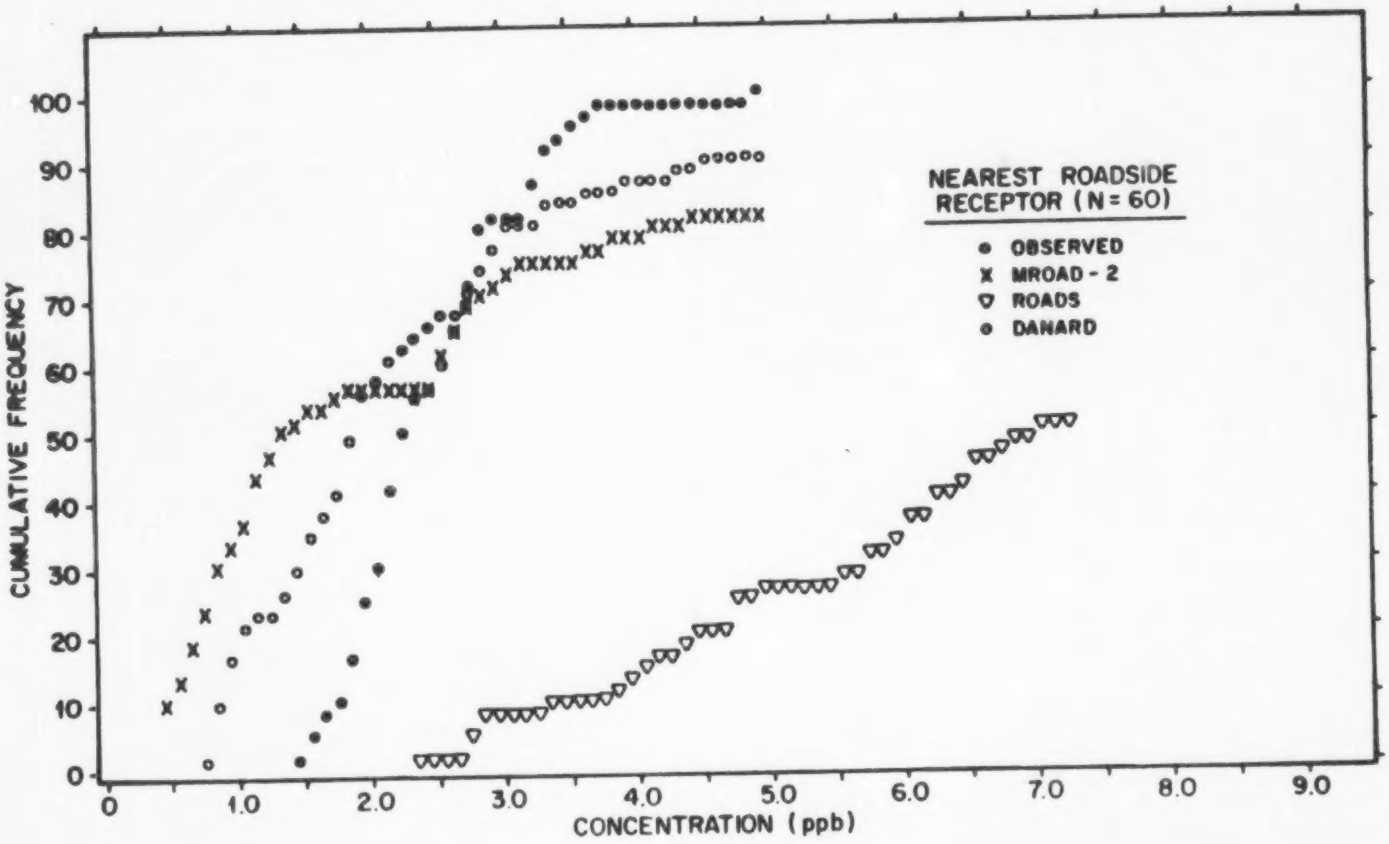

Figure 27: Same as Figure 25 except for the numerical models.

understanding of the model's ability to simulate the physical processes. Accuracy of model prediction can be identified and confidence intervals may be derived from these diagrams. In many applications, a model which has a Gaussian error curve with its peak at zero and a rapid fall off on either side is preferred. If the Gaussian shaped curve is skewed to the negative (positive), it indicates overprediction (underprediction).

The cumulative distribution of (O-P)/O for the HIWAY model is shown in Figure 28. A significant deviation from the Gaussian shape is evident in this diagram. The plot indicates that only 10% of the (O-P)/O distribution is in the interval of ± 0.05. The model overpredicts 70% of the time and underpredicts 25% of the time. The frequency distribution of (O-P)/O for the GM model, shown in Figure 29, indicates that 20% of (O-P)/O are in the interval of ± 0.05. The GM model overpredicts 32% of the time and underpredicts 58% of the time. The distribution, however, has a Gaussian shape and is skewed toward underprediction. The distribution for AIRPOL-4 (see Figure 30) shows that 13% of the time (O-P)/O is in the interval ± 0.05; overprediction is 35% and underprediction is 58% of the time. The frequency distribution of (O-P)/O for CALINE-2, shown in Figure 31, looks quite similar to that of HIWAY. However, it should be noted that CALINE-2 overpredicts to a lesser degree compared to the HIWAY model.

The distributions of (O-P)/O for the numerical models are presented in Figures 32 to 34. The MROAD2 model (see Figure 32) shows underprediction, 77% of the time, while ROADS (see Figure 33) indicates overprediction 62% of the time. The DANARD model (see Figure 34) is again skewed toward overprediction 61% of the time. These diagrams clearly indicate that for this set of data these numerical models perform no better than the Gaussian models.

More quantitative information can be obtained from the above cumulative frequency distributions. The ability of a model to predict pollutant concentrations to within a factor of 2 of the observed are derived and compared with each other in Table 13. It is evident from this table that GM and AIRPOL-4 predict concentrations within a factor of 2 of the observed more than 60% of the time.

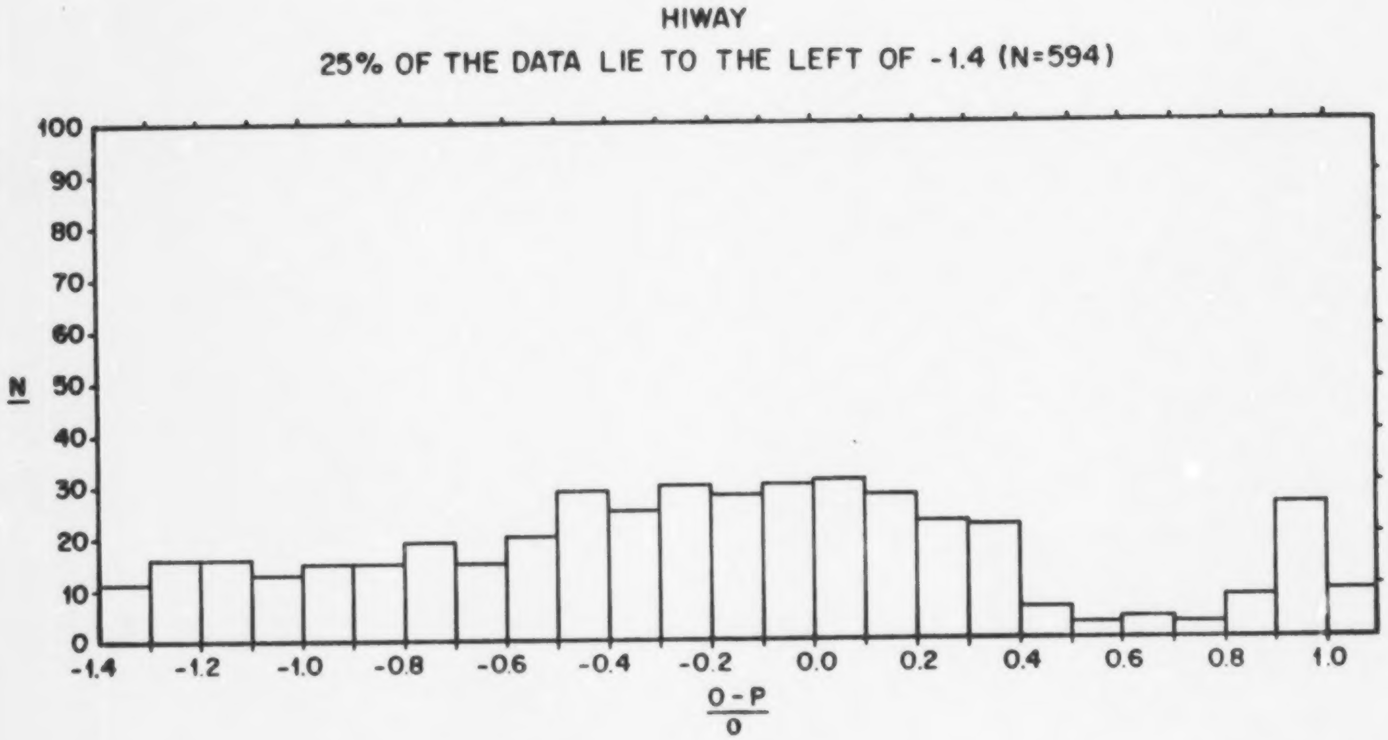

Figure 28: Cumulative frequency distribution of (O-P)/O where O is the observed concentration and P is the predicted concentration for the HIWAY model.

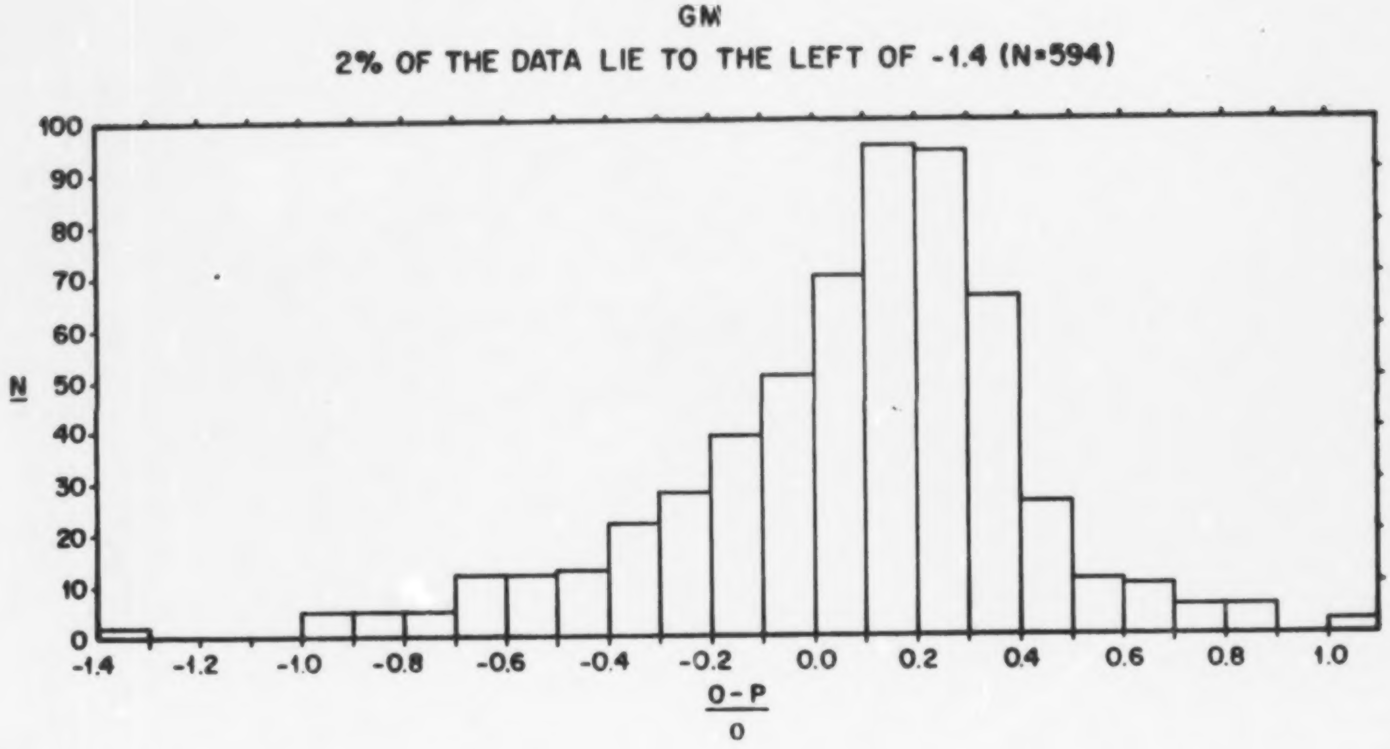

Figure 29: Same as Figure 28 except for the GM model.

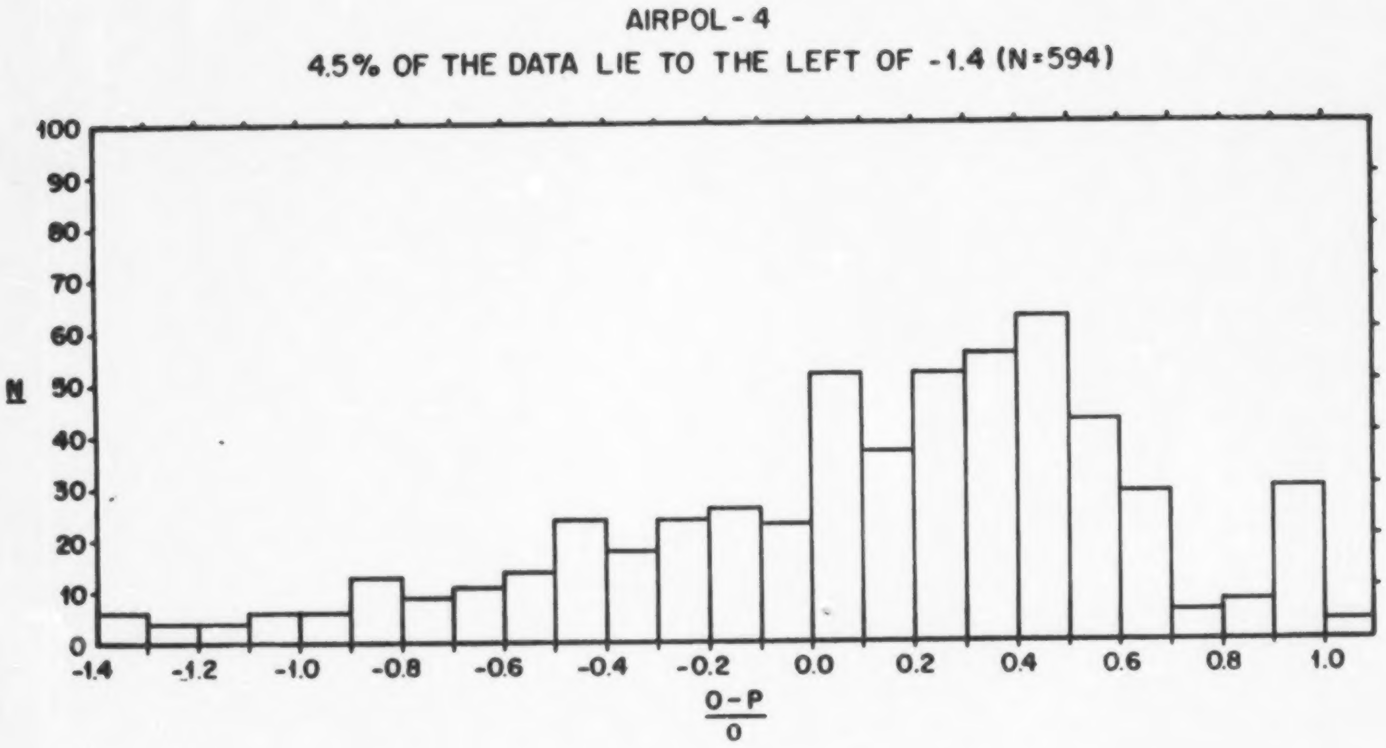

Figure 30: Same as Figure 28 except for the AIRPOL-4 model.

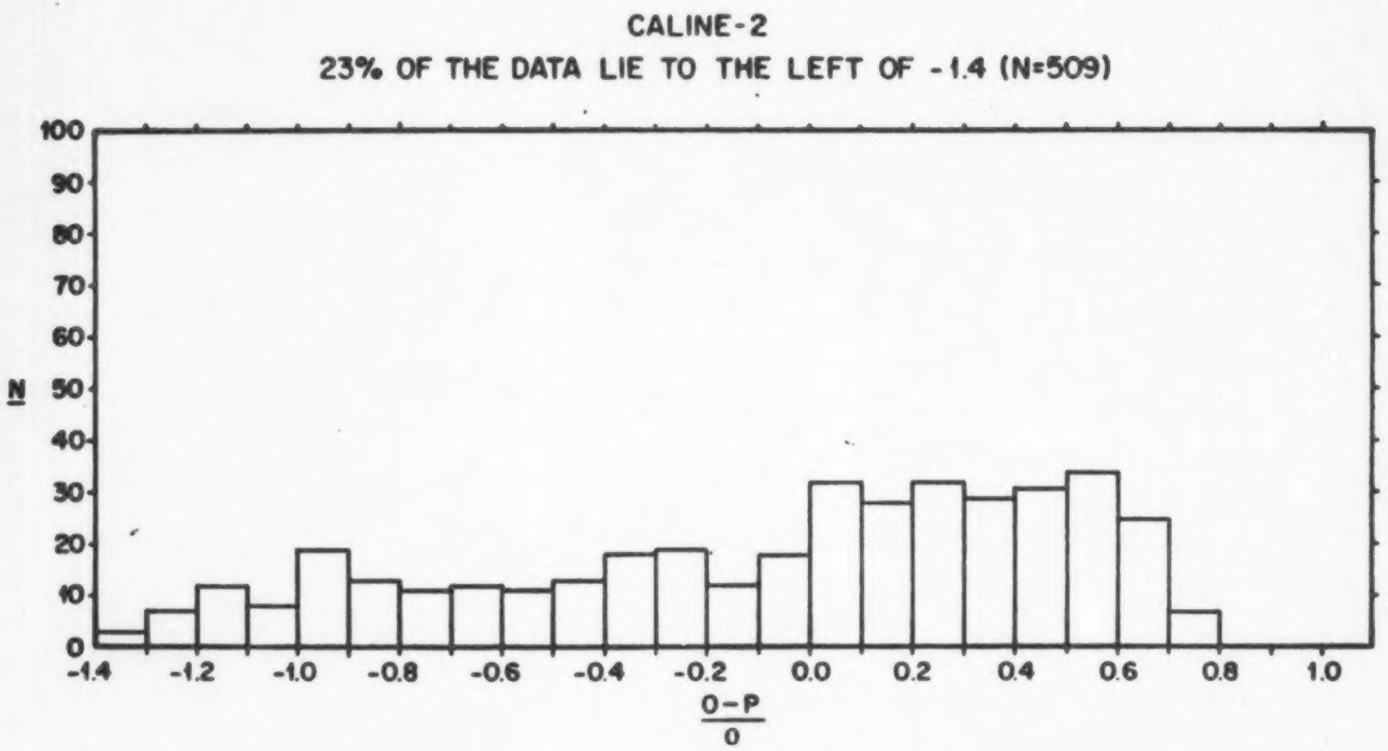

Figure 31: Same as Figure 28 except for the CALINE-2 model.

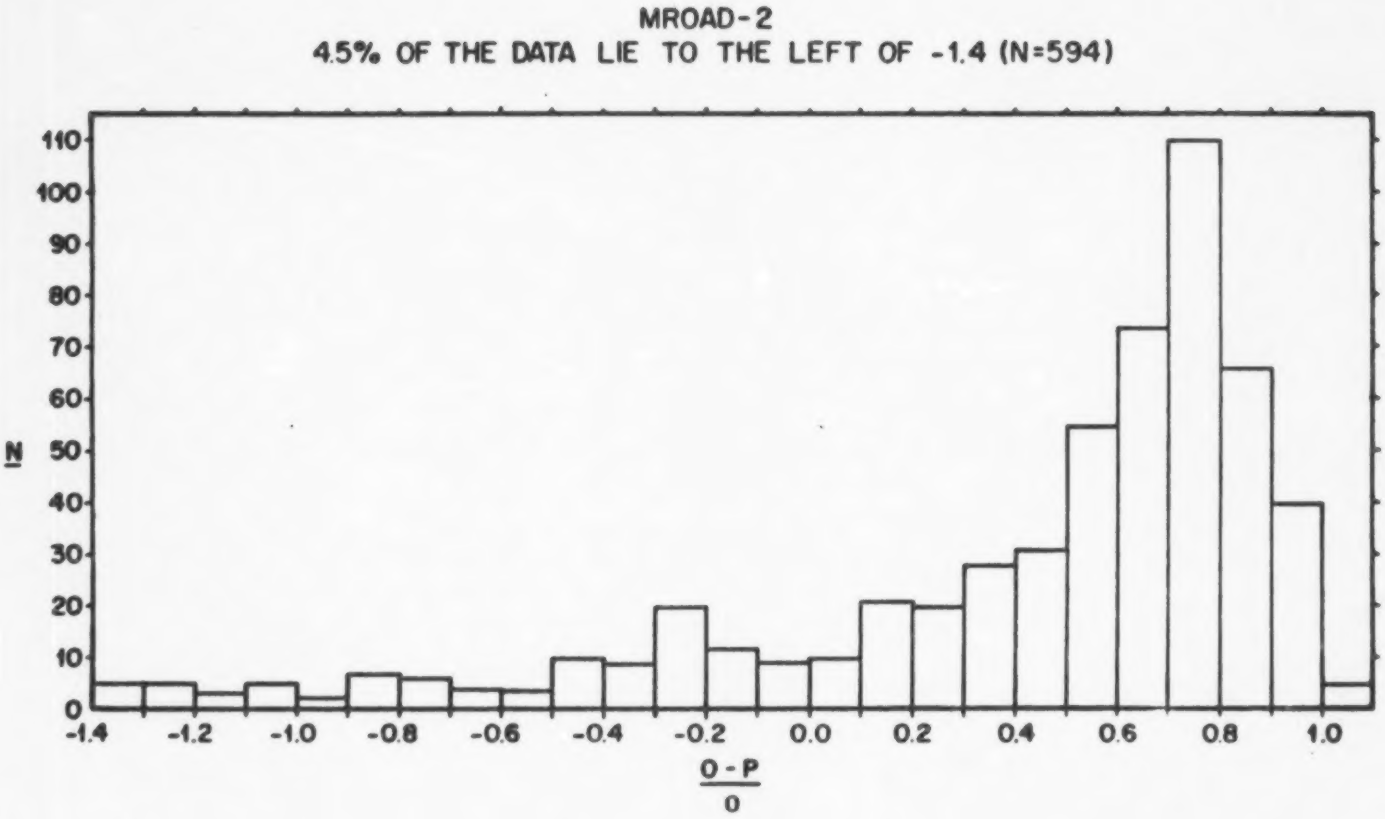

Figure 32: Same as Figure 28 except for the MROAD2 model.

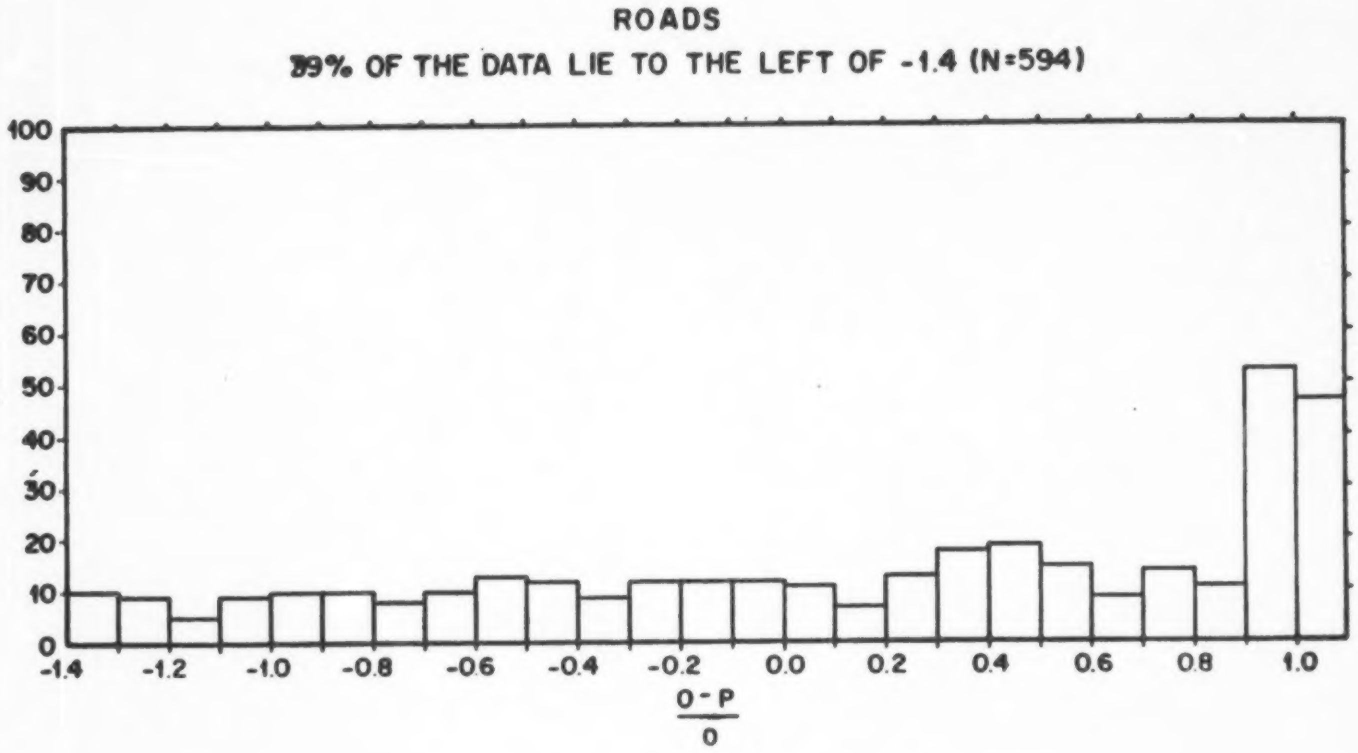

ROADS

39% OF THE DATA LIE TO THE LEFT OF -1.4 (N=594)

Figure 33: Same as Figure 28 except for the ROADS model.

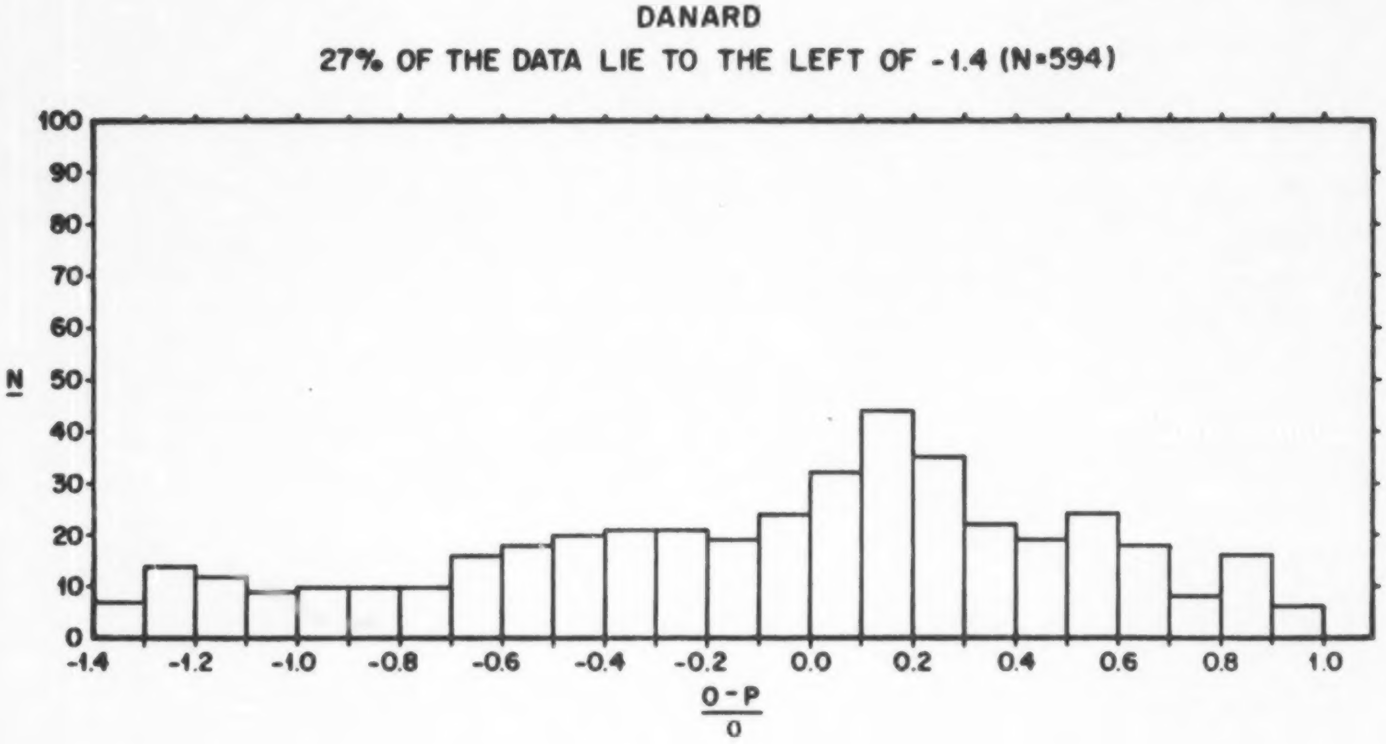

Figure 34: Same as Figure 28 except for the DANARD model.

TABLE 13

Model	Mode	Sample Size	% of prediction to within a factor of 2 (½ obs ≤ pred ≤ 2 obs)	% of exact prediction (0.95 obs ≤ pred ≤ 1.05 obs)	% of overprediction (obs < pred ≤ 2 obs)	% of underprediction (1/2 obs ≤ pred < obs)
GM	All Data	594	87	10	29	48
AIRPOL-4	All Data	594	61	7	27	27
HIWAY	All Data	594	56	5	37	14
CALINE-2	Data with > 1 m/sec wind speed	509	52	5	28	19
DAHARD	All Data	594	51	5	27	19
MROAD 2	All Data	594	28	2	13	13
ROADS	All Data	594	27	2	17	8

Table 13: Summary of the (O-P)/O where O is the observed and P is the predicted concentrations to within a factor of two of the observed are compared.

From a scientific point of view, one would expect to see that the model predictions are in close agreement with the measurements over the entire range of concentrations. However, from a regulatory point of view, the performance of the model in predicting the higher observed concentrations is of greater importance. The rationale for this regulatory viewpoint is that the models will be used to perform a worst case type analysis to ensure compliance with the air quality standards, and that the errors in measurement of low concentrations could be large.

In order to readily identify the model performance in the range of interest for the regulatory purposes, all data which was greater than half the maximum value observed per run are separated from the entire data set and the cumulative distributions of percent error are developed. The results of this analysis, summarized in Table 14, indicates that the GM model predicts concentrations 95% of the time to within a factor of 2. However, the GM model predictions are skewed toward underprediction. It is evident from this table that except for HIWAY all the other models have a tendency to underpredict in the upper part of the cumulative frequency distribution. The DANARD numerical model also appears to perform quite well in this concentration range.

The above results indicate that of all the models tested, the GM model provides by far a better simulation. Its predictions are within a factor of 2 of the observed concentrations 87% of the time. When the entire range of concentrations are considered, the ranking of models according to their decreasing performance is GM, AIRPOL-4, HIWAY, CALINE-2, DANARD, MROAD2, and ROADS. When the data in the upper part of the cumulative distribution are considered, the ranking of models according to their decreasing performance is GM, DANARD, HIWAY, AIRPOL-4, CALINE-2, MROAD2, and ROADS. Of all the models, HIWAY yields the most conservative estimates since it has the highest percentage of overprediciton in most of the statistical tests considered. Although the GM model has better statistics than the other models since it is skewed toward underprediction, it may not be useful for regulatory decision-making purposes. As a screening tool for regulatory purposes, the HIWAY model will be useful even though it is overly conservative. However, the present version of the HIWAY model for stable and parallel wind-road orientations warrants modifications to improve its predictive capability.

TABLE 14

Model	Sample Size	% of prediction to within a factor of 2 ($\frac{1}{2}$ obs $\leq$ pred $\leq$ 2 obs)	% of exact prediction (0.95 obs $\leq$ pred $\leq$ 1.05 obs)	% of overprediction (obs $<$ pred $\leq$ 2 obs)	% of underprediction ($\frac{1}{2}$ obs $\leq$ pred $<$ obs)
GM	155	95	12	19	64
HIWAY	155	70	7	43	20
AIRPOL-4	155	49	3	18	28
CALINE-2	128 (data with $\mu >$ 1m/sec)	49	4	21	24
DANARD	155	75	8	31	36
MROAD 2	155	37	3	17	17
ROADS	155	26	1	20	5

Table 14: Same as Table 13 except only data greater than half maximum observed per each sampling run is presented.

SECTION 4

IMPROVEMENTS TO THE EPA-HIWAY MODEL

Previous investigations by Chock (1977), Noll et al (1978), Rao et al (1979) and the results of the previous section indicated that the EPA-HIWAY model overestimates pollutant concentrations adjacent to the highway. This overestimation is more significant under stable atmospheric conditions and for parallel wind-road orientation angles with low wind speeds. Petersen (1978) used the wind fluctuation data in a modified version of the original HIWAY model which specifies the dispersion parameters as a function of wind fluctuation statistics and found that there was significant improvement in the model performance over the current version of the HIWAY model. This modified version of the model requires the standard deviations of the horizontal wind direction and elevation angles as a function of averaging time and sampling duration as input to the model. These sophisticated data are not generally available and the model cannot be applied without having this information. The most important finding of Petersen (1978) is that the ambient turbulence mechanisms will be properly represented when onsite turbulence data is used. Rao et al (1979), Sedefian et al (1980) and Eskridge et al (1979a, 1979b) clearly demonstrated that the dispersion in the near-field is completely dictated by the locally generated turbulence and that the ambient atmospheric stability plays an insignificant role in dispersing pollutants in the immediate vicinity of the roadway.

MODIFICATIONS TO THE HIWAY MODEL

Basically, three parameters are necessary in estimating dispersion from a ground level line source. These are the mean wind speed, and the standard deviations of the plume spread in the horizontal and vertical directions. The Gaussian dispersion equation has a singularity at zero wind speed, and hence the Gaussian assumptions become invalid at very low wind speeds. Hence, all Gaussian models perform poorly when the wind speeds are less than 1 m/sec.

Rao et al (1979) studied the effects of vehicle-induced drag due to moving vehicles on the wind profiles adjacent to the roadway, and determined that there is a pronounced acceleration of wind in the lowest 8 m, especially in the cases of wind directions nearly parallel to the roadway. Thus, even when the ambient wind speeds are quite low, near the roadway itself there is an acceleration of wind. As for the plume spread, the HIWAY model employs Pasquill-Gifford (P-G) curves extrapolated upwind to 1 m from the source. These curves were originally developed for downwind distances beginning at 100 m from a point source and, hence, do not properly describe the dispersion in the near-field. Sedefian et al (1980) indicated that the wake effects due to the moving vehicles on the roadway are superimposed upon the naturally occuring turbulence and play a dominant role in dispersing the pollutants in the near-field.

Hence, there are two possible ways to modify the line source dispersion equation to account for the enhanced dispersion due to the traffic flow, namely, (1) application of an vehicle-induced drag flow factor, and (2) application of a new set of dispersion curves that properly reflect the turbulence characteristics adjacent to the roadways. In this section, a new set of dispersion curves applicable for pollutant dispersion estimation near roadways are developed based on the data collected in the General Motors (GM) Study and in the New York (NY) State Study. Further, an empirical vehicle-induced drag flow factor is developed to handle pollutant dispersion under low wind speed conditions when traffic-generated effects dominate dispersion.

Wind Speed Correction Factor

As previously indicated, the assumptions in the Gaussian equation are violated under low wind speed conditions. Since the concentration of the pollutants is inversely proportional to the wind speed, the concentration approaches infinity asymptotically as the wind speed approaches zero. This situation is obviously unrealistic. Carpenter and Clemaña (1975) argued that the inverse linear relationship is valid only for relatively high wind speeds, and hence, requires a correction factor for low wind speeds. Based on observational data, they suggested that the concentration is inversely proportional to $(U + 1.92\ e^{-0.22U})$ where U is the ambient wind speed. This relation suggests that the concentration is inversely proportional to 1.92 at zero wind speed, and as the wind speed increases the concentration becomes inversely proportional to U. Since the original HIWAY model performed poorly for low wind speeds, the wind speed correction formulation as suggested by Carpenter and Clemaña is incorporated into a version of the HIWAY model (noted as HIWAY #2).

Vehicle-Induced Drag Flow Factor

Analysis of the GM data revealed that the drag factor must be a function of the wind-road orientation angle. This is because the amount of acceleration in the lower layers is most significant under parallel wind-road orientation (see Rao et al, 1979). Hence, an empirical drag factor which is a function of the wind-road angle is developed and is incorporated into the HIWAY model (HIWAY #4). The relation developed is $U = AU_o^{0.164}\cos^2\theta$ where U is the adjusted wind speed used in the model, U_o is the ambient wind speed (m/sec), θ is the wind-road angle, and A is a constant related to the traffic speed. It is observed that A equals 1.85 for the traffic speed conditions such as those simulated in the GM experiment. This relation takes its full effect for parallel wind ($\theta = 0$) situations and has no effect for perpendicular wind cases. If the ambient wind speed, U_o, is less than the wind speed, U, computed according to the above relation, then only the adjusted wind speed, U, is used in the model. If the ambient wind speed is greater than the adjusted wind speed, no changes to the wind speed are made (i.e. if $U_o \geq U$, then $U = U_o$). Thus, this allows correction for only low ambient wind speed situations (when ambient wind speeds are less than 2 m/sec).

Dispersion Parameters

The applicability of the dispersion values used in the HIWAY model can be evaluated by comparing the calculated σ_z, standard deviation of the plume spread in the vertical, to those used in the HIWAY model. Since measurements of concentrations at various receptors downwind of the source and meteorological conditions during the experiment are available, the vertical dispersion parameter can be computed from the line source equation (Turner, 1970).

$$C = 2/\pi(Q/\bar{u}\ \sin\theta\ \sigma_z)\ \exp -(\tfrac{1}{2}(Z^2/\sigma_z^2)) \qquad (17)$$

Where C is the observed concentration, $\bar{u}$ is the mean wind speed, θ is the angle between the wind direction and the orientation of the road ($60^\circ \leq \theta \leq 90^\circ$), Z is the height of the receptor, and σ_z is the vertical diffusion parameter. At each tower location, using the Gaussian plume assumption that σ_z is not a function of height and that the wind is uniform in the layer, σ_z can be calculated by transposing equation (17) into the form

$$\sigma_z^2 = (Z_2^2 - Z_1^2)/2\ln(C_1/C_2) \qquad (18)$$

Where Z_2 and Z_1 are the two levels at a given downwind distance at which C_2 and C_1 are the concentrations measured. In equation (18), the concentrations at heights 0.5 m (Z_1) and 3.5 m (Z_2) at the nearest roadside tower are used to compute σ_z. Once this value is known, the variation of σ_z with downwind distance (x) is calculated from the relation

$$C(\text{at } x_1)/C(\text{at } x_2) = (\sigma_{z,x_2}/\sigma_{z,x_1})\ \exp\left[\frac{Z^2}{2\sigma^2_{z,x_1}\sigma^2_{z,x_2}}(\sigma^2_{z,x_1} - \sigma^2_{z,x_2})\right] \qquad (19)$$

The concentration at the 0.5 m (Z) height is used to calculate σ_z at each downwind distance. Figure 35 provides a comparison between the computed σ_z values using both the GM and NY data sets, and those used in the HIWAY model. The local atmospheric stability for each experimental run at the GM site is determined according to the methods outlined in Rao et al (1980). Since most of the experiments of the NY site were conducted under unstable situations, the stability class B is assumed for all experiments. It is evident from this diagram that the computed σ_z values for all ambient stability conditions lie within the stability categories A to C of the P-G curves. Petersen (1978) specified the plume spread in the horizontal (σ_y) and vertical (σ_z) directions as a function of standard deviations of the azimuth angle (σ_θ) and elevation angle (σ_ϕ) and found that for downwind distances less than 300 m, dispersion is typically associated with P-G dispersion classes B to C. These results clearly indicate that the present dispersion values in the HIWAY model are unrealistic and need to be modified.

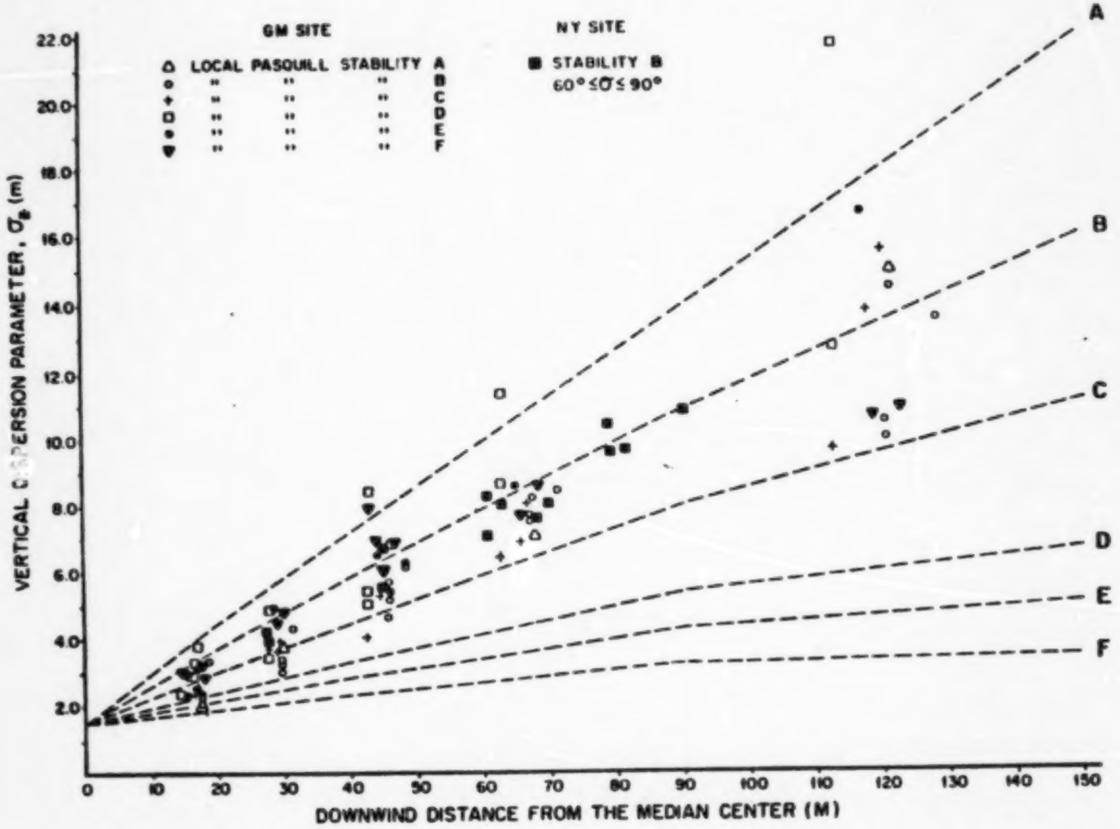

Figure 35: Comparision between σ_z specified as a function of downwind distance and atmospheric stability according to P-G curves and those computed by solving the Gaussian equation with the observed concentration data in both the GM and NY experiments.

The calculated σ_z from equation (18) at the nearest roadside receptor is plotted against the cross-road wind speed in Figure 36, where the actual local stability for each data point is also indicated in the diagram. These results show that σ_z must be a function of not only atmospheric stability but also cross-road wind speeds. Under low cross-road wind speeds, the plume takes a longer time to reach a receptor away from the source region, and, consequently, the local turbulence mechanism has a longer time to act upon the plume and spread it a great deal more.

Based on the knowledge gained on the influence of the local turbulence over the naturally occurring turbulence, the vertical dispersion parameter is defined as

$$\sigma_z^2 = \sigma_{z_t}^2 + \sigma_{z_a}^2 \qquad (20)$$

where σ_{z_t} and σ_{z_a} represent contributions from wake-induced turbulence and ambient turbulence, respectively. The contribution of the wake effects to the initial dispersion is given as

$$\sigma_{z_t} = 3.57 - 0.53U_\perp \qquad (21)$$

where $U_\perp$ is the cross-road wind speed (See Figure 36) in m/sec. For all cross-road wind speeds greater than 3.91 m/sec, σ_{z_t} is held constant at 1.5 m. The ambient atmospheric stability is defined in terms of three stability classes, namely, unstable, neutral and stable. The contribution of ambient stability to the dispersion is specified as

$$\sigma_{z_a} = \begin{cases} 110.62x^{0.93198} & \text{for unstable} \\ 86.49x^{0.92332} & \text{for neutral} \\ 61.14x^{0.91465} & \text{for stable} \end{cases} \qquad (22)$$

where x is the downwind distance from the source in kilometers. In order to be consistent with the above formulation, the standard deviation in the cross-wind direction, σ_y, is specified as

$$\sigma_y^2 = \sigma_{y_t}^2 + \sigma_{y_a}^2 \qquad (23)$$

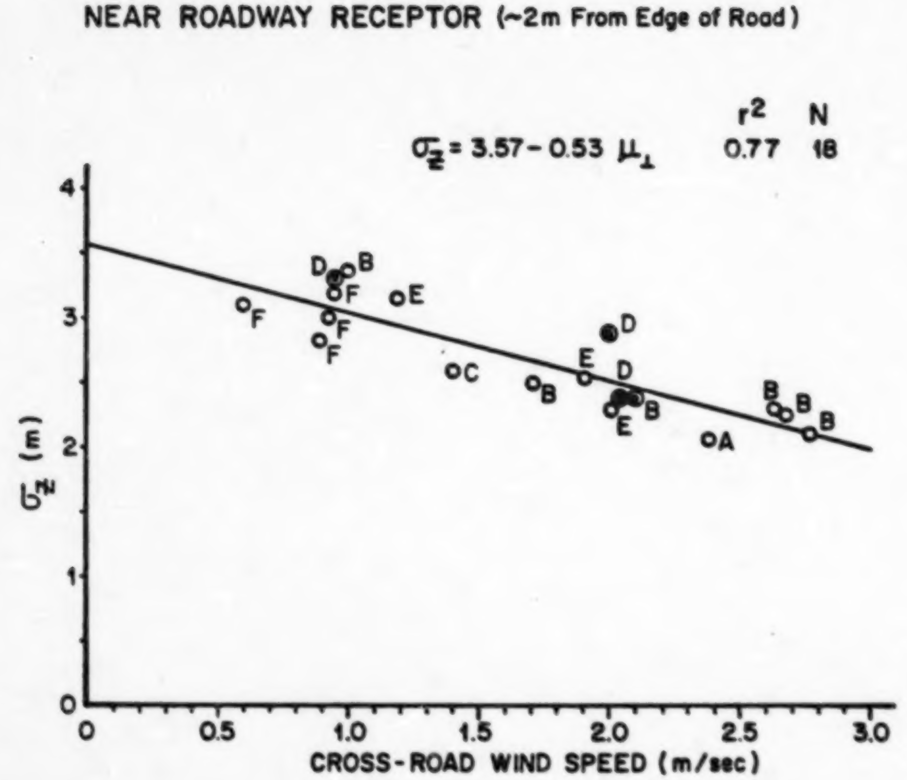

Figure 36: Computed σ_z at the nearest roadside receptor as a function of cross-road wind speed.

where $\sigma_{y_t} = 2\sigma_{z_t}$; and σ_{y_a} is defined as

$$\sigma_{y_a} = 1000\ (x)\ \sin\theta/(2.15\cos\theta) \tag{24}$$

Here x is in kilometers and θ is specified as

$$\theta = \begin{cases} (18.333-1.8096\ln x)/57.2958 & \text{for unstable} \\ (14.333-1.7706\ln x)/57.2958 & \text{for neutral} \\ (12.500-1.0857\ln x)/57.2958 & \text{for stable} \end{cases} \tag{25}$$

In the above equation, both σ_z and σ_y are in meters.

The present formulation for the dispersion parameters eliminates the concept of virtual point source used in the original HIWAY model. The new set of dispersion curves, computed according to the above equations, are compared to the P-G curves of the HIWAY model in Figure 37.

MODEL TESTING AND COMPARISONS

The following versions of the HIWAY model are employed to simulate the tracer release experiments conducted in the GM and NY study.

HIWAY#1 - original HIWAY model
HIWAY#2 - HIWAY model with the wind speed correction factor suggested by Carpenter and Clemaña (1975)
HIWAY#3 - HIWAY model with the modified set of dispersion curves
HIWAY#4 - HIWAY model with the modified dispersion curves and the vehicle-induced drag flow factor

The performances of each of the above versions of the HIWAY model are compared to the GM model (Chock, 1977) CALINE-3 model (Benson, 1979), and the numerical wake model (Eskridge et al, 1979). The same meteorological conditions described in the previous section for the GM data set, and Sistla et al (1979) for the NY data set are used in these model evaluations.

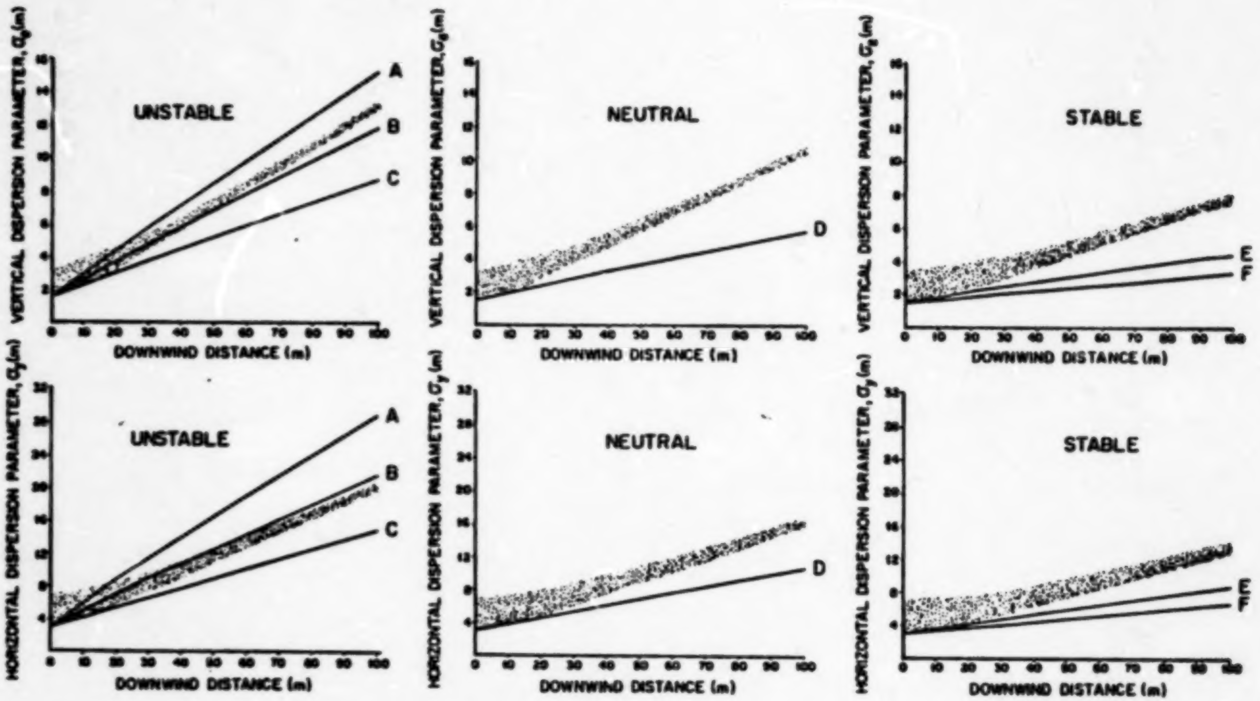

Figure 37: Comparison of the new dispersion curves (shaded areas) to the P-G dispersion curves (solid lines) used in the original HIWAY model. The dispersion parameters (σ_y,σ_z) are given as a function of downwind distance for each stability class. The upper bound of the new dispersion curves represents the values used for zero cross-road wind speeds, while the lower bound is for cross-road wind speeds greater than 3.91 m/sec.

Regression Analysis

The GM data are segregated according to wind-road orientation angle and the results of regression analysis are shown in Table 15. Although the correlation when all data combined for HIWAY #3 is about the same as HIWAY #1, the slope is about three times that of HIWAY #1. This indicates that the overpredictions of the original HIWAY are reduced somewhat in the modified HIWAY model. The simulation of HIWAY #4, which employs a drag flow factor as a function of wind-road orientation angle, is much better than the other HIWAY versions, and is quite comparable to the simulation of the GM model. The numerical wake model developed by Eskridge et al (1979) has an r^2 of 0.63, a slope of 0.77, an intercept of 0.18, and a standard error of estimate of 0.47 for a sample size of 551 data points. The regression results for HIWAY #4 are quite comparable to those of the wake model for this simple at-grade roadway configuration.

The results also show that the HIWAY #4 simulation is much better than the CALINE-3 model. When the data are divided according to the stability classes (see Table 16), again HIWAY #3 has a better slope than HIWAY #1. The correlations of HIWAY #4 show even further improvement over HIWAY #3. HIWAY #4 shows a considerable improvement over HIWAY #1 and CALINE-3 for stable atmospheric conditions. When the data are grouped according to wind speed class (see Table 17), HIWAY #4 provides a better simulation than the other HIWAY versions and CALINE-3 for low wind speeds.

The vehicle-induced drag flow factor is applied only if the adjusted wind speed according to the relation $1.85\ U_o^{0.164} \cos^2 \theta$ is greater than the ambient wind speed (U_o). It should be noted that this correction is not applicable when U_o approaches zero. No attempts were made to make the correction valid for $U_o = 0$ since the basic Gaussian dispersion equation becomes invalid at this point. The cut-off wind speed is about 30 cm/sec. The reason for this cut-off is that commonly used wind instruments themselves cannot measure wind speeds reliably when the wind speeds are less than about 30 cm/sec.

TABLE 15

DATA SUBSET	STATISTICAL PARAMETER	HIWAY #1	HIWAY #2	HIWAY #3	HIWAY #4	GM	CAL-3
	r^2	0.65	0.73	0.81	0.81	0.92	0.82
Perpendicular	b	0.41	1.17	0.80	0.80	0.99	1.02
	a	0.37	0.21	0.12	0.12	0.12	0.10
$60^\circ \leq \theta \leq 90^\circ$	$S_{o/p}$	0.39	0.34	0.29	0.29	0.19	0.28
	R	0.75	1.57	0.94	0.94	1.15	1.16
	N	173	173	173	173	173	173
	r^2	0.37	0.52	0.51	0.61	0.77	0.53
Oblique	b	0.22	0.78	0.49	0.66	0.97	0.63
	a	0.65	0.44	0.41	0.27	0.25	0.39
$30^\circ \leq \theta < 60^\circ$	$S_{o/p}$	0.60	0.52	0.52	0.47	0.36	0.51
	R	0.61	1.39	0.82	0.89	1.15	1.03
	N	128	128	128	128	128	128
	r^2	0.24	0.64	0.28	0.71	0.83	0.23
Parallel	b	0.08	0.53	0.23	0.91	0.94	0.21
	a	0.80	0.27	0.69	-0.04	0.03	0.77
$0^\circ \leq \theta < 30^\circ$	$S_{o/p}$	0.67	0.46	0.65	0.41	0.32	0.68
	R	0.40	0.73	0.72	0.88	1.00	0.92
	N	293	293	293	293	293	293
	r^2	0.26	0.54	0.35	0.70	0.83	0.29
All Data	b	0.11	0.54	0.31	0.81	0.94	0.30
Combined	a	0.75	0.42	0.58	0.10	0.12	0.67
	$S_{o/p}$	0.64	0.50	0.59	0.40	0.30	0.62
	R	0.50	0.96	0.79	0.89	1.06	1.00
	N	594	594	594	594	594	594

Table 15: Same as Table 9 except the models compared here are GM, HIWAY #1, HIWAY #2, HIWAY #3, HIWAY #4 and CALINE-3. One additional parameter, R, is the ratio of the mean observed concentration to the mean predicted concentration for that data subset. Here again, the data are segregated according to wind-road orientation angle.

TABLE 16

DATA SUBSET	STATISTICAL PARAMETER	HIWAY #1	HIWAY #2	HIWAY #3	HIWAY #4	GM	CAL-3
Unstable (A to C)	r^2	0.61	0.68	0.60	0.76	0.91	0.68
	b	0.54	1.10	0.72	0.99	1.18	1.25
	a	0.22	0.11	0.15	-0.03	0.04	0.07
	S_o/p	0.37	0.34	0.38	0.29	0.18	0.34
	R	0.76	1.29	0.89	0.95	1.24	1.37
	N	276	276	276	276	276	276
Neutral (D)	r^2	0.69	0.57	0.75	0.78	0.80	0.76
	b	0.45	0.65	0.90	1.02	1.01	1.20
	a	0.18	0.25	0.03	-0.05	0.05	-0.02
	S_o/p	0.39	0.46	0.35	0.32	0.31	0.34
	R	0.56	0.89	0.93	0.97	1.06	1.17
	N	100	100	100	100	100	100
Stable (E & F)	r^2	0.23	0.52	0.29	0.65	0.82	0.24
	b	0.08	0.46	0.22	0.73	0.90	0.21
	a	0.93	0.51	0.80	0.15	0.07	0.86
	S_o/p	0.75	0.60	0.72	0.50	0.36	0.74
	R	0.37	0.82	0.68	0.83	0.95	0.78
	N	218	218	218	218	218	218
Downwind Ground Level (0.5m) Receptors Only	r^2	0.21	0.53	0.34	0.68	0.84	0.34
	b	0.09	0.57	0.33	0.84	0.99	0.37
	a	1.00	0.50	0.78	0.18	0.12	0.86
	S_o/p	0.78	0.60	0.71	0.50	0.35	0.71
	R	0.47	0.95	0.88	0.98	1.09	1.17
	N	260	260	260	260	260	260

Table 16: Same as Table 15 except the data are segregated according to stability class.

TABLE 17

DATA SUBSET	STATISTICAL PARAMETER	HIWAY #1	HIWAY #2	HIWAY #3	HIWAY #4	CM	CAL-3
$U < 1$ m/sec	r^2	0.24	0.36	0.34	0.67	0.82	0.30
	b	0.05	0.36	0.16	0.62	0.78	0.16
	a	1.03	0.84	0.85	0.22	0.26	0.91
	S_o/p	0.74	0.68	0.69	0.48	0.36	0.70
	R	0.29	1.12	0.49	0.75	0.98	0.58
	N	85	85	85	85	85	85
$1 \leq U < 2.5$ m/sec	r^2	0.65	0.60	0.71	0.74	0.87	0.67
	b	0.40	0.66	0.84	0.93	1.10	1.02
	a	0.30	0.34	0.01	-0.05	0.02	0.09
	S_o/p	0.43	0.46	0.39	0.37	0.26	0.42
	R	0.59	1.02	0.85	0.88	1.12	1.13
	N	339	339	339	339	339	339
$U \geq 2.5$ m/sec	r^2	0.69	0.68	0.84	0.84	0.82	0.79
	b	0.41	0.53	1.18	1.18	0.86	1.41
	a	0.24	0.25	-0.07	-0.07	0.12	-0.02
	S_o/p	0.37	0.38	0.27	0.27	0.29	0.31
	R	0.58	0.79	1.09	1.09	1.01	1.38
	N	170	170	170	170	170	170
All Data With $U > 1$ m/sec	r^2	0.66	0.61	0.72	0.75	0.84	0.68
	b	0.41	0.61	0.88	0.95	1.00	1.08
	a	0.28	0.32	0.03	-0.02	0.07	0.09
	S_o/p	0.41	0.44	0.38	0.36	0.28	0.40
	R	0.59	0.94	0.91	0.94	1.09	1.20
	N	509	509	509	509	509	509

Table 17: Same as Table 15 except the data are segregated according to wind speed class.

When the data with wind speeds greater than 1 m/sec are used, the simulation of HIWAY #3 is quite close to that of HIWAY #4 and CALINE-3. Although the correlation for HIWAY #1 is comparable to that of the modified versions, the slope is still less desirable. These results also indicate that the inclusion of the wind speed correction alone such as the one suggested by Carpenter and Clemaña (HIWAY #2) does not significantly improve the model's ability to simulate the dispersion process.

The spatial variation of the regression statistics of all the HIWAY versions and the GM model is shown in Table 18. These results show that the predictions of HIWAY #4 are far better than the other HIWAY versions and CALINE-3, and are comparable to the GM model for receptors close to the roadway. In general, all models appear to overpredict as the distance from the road increases.

Table 19 presents the distribution of fractional error of HIWAY #1 and HIWAY #4 for spatial variation by stability classification for wind speeds greater than 1 m/sec. The fractional error is defined as the summation of the difference between the observed and predicted divided by the average of the observed and predicted $((2/N)\Sigma(O_i-P_i)/(O_i+P_i))$. The fracional error has the same numerical value although different signs for either an overprediction of n times or an underprediction of n^{-1} times (e.g. a prediction of twice observed yields a value of -2/3 while half of observed yields +2/3). Therefore, a negative fractional error indicates an overall tendency to overpredict, while the magnitude itself indicates the degree of this tendency. Table 20 presents the standard deviations of the fractional errors in Table 19. Table 21 shows the number of data points used to compute the values in Tables 19, 20 and 22. A comparison between HIWAY #1 and HIWAY #4 from these tables indicates that HIWAY #4 still retains the conservative nature of HIWAY #1, while reducing considerably the tendency to grossly overpredict.

Table 22 presents the distribution of absolute fractional error for GM, HIWAY #1, HIWAY #4 and CALINE-3, segmented in the same fashion as the previous tables. The absolute fractional error is computed in the same manner as the fractional error, but the absolute value of difference between the observed and predicted is used in the calculation. Thus, both an

TABLE 18

Data Subset	Statistical Parameter	HIWAY #1	HIWAY #3	HIWAY #4	GM	CAL-3
Towers 2 & 4 (4 meters from highway)	r^2	0.27	0.31	0.75	0.86	0.26
	b	0.10	0.26	0.90	0.92	0.26
	a	1.11	0.93	0.09	0.22	1.00
	$S_{o/p}$	0.88	0.86	0.52	0.39	0.89
	R	0.52	0.80	0.96	1.09	0.94
	N	182	182	182	182	182
Tower 5 (15 meters from highway)	r^2	0.55	0.54	0.63	0.75	0.45
	b	0.30	0.58	0.72	0.89	0.84
	a	0.50	0.33	0.21	0.18	0.31
	$S_{o/p}$	0.36	0.37	0.33	0.27	0.40
	R	0.60	0.87	0.91	1.09	1.22
	N	137	137	137	137	137
Towers 1 & 6 (30 meters from highway)	r^2	0.17	0.27	0.43	0.56	0.20
	b	0.05	0.17	0.41	0.73	0.15
	a	0.65	0.55	0.36	0.19	0.60
	$S_{o/p}$	0.32	0.30	0.27	0.23	0.32
	R	0.41	0.68	0.80	0.99	0.89
	N	183	183	183	183	183
Tower 7 (50 meters from highway)	r^2	0.73	0.31	0.40	0.77	0.32
	b	0.31	0.33	0.42	0.60	0.45
	a	0.22	0.39	0.33	0.17	0.40
	$S_{o/p}$	0.15	0.20	0.19	0.14	0.20
	R	0.61	0.83	0.87	1.00	1.23
	N	46	46	46	46	46
Tower 8 (100 meters from highway)	r^2	0.48	0.41	0.50	0.68	0.33
	b	0.21	0.45	0.55	0.55	0.46
	a	0.28	0.16	0.13	0.17	0.21
	$S_{o/p}$	0.14	0.14	0.13	0.11	0.15
	R	0.60	0.80	0.83	0.93	1.06
	N	46	46	46	46	46

Table 18: Same as Table 15 except the data are segregated according to source-receptor location.

Table 19

Distance/Stability	HIWAY #1				HIWAY #4			
	Unstable	Neutral	Stable	All	Unstable	Neutral	Stable	All
4 m	-0.21	-0.05	-0.08	-0.14	-0.14	-0.12	-0.08	-0.12
15 m	-0.14	-0.36	-0.45	-0.26	-0.07	-0.11	-0.12	-0.08
30 m	-0.30	-0.37	-0.42	-0.35	-0.17	-0.10	-0.19	-0.16
50 m	-0.19	-0.81	-1.00	-0.51	0.00	-0.05	-0.20	-0.06
100 m	-0.20	-0.90	-1.25	-0.60	0.02	-0.11	-0.51	-0.15
All	-0.21	-0.35	-0.42	-0.30	-0.10	-0.10	-0.17	-0.12

Table 19: Distribution of Fractional Error by stability and distance for GM data, when the wind speed was greater than 1 m/sec, for HIWAY #1 and HIWAY #4.

Table 20

Distance/Stability	HIWAY #1				HIWAY #6			
	Unstable	Neutral	Stable	All	Unstable	Neutral	Stable	All
4 m	0.48	0.82	0.98	0.74	0.49	0.37	0.42	0.45
15 m	0.39	0.70	0.83	0.61	0.35	0.34	0.40	0.36
30 m	0.40	0.67	0.94	0.68	0.34	0.37	0.27	0.33
50 m	0.43	0.37	0.14	0.52	0.38	0.50	0.22	0.38
100 m	0.39	0.41	0.24	0.59	0.30	0.55	0.30	0.42
All	0.43	0.74	0.93	0.68	0.39	0.39	0.37	0.39

Table 20: Distribution of Standard Deviation of Fractional Errors presented in Table 19.

TABLE 21

Distance / Stability	Unstable	Neutral	Stable	All
4	75	27	50	152
15	69	21	32	122
30	75	27	51	153
50	23	7	11	41
100	23	7	11	41
All	265	89	155	509

Table 21: Number of data points for each category used in analyses of Tables 19, 20, and 21.

TABLE 22

Model	Distance (m) \ Stability	Unstable	Neutral	Stable	All
GM	4	0.43	0.29	0.26	0.37
	15	0.36	0.31	0.22	0.31
	30	0.24	0.29	0.23	0.25
	50	0.31	0.38	0.24	0.31
	100	0.34	0.39	0.59	0.41
	ALL	0.35	0.31	0.26	0.32
HW-1	4	0.40	0.65	0.80	0.58
	15	0.33	0.67	0.84	0.52
	30	0.39	0.65	0.94	0.62
	50	0.33	0.80	1.00	0.59
	100	0.36	0.90	1.25	0.69
	ALL	0.37	0.69	0.90	0.59
HW-4	4	0.39	0.29	0.32	0.35
	15	0.27	0.27	0.35	0.29
	30	0.29	0.28	0.27	0.28
	50	0.26	0.38	0.25	0.28
	100	0.24	0.40	0.51	0.34
	ALL	0.31	0.30	0.32	0.31
CAL-3	4	0.46	0.44	0.40	0.44
	15	0.49	0.42	0.31	0.43
	30	0.46	0.43	0.28	0.39
	50	0.60	0.45	0.16	0.46
	100	0.51	0.45	0.50	0.50
	ALL	0.48	0.43	0.33	0.43

Table 22: Distribution of Absolute Fractional Error by stability and distance for GM data, when wind speed is greater than 1 m/sec, for GM, HIWAY #1, HIWAY #4, and CALINE-3 models.

overprediction of n times and underprediction of n^{-1} times yield the same value (e.g. a prediction of either twice or half observed yield a value of 2/3). Therefore, the absolute fractional error shows a model's average ability to predict within a certain factor (an absolute fractional error of 0.4 indicates a factor of 1.5, while 0.67 corresponds to a factor of 2, and 1.0 is a factor of 3). Table 22 shows that HIWAY #4 is comparable to GM in performance, and a significant improvement over HIWAY #1.

Scatter plots of observed and predicted concentrations for HIWAY #1, HIWAY #4, GM and CALINE-3 are presented in Figures 38. Another interesting way of looking at the model's ability in predicting concentrations is shown in Figure 39. Here a tabular presentation of bivariate frequency distribution of observed versus predicted concentrations in various concentration intervals is given for the original HIWAY, HIWAY #4, GM and CALINE-3 models. Values in the squares along the position diagonal represent "successful predictions" and thus, readily identify the success of the model at different observed concentration levels. The total number of data points in each plot vary because only the predicted concentrations of each model falling within the range of observed concentration are included in the plot. It is evident from this plot that the GM model has 80% of the data within the bracketed area of successful predictions while the orginal HIWAY model has only 49% of the data in this region. The HIWAY #4 model has 71% of the data in the region of successful predictions while CALINE-3 has 66% of the data in this region. For the GM model, 37.5% of the data falls on the one-to-one line, 36.9% of the data on the one-to-one line for HIWAY #4, 30.5% of the data for the CALINE-3 model and 23.4% of the data for HIWAY #1 fall on the observed equals predicted line.

Cumulative Frequency Distributions

In order to further assess the model performance, various frequency distribution plots are developed. These plots depict the model performance in an overall statistical sense rather than the usual one-to-one relationship afforded by the regression statistics. Figure 40 shows the frequency distribution of observed concentration and the concentration distributions predicted by the HIWAY #1, HIWAY #3, and HIWAY #4 models. It is evident from this

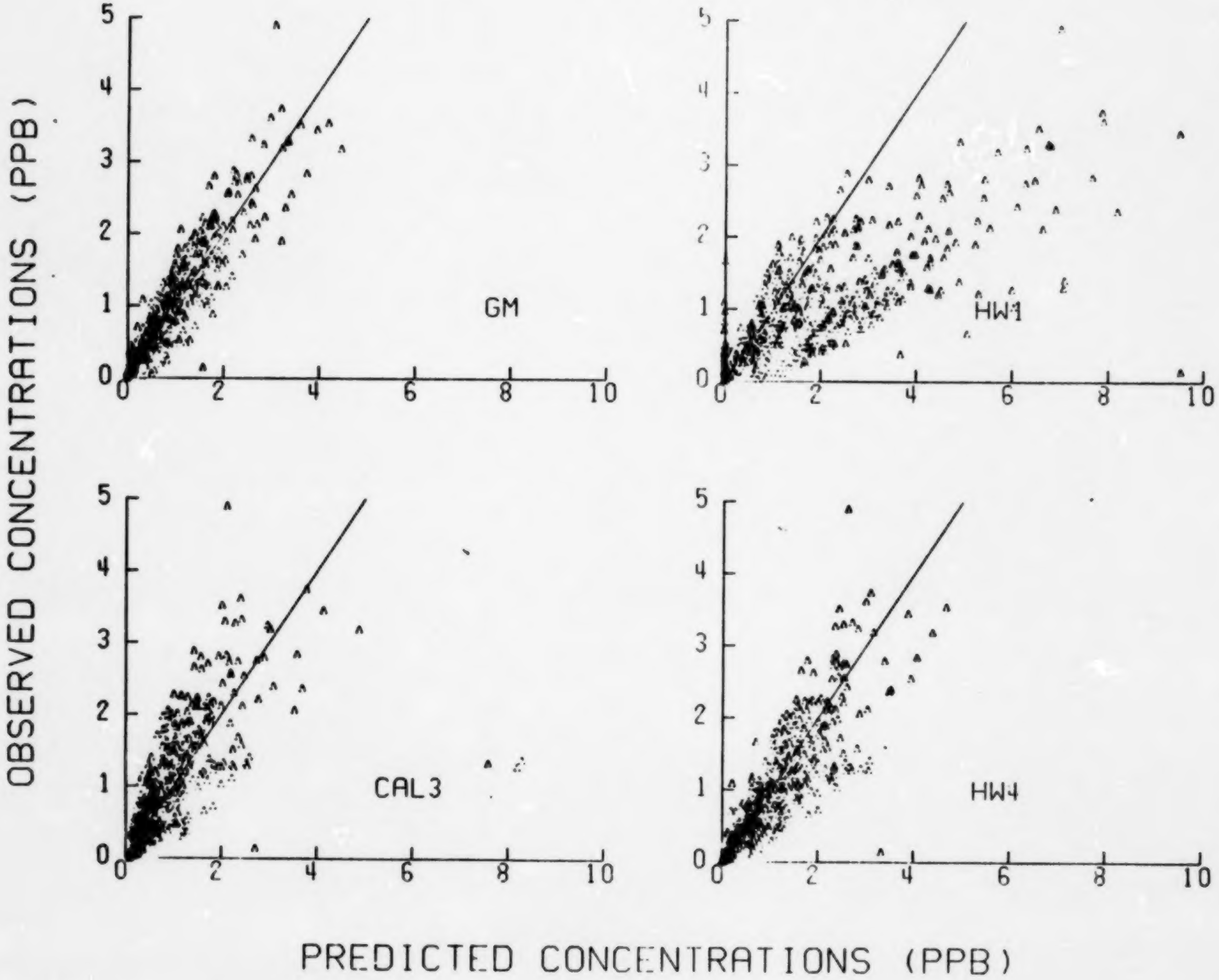

Figure 38: Scatter plots showing the observed versus predicted concentrations for HIWAY #1, HIWAY #4, GM and CALINE-3.

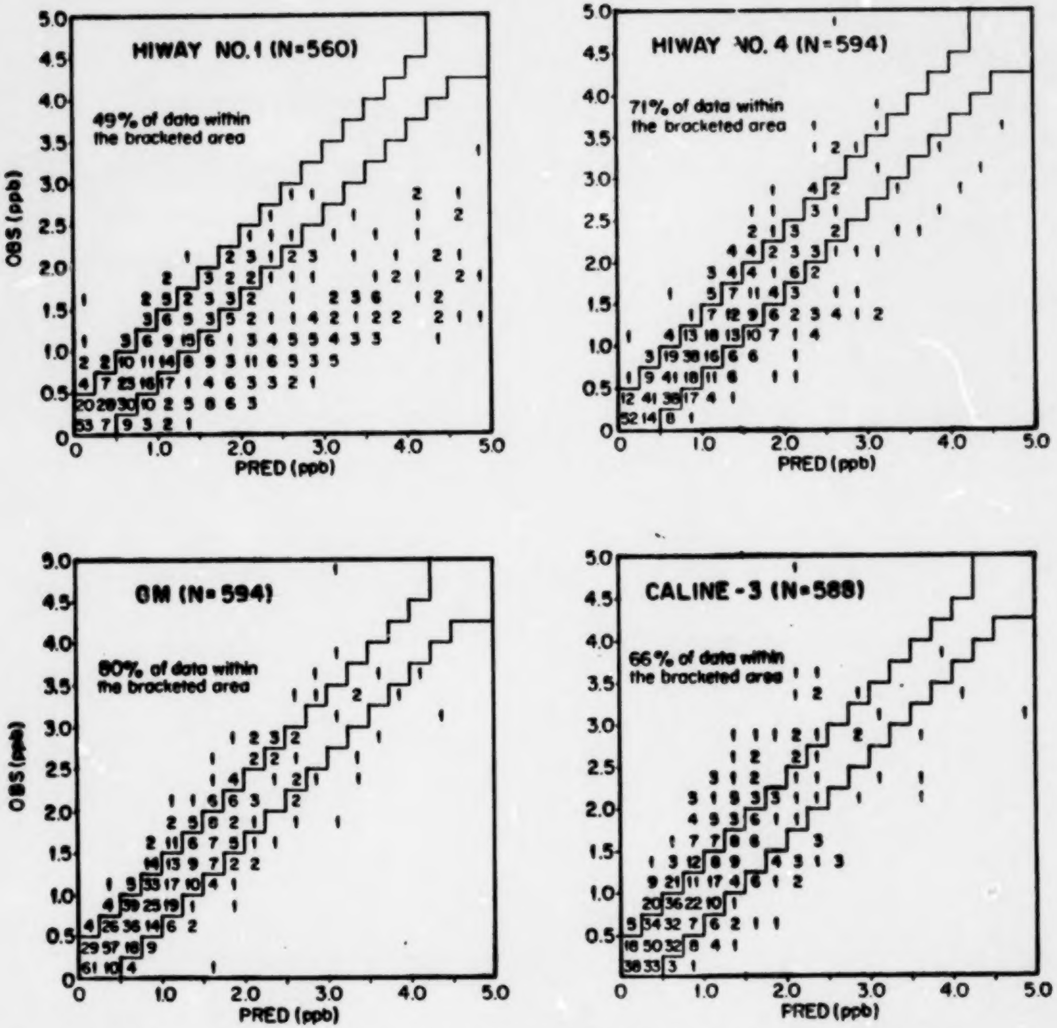

Figure 39: Bivariate frequency distributions of the observed versus predicted concentrations for HIWAY #1, HIWAY #4, GM and CALINE-3.

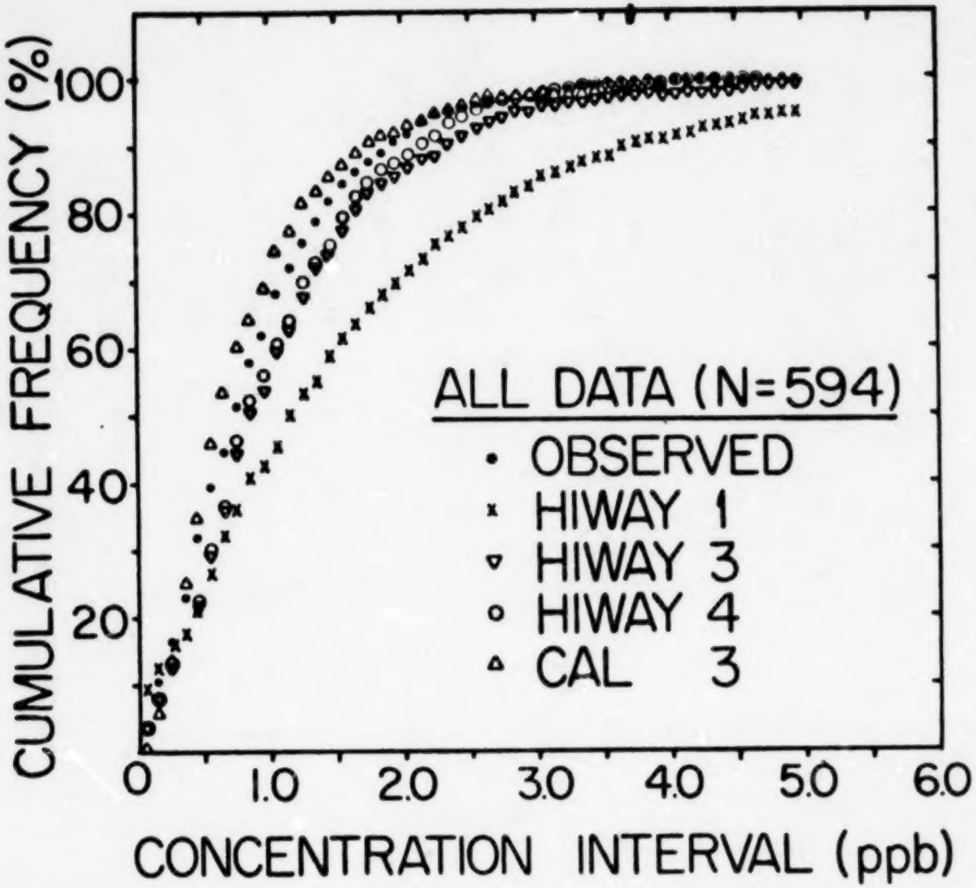

Figure 40: Cumulative frequency distribution of observed concentration is compared to the distribution provided by HIWAY #1, HIWAY #3, HIWAY #4 and the CALINE-3 models.

plot that HIWAY #3 and HIWAY #4 simulate the observed concentration distributions quite well compared to the original HIWAY model. The original HIWAY model consistently overestimates the concentrations.

The cumulative frequency plots of (O-P)/O where O is the observed and P is the predicated concentration give more insight into the model's behavior. Such plots for the HIWAY #4 and CALINE-3 models are shown in Figures 41 and 42. It is preferable that these plots have a Gaussian shape with the peak at zero and rapid fall off on either side. HIWAY #1 yields a distribution pattern (see Figure 28) that deviates very significantly from the GM model (see Figure 29).

It is possible to derive information as to how the model simulates the dispersion mechanism by comparing (O-P)/O cumulative plots of normalized concentrations. The normalization is done by dividing each data point predicted by the model by the corresponding maximum predicted from that run. The observed data for that run is also normalized by the observed maximum for the run. In this way, any uncertainties in the estimation of source strength and meteorological variables will be removed since direct comparisons of observed and predicted concentration profiles can be made. The spatial variations of concentration is related only to the spatial variation of dispersion parameters. Hence, comparison of normalized concentration profiles will provide information on how well a model handles the diffusion process.

Comparing the cumulative plots of $(O_n-P_n)/O_n$, where the subscript n denotes normalized concentrations, for HIWAY #1 (see Figure 43) and HIWAY #4 (see Figure 44), it is seen that the distribution for the former is not as smooth as the latter. The distribution for HIWAY #4 is skewed to the negative side indicating that the predicted concentration profile is more than the observed profile thereby yielding conservative estimates of pollutant levels. The distribution for the GM model (see Figure 45) has a Gaussian shape while HIWAY #4 resembles more of a log-normal curve with negative skewness. It is of particular interest to note that the distribution for HIWAY #4 reaches its peak about zero and rapidly falls off to the right of the peak. This feature is quite important for a regulatory model since environmental health decisions will be made using the model predictions. The regression statistics for

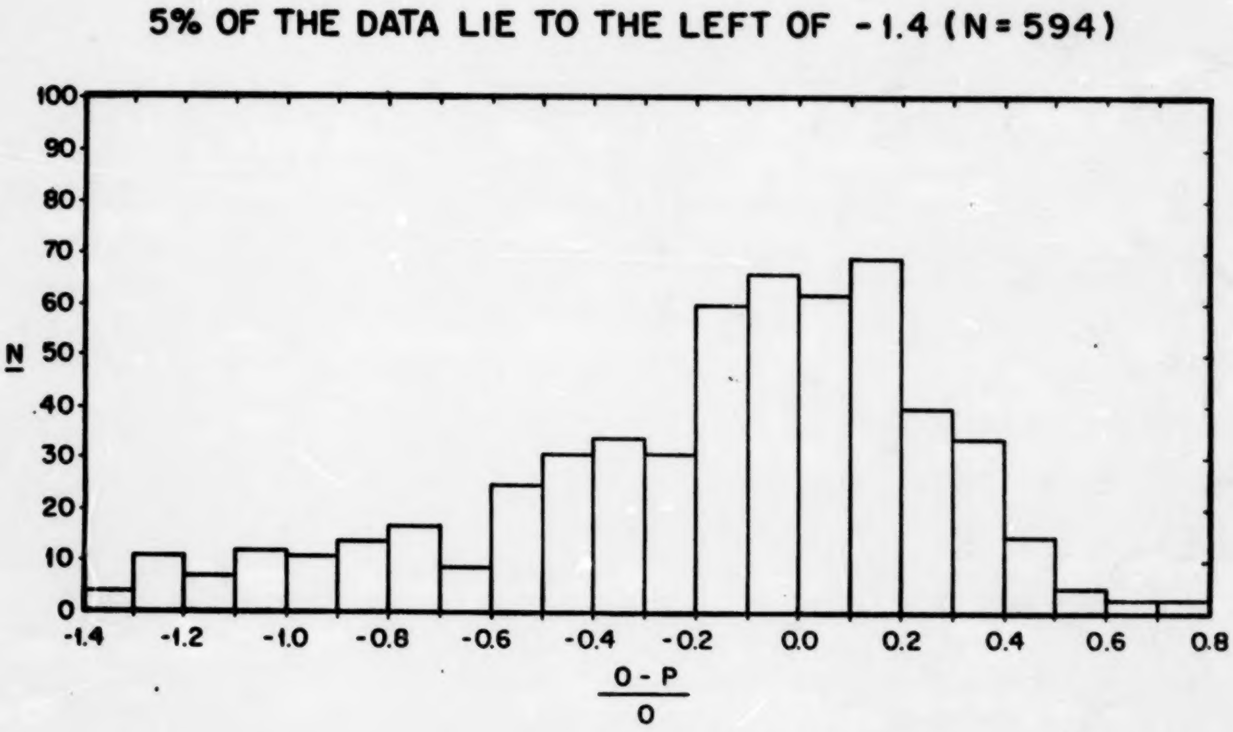

Figure 41: Same as Figure 28 except for the HIWAY #4 model.

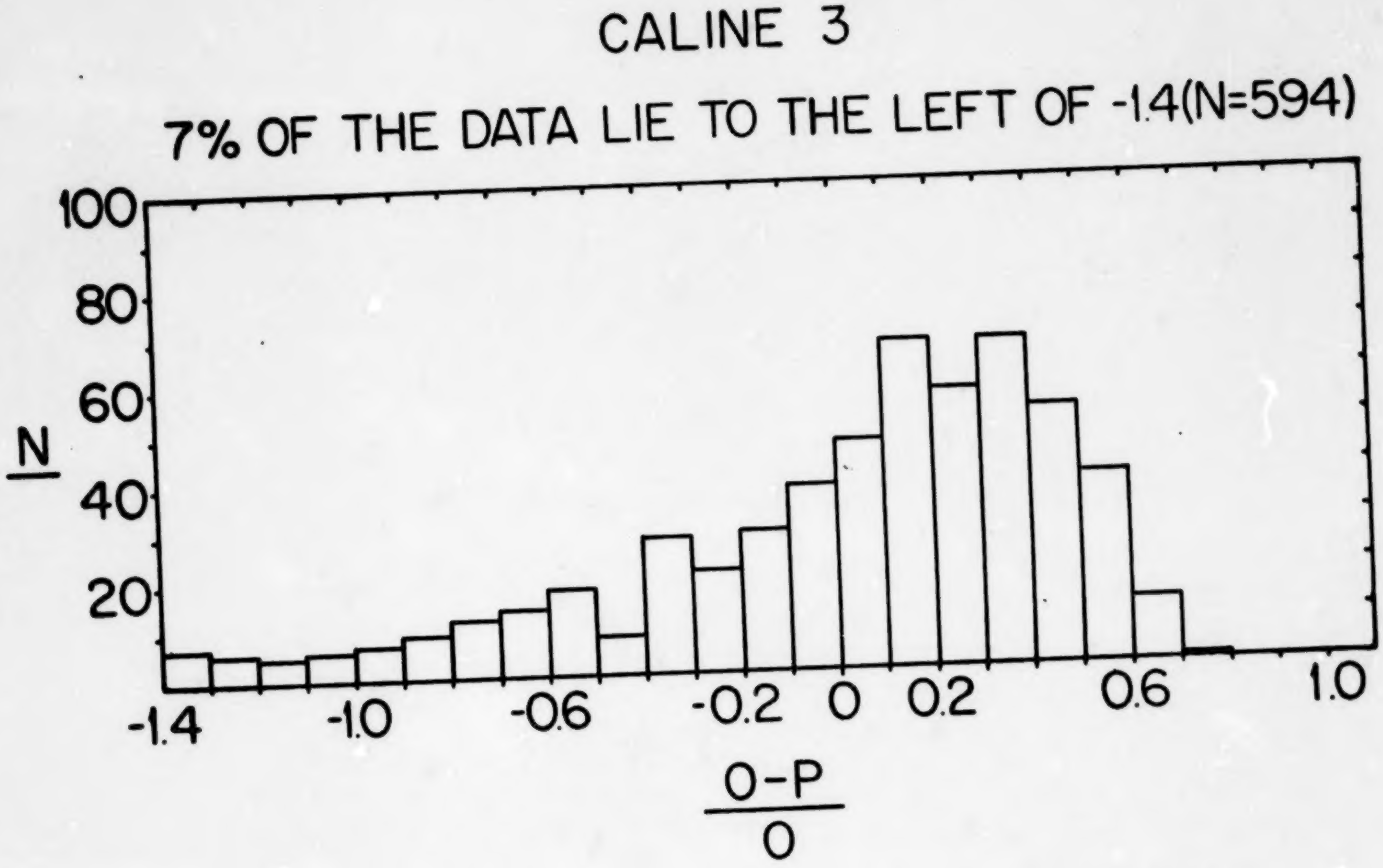

Figure 42: Same as Figure 28 except for the CALINE-3 model.

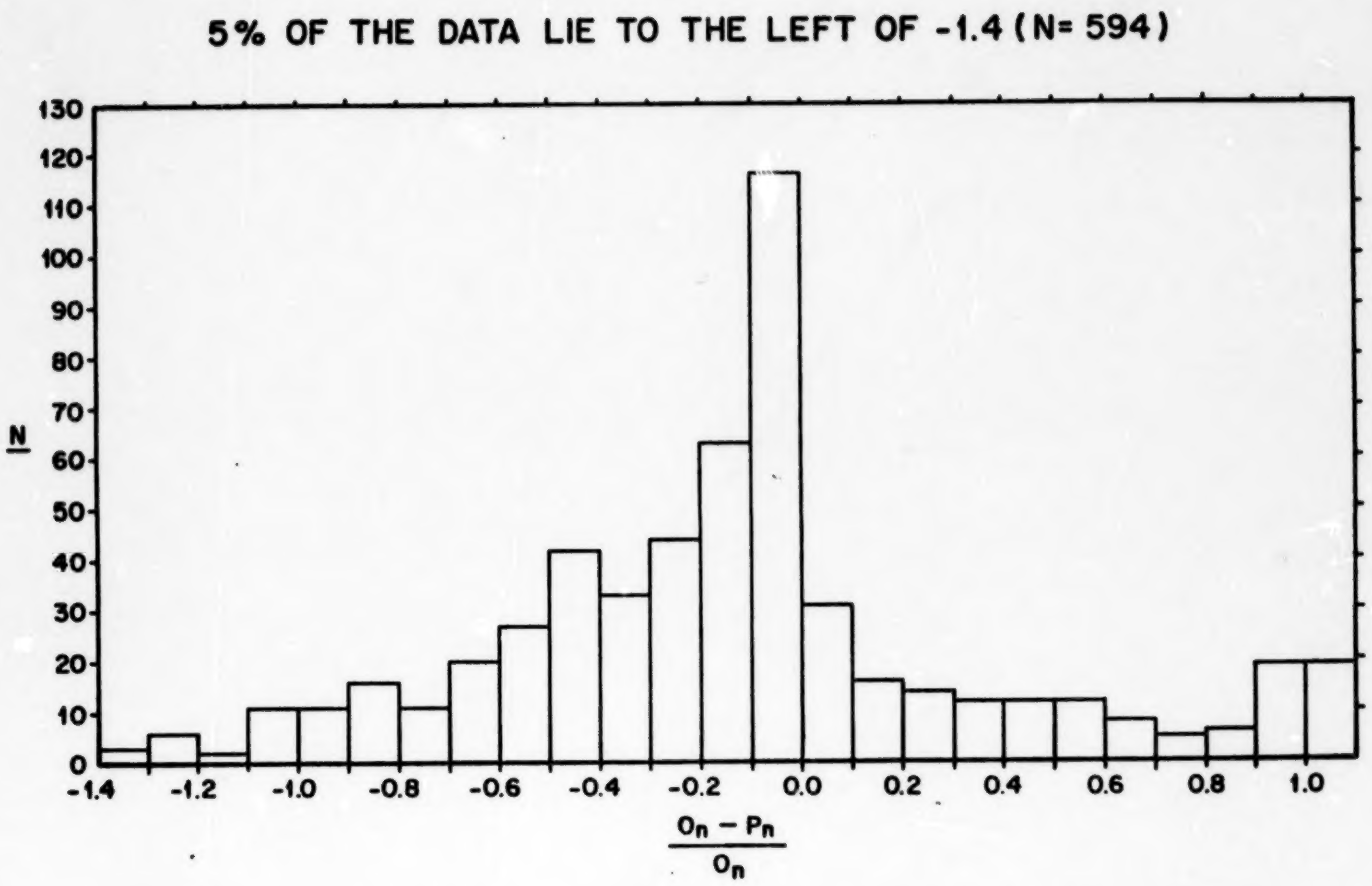

Figure 43: Cumulative plots of normalized concentrations for $(O_n - P_n)/O_n$ for the original HIWAY model. The observed and predicted concentration at various locations for a given run are divided by their corresponding maximums for that run.

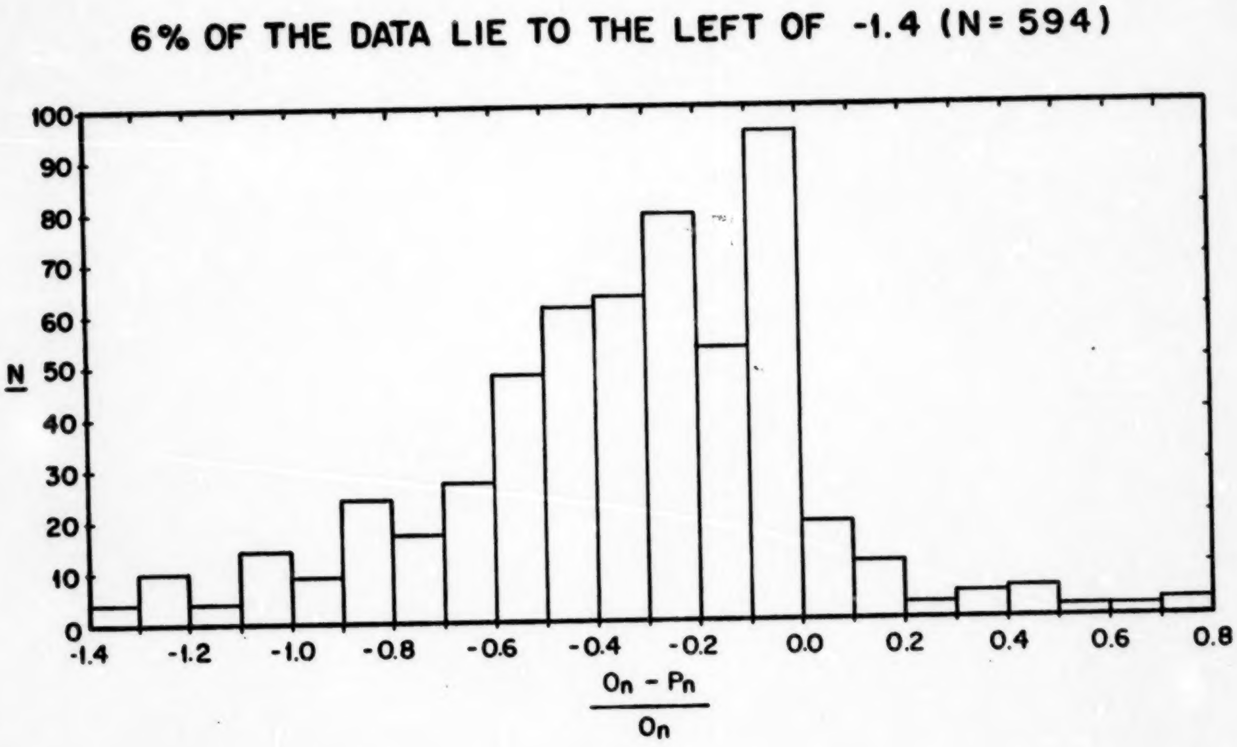

Figure 44: Same as Figure 43 except for the HIWAY #4 model.

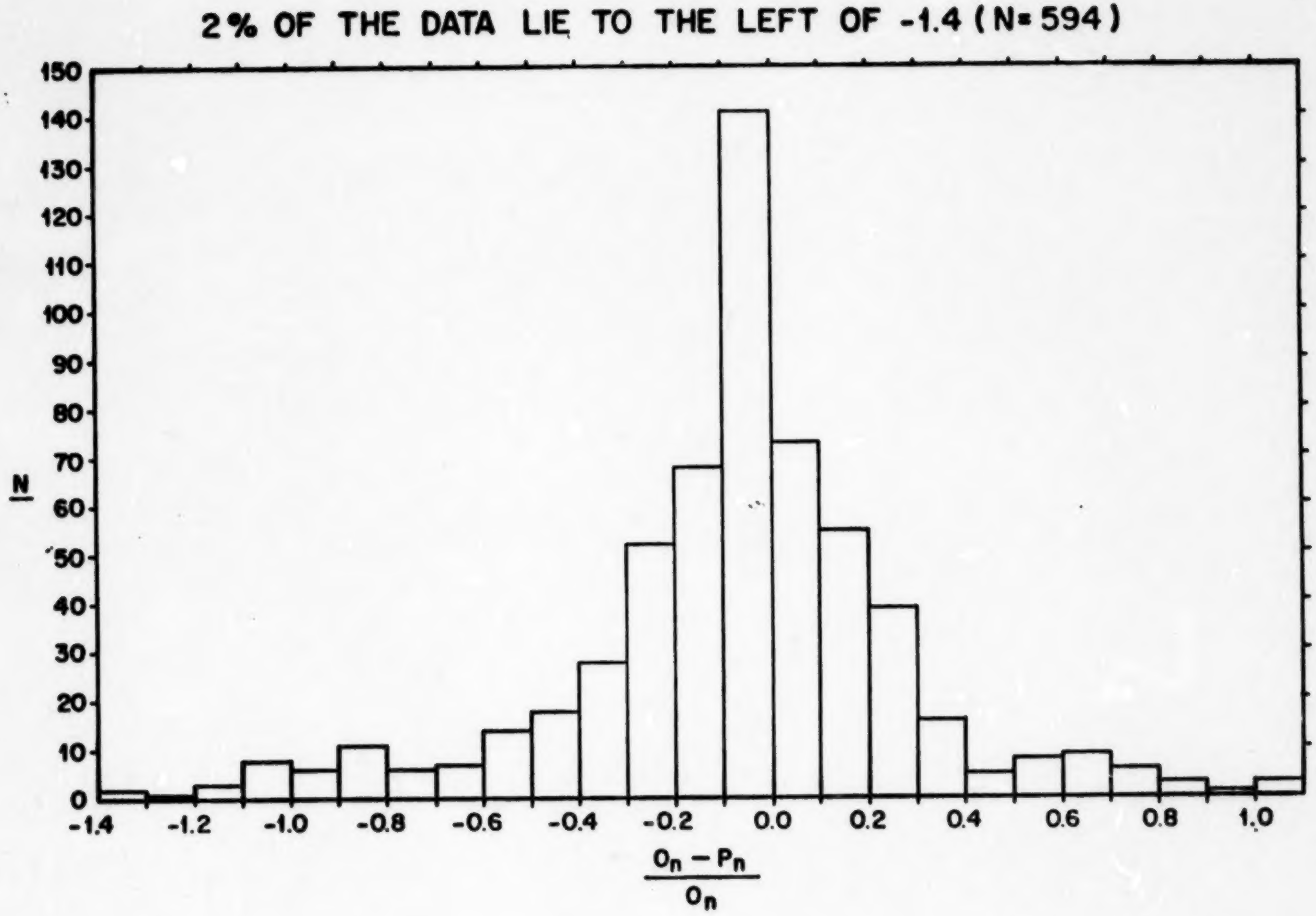

Figure 45: Same as Figure 43 except for the GM model.

normalized predictions and observations after removing mutual values of unity are given in Table 23. These results indicate that when all the data are considered, HIWAY #3 and HIWAY #4 simulate the dispersion process better than HIWAY #1 and CALINE-3, and are as good as the GM model.

The original HIWAY and the modified HIWAY version are employed to simulate the experiments conducted in the New York study. Table 24 presents the regression statistics for the HIWAY #1, HIWAY #4, GM, and the CALINE-3 models for the New York data set. These results also show significant improvement of the HIWAY #4 model over the original HIWAY model. The results of HIWAY #4 (using the same vehicle-induced drag factor developed with the GM data set) are quite comparable to those of the GM model.

More quantitative information as to the actual percentage of prediction to within a factor of 2 of the observed concentration are derived from (O-P)/O and the results are summarized in Table 25. For the GM data set, it is evident from this table that the original HIWAY model predicts concentrations 56% of the time to within a factor of 2 of the observed, while the modified models (HIWAY #3 and HIWAY #4) show a prediction to within a factor of 2 of the observed in excess of 80% of the time. However, it should be noted that the predictions are skewed toward overestimation. Although the GM model has by far the best percentage in the category of within a factor of 2, it is skewed toward underestimation.

Table 26 presents the regression results for data, when the wind speed was greater than 1 m/sec, by stability classification. Table 27 presents the (O-P)/O prediction results for the above stable data, while Table 28 has the corresponding unstable data. Only GM and HIWAY #4 simulate the concentration field 90% of the time within a factor of two and display a skewness toward overprediction for the stable atmospheric conditions, when the wind speed is greater than 1 m/sec.

For regulatory purposes, the ability of a model in providing accurate estimates of pollutant levels in the upper percentile of concentration is of greater importance than the overall predictability in the entire range of

TABLE 23

DATA SUBSET	STATISTICAL PARAMETER	HIWAY #1	HIWAY #3 & #4	GM	CAL-3
All Data	r^2	0.61	0.85	0.79	0.67
	b	0.65	0.76	0.85	0.89
	a	0.08	-0.01	0.03	-0.03
	$S_{o/p}$	0.12	0.07	0.08	0.11
	N	533	533	533	533

Table 23: Regression statistics between normalized observed and normalized predicted values for the original HIWAY, HIWAY #3, and HIWAY #4, CALINE-3 and the GM model for the GM data set. The regression analysis here shows how well the models predict the concentration profile.

TABLE 24

Data Subset	Model	r^2	b	a	$S_{o/p}$	N	Mean Observed	Mean Predicted
Parallel	GM	0.92	0.93	0.33	0.65	39	3.34	3.25
	New HIWAY #4	0.81	0.66	0.71	1.02	39	3.34	3.97
	HIWAY #1	0.72	0.39	1.16	1.24	39	3.34	5.52
	CALINE-3	0.61	1.37	0.82	1.44	39	3.34	1.84
Oblique	GM	0.73	0.97	0.28	0.88	53	2.16	1.93
	HIWAY #4	0.74	0.81	0.24	0.86	53	2.16	2.36
	HIWAY #1	0.57	0.56	0.54	1.12	53	2.16	2.89
	CALINE-3	0.43	1.39	0.29	1.28	53	2.16	1.35
Perpendicular	GM	0.87	0.83	0.62	0.75	41	2.89	2.72
	HIWAY #4	0.86	0.63	0.77	0.79	41	2.89	3.35
	HIWAY #1	0.67	0.39	1.36	1.21	41	2.89	3.95
	CALINE-3	0.68	0.85	0.91	1.19	41	2.89	2.32
U < 2 m/sec	GM	0.89	0.84	0.66	0.75	34	3.48	3.36
	HIWAY #4	0.91	0.63	0.68	0.67	34	3.48	4.47
	HIWAY #1	0.73	0.33	1.45	1.17	34	3.48	6.24
	CALINE-3	0.69	0.91	0.83	1.26	34	3.48	2.92
2 ≤ U ≤ 5 m/sec	GM	0.80	0.88	0.58	0.95	59	3.09	2.86
	HIWAY #4	0.70	0.69	0.68	1.14	59	3.09	3.48
	HIWAY #1	0.61	0.52	0.98	1.30	59	3.09	4.06
	CALINE-3	0.42	1.31	0.79	1.60	59	3.09	1.76
U > 5 m/sec	GM	0.88	1.06	0.02	0.40	40	1.54	1.43
	HIWAY #4	0.86	1.05	-0.03	0.43	40	1.54	1.50
	HIWAY #1	0.85	0.79	-0.02	0.45	40	1.54	1.96
	CALINE-3	0.55	2.18	-0.38	0.78	40	1.54	0.88
Stability 2	GM	0.78	0.88	0.84	0.94	46	3.42	2.93
	HIWAY #4	0.70	0.63	1.08	1.10	46	3.42	3.72
	HIWAY #1	0.55	0.34	1.84	1.35	46	3.42	4.67
	CALINE-3	0.49	1.40	0.94	1.43	46	3.42	1.77
Stability 3	GM	0.93	0.96	0.14	0.52	54	2.33	2.29
	HIWAY #4	0.89	0.80	0.21	0.64	54	2.33	2.66
	HIWAY #1	0.85	0.59	0.34	0.76	54	2.33	3.36
	CALINE-3	0.67	1.39	0.15	1.13	54	2.33	1.57
Stability 4	GM	0.78	0.87	0.30	0.68	27	1.89	1.84
	HIWAY #4	0.79	0.75	0.25	0.67	27	1.89	2.18
	HIWAY #1	0.63	0.48	0.51	0.86	27	1.89	2.87
	CALINE-3	0.63	1.23	0.14	0.88	27	1.89	1.42
Stability 6	GM	0.95	0.77	0.61	0.68	6	4.66	5.28
	HIWAY #4	0.97	0.59	-0.34	0.53	6	4.66	7.35
	HIWAY #1	0.66	0.29	1.95	1.86	6	4.66	9.36
	CALINE-3	0.90	0.93	-0.57	1.00	6	4.66	5.64
All Data	GM	0.86	0.90	0.43	0.78	133	2.73	2.56
	HIWAY #4	0.81	0.68	0.59	0.90	133	2.73	3.14
	HIWAY #1	0.66	0.42	1.07	1.20	133	2.73	3.98
	CALINE-3	0.54	1.03	0.88	1.39	133	2.73	1.46

Table 24: Ensemble regression statistics for the original HIWAY, HIWAY #4, CALINE-3 and the GM model for the New York data set.

TABLE 25

Model	Mode	Sample Size	% of Prediction Within a Factor of 2	% of Exact Prediction	% of Overprediction (Obs < Pred ≤ 2 Obs)	% of Underprediction (1/2 Obs ≤ Pred ≤ Obs)
GM	All GM Data	594	88	10	27	48
	U > 1 m/sec	509	87	10	22	55
HIWAY #1	All GM Data	594	56	5	37	14
	U > 1 m/sec	509	61	6	39	16
HIWAY #2	All GM Data	594	62	6	30	26
	U > 1 m/sec	509	64	6	31	27
HIWAY #3	All GM Data	594	82	10	41	30
	U > 1 m/sec	509	86	11	43	32
HIWAY #4	All GM Data	594	85	11	44	30
	U > 1 m/sec	509	87	11	43	33
CAL-3	All GM Data	594	71	7	28	36
	U > 1 m/sec	509	69	6	25	38
GM	All N.Y. Data	133	80	14	30	36
HIWAY #1	All N.Y. Data	133	72	7	42	23
HIWAY #4	All N.Y. Data	133	87	12	48	27
CAL-3	All N.Y. Data	133	51	3	18	30

Table 25: Quantitative evaluation of the dispersion models tested. Here, the model's ability to predict concentrations to within a factor of two of the observed are compared.

Data Subset	Statistical Parameter	GM	HIWAY #1	HIWAY #4	CALINE-3	AIRPOL-4	MROAD2	ROADS	DANARD
Unstable (A to C)	r^2	0.91	0.65	0.77	0.69	0.68	0.67	0.65	0.31
	b	1.19	0.62	1.01	1.30	1.50	1.67	0.32	0.45
	a	0.04	0.18	-0.04	0.06	0.01	0.33	0.34	0.32
	$S_{o/p}$	0.18	0.35	0.29	0.33	0.33	0.34	0.35	0.49
	R	1.26	0.80	0.96	1.42	1.53	2.89	0.56	0.74
	N	265	265	265	265	265	265	265	265
Neutral (D)	r^2	0.79	0.69	0.81	0.75	0.64	0.72	0.63	0.16
	b	1.02	0.46	1.11	1.23	0.89	1.15	0.19	0.24
	a	0.04	0.17	-0.09	-0.02	0.09	0.35	0.46	0.53
	$S_{o/p}$	0.32	0.39	0.30	0.35	0.42	0.37	0.42	0.64
	R	1.07	0.56	1.01	1.21	0.99	1.88	0.38	0.56
	N	89	89	89	89	89	89	89	89
Stable (E & F)	r^2	0.85	0.75	0.71	0.70	0.65	0.55	0.58	0.09
	b	1.01	0.40	0.92	1.10	0.69	0.39	0.12	0.09
	a	-0.09	0.14	-0.05	-0.09	0.16	0.59	0.57	0.84
	$S_{o/p}$	0.33	0.42	0.45	0.46	0.49	0.56	0.54	0.80
	R	0.95	0.46	0.88	1.02	0.80	0.84	0.25	0.37
	N	155	155	155	155	155	155	155	155

Table 26: Regression summary of all models by stability classification for GM data when wind speed was greater than 1 m/sec.

Model	Sample Size	% of prediction to within a factor of 2 (1/2 obs ≤ pred ≤ 2 obs)	% of prediction within ± 5% of the observed (1.05 obs < pred < 0.95 obs)	% of overprediction (1.05 obs < pred ≤ 2 obs)	% of underprediction (1/2 obs ≤ pred < 0.95 pred)	% of data >2 x observed
GM	155	96	10	53	33	3%
HIWAY #1	155	26	1	20	5	60%
HIWAY #4	155	90	6	56	28	10%
CALINE-3	155	87	7	38	42	13%
AIRPOL-4	155	70	4	49	17	14%
MROAD2	155	56	4	34	18	9%
ROADS	155	11	3	5	3	56%
DANARD	155	42	5	24	13	48%

Table 27: Summary of (O-P)/O for stable case data used in Table 26.

Model	Sample Size	% of prediction to within a factor of 2 (1/2 obs ≤ pred ≤ 2 obs)	% of prediction within ± 5% of the observed (1.05 obs < pred < 0.95 obs)	% of overprediction (1.05 obs < pred ≤ 2 obs)	% of underprediction (1/2 obs ≤ pred < 0.95 pred)	% of data >2 x observed
GM	265	90	7	13	70	1%
HIWAY #1	265	86	9	51	26	12%
HIWAY #4	265	90	12	38	40	10%
CALINE-3	265	74	4	19	51	8%
AIRPOL-4	265	78	7	13	58	3%
MROAD2	265	16	0	2	14	1%
ROADS	265	56	5	32	19	32%
DANARD	265	62	6	28	28	24%

Table 28: Summary of (O-P)/O for unstable case data used in Table 26.

concentration. To show how the modified model behaves in the upper portion of the cumulative frequency distribution, measured concentrations greater than half the maximum observed concentration for a given run are separated out and the capability of the models in predicting concentrations to within a factor of 2 is presented in Table 29. The modified HIWAY models show considerable improvement over the original HIWAY version. It should be noted that the CALINE-3 simulation in the upper concentration range for the GM data set is similar to that of the original HIWAY model. However, the CALINE-3 model is skewed toward underprediction. CALINE-3 performed poorly with the NY data set. For the GM data set, the GM model shows an exact prediction of 12% and an overprediction of 19% while HIWAY #4 shows 14% and 37% respectively. A similar trend can be seen when the analysis is applied to the N.Y. Data set.

The upper half of the cumulative frequency distribution (50th to 100th percentile of high concentrations) was also analyzed for the percentages within a factor of two and is presented in Table 30. Table 31 presents all data in the upper half of the cumulative frequency distribution for winds speeds greater than 1 m/sec. Tables 30 and 31 also include the models' regression statistics and means for these respective data sets. As can be seen, the same general trends of model behavior hold for these data sets as has been discussed previously. These results clearly demonstrate that HIWAY #4 provides a realible simulation of the dispersion process and could be confidently used by the regulatory agencies in assessing air quality impact of line sources.

Model Sensitivity to Wind Direction

In order to see the sensitivity of the model predictions to the wind-road orientation angles, contours of normalized concentration ($\chi_p u/Q$ where χ_p is the predicted concentration) for the original HIWAY model and HIWAY #3 for stable atmospheric conditions as a function of wind-road angle and distance from the median are developed and shown in Figure 46. Also included in this diagram are the contours of observed ($\chi_o u/Q$ where χ_o is the measured concentration) and those predicted by the GM model for stable atmospheric conditions for the purpose of comparison with the original and modified HIWAY models.

TABLE 29

Model	Mode	Sample Size	% of Prediction within a Factor of 2	% of Exact Prediction	% of Overprediction (Obs < Pred ≤ 2 Obs)	% of Underprediction (1/2 Obs ≤ Pred ≤ Obs)
GM	GM Data	155	95	12	19	64
HIWAY #1	GM Data	155	70	7	43	20
HIWAY #2	GM Data	155	65	5	23	37
HIWAY #3	GM Data	155	96	13	37	46
HIWAY #4	GM Data	155	97	14	37	46
CAL-3	GM Data	155	70	7	14	49
GM	N.Y. Data	60	100	17	30	53
HIWAY #1	N.Y. Data	60	82	8	43	31
HIWAY #4	N.Y. Data	60	100	13	50	37
CAL-3	N.Y. Data	60	47	3	9	35

Table 29: Same as Table 25 except only data greater than half maximum observed per each run is presented.

TABLE 30

Model	Sample Size	% of Prediction to within a factor of 2 (1/2 Obs ≤ Pred ≤ 2 Obs)	% of Exact Prediction (0.95 Obs ≤ Pred ≤ 1.05 Obs)	% of Over-Prediction (1.05 Obs ≤ Pred ≤ 2 Obs)	% of Under-Prediction (1/2 Obs ≤ Pred ≤ 0.95 Obs)	r^2	Slope	Intercept	Standard Error of Estimate	Mean Observed	Mean Predicted
GM	297	99	11	26	62	0.74	0.82	0.36	0.35	1.50	1.38
HIWAY #1	297	59	4	39	16	0.17	0.06	1.31	0.62	1.50	3.09
HIWAY #4	297	96	12	43	41	0.52	0.67	0.44	0.47	1.50	1.58
CALINE-3	297	86	8	19	59	0.18	0.17	1.25	0.61	1.50	1.44
AIRPOL-4	297	78	6	28	44	0.29	0.39	0.98	0.57	1.50	1.33
M ROAD 2	297	39	2	19	18	0.17	0.06	1.38	0.61	1.50	2.08
ROADS	297	29	3	19	7	0.18	0.02	1.36	0.61	1.50	5.85
DANARD	297	69	6	34	29	0.05	0.06	1.35	0.66	1.50	2.66

Table 30: Summary of (O-P)/O for the upper half (50th through 100th percentile) of the observed GM data cumulative frequency distribution.

TABLE 31

Model	Sample Size	% of Prediction to within a factor of 2 (1/2 Obs ≤ Pred ≤ 2 Obs)	% of Exact Prediction (0.95 Obs ≤ Pred ≤ 1.05 Obs)	% of Over-Prediction (1.05 Obs ≤ Pred ≤ 2 Obs)	% of Under-Prediction (1/2 Obs ≤ Pred ≤ 0.95 Obs)	r^2	Slope	Intercept	Standard Error of Estimate	Mean Observed	Mean Predicted
GM	241	99	10	24	65	0.73	0.91	0.27	0.34	1.46	1.31
HIWAY #1	241	65	5	43	17	0.49	0.31	0.71	0.47	1.46	2.45
HIWAY #4	241	98	12	38	48	0.54	0.82	0.27	0.44	1.46	1.44
CALINE-3	241	86	5	15	66	0.55	0.85	0.52	0.44	1.46	1.10
AIRPOL-4	241	75	5	33	37	0.35	0.48	0.82	0.53	1.46	1.32
M ROAD 2	241	36	2	18	16	0.31	0.28	1.14	0.55	1.46	1.14
ROADS	241	34	2	24	8	0.48	0.10	1.02	0.47	1.46	4.30
DANARD	241	69	7	34	28	0.04	0.06	1.31	0.65	1.46	2.48

Table 31: Same as Table 30, except only data when the wind speed was greater than 1m/sec is presented.

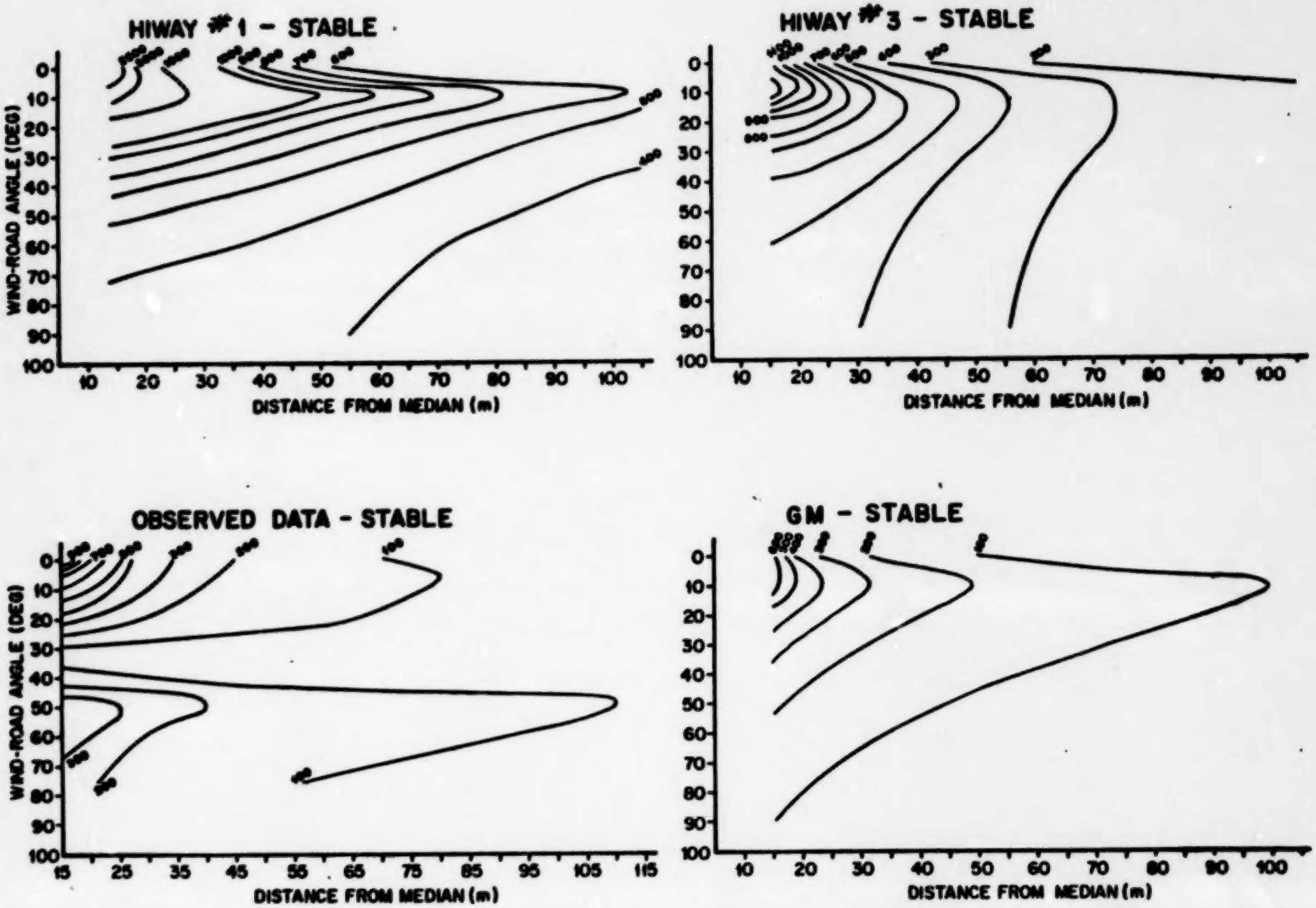

Figure 46: Variation of normalized concentrations ($\chi u/Q$) with horizontal distance and wind-road angle (in degrees) for E-stability as computed from the original HIWAY (HIWAY #1), and observed data; modified HIWAY (HIWAY #3), and the GM model.

Only results for HIWAY #3 are included since it has been shown (see Table 23) that the simulation of dispersion process of HIWAY #3 and HIWAY #4 are similar, except that HIWAY #4 has adrag factor to handle special situations such as low wind speed conditions. These plots for the model predictions are developed for unit wind speed and unit source strength for a receptor height of 2 m. Whereas the maximum measured value is of the order of 900 Km^{-1} adjacent to the roadway for near parallel wind conditions, the original HIWAY model predicts a value of 4000 Km^{-1} for F-stability, and 2500 Km^{-1} for E-stability. The modified HIWAY model predicts 1100 Km^{-1} for stable situations. The GM model, on the other hand, predicts a value of 600 Km^{-1} in the immediate vicinity of the roadway for near parallel wind situations. These diagrams clearly indicate that the predictions of the modified HIWAY model are much better than the original HIWAY model and are in good agreement with the measured data.

CARBON MONOXIDE DATA

The Carbon Monoxide data, collected in the NY experiment were also modeled. For this analysis, the GM, HIWAY #1, and HIWAY #4 models were evaluated. Of the 318 hours of data, 260 runs were considered. The others were excluded either because the stability was unknown, or the CO and wind data indicated different downwind receptors. Predicted or measured zero concentrations were included in the regression analysis. The emission rate was estimated using AP-42 Supplement 5 factors. Traffic conditions went from light to heavy, stop and go. Reference should be made to Rao et al (1979) for further details on the data management and modeling techniques.

Table 32 presents the ensemble regression statistics for both the ground-level and all points data sets, as well as the normalized values. The improvements to the orginal HIWAY model are once again seen, as is GM's tendency to underpredict.

CALIBRATION OF MODELS

Much has been said about the applicability of using a "calibrated" model for prediction purposes. A regression is generally performed between a chosen

Table 32

	Model	r^2	Slope	Intercept	SEE	$\overline{\text{OBS}}$	$\overline{\text{PRED}}$
All Data	HIWAY #1	0.23	0.159	0.98	0.93	1.29	1.98
(2m to 16m)	HIWAY #4	0.38	0.442	0.71	0.83	1.29	1.32
N = 1062	GM	0.45	0.655	0.63	0.79	1.29	1.02
Ground Data	HIWAY #1	0.15	0.112	1.38	0.99	1.71	2.89
(2m)	HIWAY #4	0.30	0.371	1.05	0.89	1.71	1.79
N = 639	GM	0.37	0.571	0.91	0.85	1.71	1.39
All Normalized	HIWAY #1	0.54	0.645	0.23	0.23	0.57	0.53
(2m to 16m)	HIWAY #4	0.69	0.813	0.10	0.19	0.57	0.58
N = 1062	GM	0.71	0.821	0.10	0.18	0.57	0.57
Ground Normalized	HIWAY #1	0.31	0.627	0.23	0.24	0.73	0.79
(2m)	HIWAY #4	0.51	0.804	0.11	0.20	0.73	0.77
N = 639	GM	0.56	0.854	0.07	0.19	0.73	0.77

Table 32: Ensemble regression statistics for the Carbon Monoxide data collected in the NY experiment. The HIWAY #1, HIWAY #4 and GM models are presented for ground-level and all sampling points concentrations, as well as for the normalized values.

Table 33

Sub-Set	N	r^2	b	a	So/p	$\bar{O}$	$\bar{P}$
1	101	.77	.88	-.01	.35	0.87	1.00
2	100	.69	.88	-.01	.43	0.97	1.11
3	94	.58	.66	.26	.50	1.06	1.21
4	94	.74	.74	.06	.41	1.09	1.39
5	100	.87	1.04	-.07	.26	.94	.98
6	105	.74	1.06	.02	.30	.83	.76
All Data	594	.70	.81	.10	.40	0.96	1.07

Table 33: Ensemble regression statistics for GM data sub-sets using HIWAY #4.

model and a small data set taken at prototype sites. The regression line equation is then used for future predictions, rather than just the models predictions.

In an effort to yield information on the practicality of this method, the two large data sets were sub-divided in chronological order. The GM tracer data set was seperated into 6 sub-groups, while the NY carbon monoxide data were divided into 5 sub-sets. The HIWAY #4 predictions were used in this analysis. Table 33 presents the regression results for the GM data. Table 34 has the regression results for all sampling heights for the CO data, while data in Table 35 is limited to the 2 meter height.

The significant differences of the slope and intercept between various subsets would seem to indicate credence to those who question the appropriateness of using the regression curve. This is augmented if one compares anyone of the all data regression lines to their respective regressions for stabilities, wind directions or speeds. Great care should be exercised when deciding whether to use a calibration line, since it might decrease the accurracy of the model even further. In realty, the regression line is strictly valid for the data set that was used in the least-squares regression.

Table 34

Sub-Set	N	r^2	b	a	So/p	$\bar{O}$	$\bar{P}$
1	216	0.62	.76	.29	.59	1.06	1.01
2	228	0.45	.62	.80	.85	1.38	.93
3	188	0.49	.41	.61	.70	1.33	1.77
4	200	0.29	.30	.90	.90	1.46	1.86
5	230	0.36	.53	.62	.86	1.23	1.16
All Data	1062	0.38	.44	.71	.83	1.29	1.32

Table 34: Ensemble regression statistics for NY CO data sub-sets using HIWAY #4.

Table 35

Sub-Set	N	r^2	b	a	So/p	$\bar{O}$	$\bar{P}$
1	126	0.51	.67	.55	.70	1.49	1.41
2	120	0.39	.54	1.06	.98	1.85	1.46
3	140	0.42	.37	.74	.75	1.56	2.19
4	134	0.27	.26	1.26	.86	1.83	2.18
5	119	0.21	.40	1.21	.92	1.83	1.58
All (2m)	639	0.30	.37	1.05	0.89	1.71	1.79

Table 35: Same as Table 34, but for ground level measurements only.

SECTION 5

CONCLUSIONS

The General Motors Sulfate dispersion experiment provided an opportunity to complement previous investigations (Chock, 1977; Eskridge et al, 1979; and Rao et al, 1979) of the characteristics of traffic-generated turbulence and its impact on the near-field dispersion process. The experimental controls imposed on the traffic flow allowed a more precise identification of relationships between atmospheric parameters and the traffic-induced turbulence than has been gained in the earlier experiments. Based on the analysis of wind field data and the evaluation of the models, the following conclusions can be drawn:

(1) The dynamics of air flow near the roadway are completely dictated by the wake effects due to the traffic flow. The wake effects decrease with distance from the source region according to a power law. The wake turbulent kinetic energy generated by the traffic flow decays to 1/10 of its maximum value in about 15 sec of transport downwind.

(2) The kinematic analysis shows significant distortions of the wind field close to the roadway. It is observed that there is a pronounced acceleration of the the wind at lower levels adjacent to the roadway due to the drag induced by the moving vechicles especially under parallel wind-road orientation with low ambient wind speeds.

(3) For wind directions perpendicular to the roadway, the magnitude of the traffic effects at the lowest observational height (1.5 m) is inversely related to the ambient wind speed. For the cases of parallel wind opposing the traffic flow, the traffic effects are substantial and are directly related to the wind speed.

(4) The observed increase of spectral energy in the high frequency range downwind of the roadway is used to determine the sizes of the traffic-generated eddies. The eddy sizes are found to be less than 3 m in the

vertical direction and less than 5 m in the horizontal direction. The time scale associated with these eddies is found to be in the range of 3 to 8 sec, depending upon the ambient atmospheric stability.

(5) The size of the traffic-generated eddy is used to determine the enhancement of diffusivities and dispersion parameters associated with the traffic. It is found that the dispersion in the immediate vicinity of the highway is dominated by the traffic with its influence decreasing considerably faster at further downwind distances and at higher elevations. However, for low wind speed situations the traffic contribution to the total diffusivity is still about 50% at a downwind distance of 30 m.

(6) A simple method is suggested for incorporating the traffic effect into diffusion models by the inclusion of wake diffusivities and dispersion parameters.

(7) Five Gaussian (GM, HIWAY, AIRPOL-4, and CALINE-2, and CALINE-3) and three numerical (DANARD, MROAD2, and ROADS) have been evaluated using the tracer data from the GM experiment. Of all the models tested here, the GM model provides by far a better simulation than the other models. This is not surprising since the GM model was developed from this data set. The GM model predicts concentrations 87% of the time to within a factor of two of the observed concentrations.

(8) When the entire range of concentrations is included in the analysis, the ranking of currently used models according to their decreasing performance is GM, AIRPOL-4, HIWAY, CALINE-2, DANARD, MROAD2, and ROADS.

(9) When the data in the upper half of the cumulative distribution are considered, the ranking of the models according to their decreasing performance is found to be GM, HIWAY #4, CALINE-3, AIRPOL-4, DANARD, HIWAY #1, MROAD2, and ROADS. Although the GM model provides a better simulation than the other models, it is skewed towards underprediction.

(10) Of all these models, HIWAY yields the most conservative estimates since it has the highest percentage of data in the category of overprediction in most of the statistical tests considered. This feature is desirable for a regulatory model since environmental health decisions will be made using the model predictions. However, the current version of HIWAY provides unacceptable overpredictions especially under stable atmospheric conditions and parallel wind-road orientations with low wind speeds.

(11) This overestimation in the HIWAY model is due to the fact that the model's dispersion parameters do not properly account for the traffic-induced turbulence near roadways. The Pasquill-Gifford (P-G) dispersion curves used in the model are modified to properly reflect the turbulence characteristics adjacent to the roadways. Further, an empirical vehicle-induced drag flow factor as a function of the wind-road orientation angle, which in a rough way accounts for the change in the mean wind field due to the moving vehicles, is developed to handle pollutant dispersion under low ambient wind speed conditions.

(12) When the original P-G curves used in the HIWAY model are replaced by the new dispersion curves and the drag flow factor is included, the performance of the HIWAY model is significantly improved.

(13) Several statistical tests are applied to compare the simulation capabilities of the original and modified versions of the HIWAY model. Comparisons of the results of the modified HIWAY with the results of the GM and the third-generation California line source model, CALINE-3, show that the revised HIWAY simulation is much better than CALINE-3 and is quite comparable to that of the GM model.

(14) Whereas the current version of the HIWAY model predicts concentrations to within a factor of two of the observed concentrations 56% of the time, the revised HIWAY predicts concentrations 85% of the time when the entire range of concentrations is considered. When the data in the 50th through 100th percentile are considered in the analysis, the current version of HIWAY predicts concentrations 59% of the time to within a factor of two of the observed concentrations and the revised HIWAY predicts concentrations to within a factor of two of the observed concentrations 96% of the time. The same trend is seen when the models are applied to the New York tracer experimental data.

(15) Although the revised HIWAY model does not have as good regression statistics as the GM model in some cases, the revised HIWAY has a slight tendency to be conservative. This is desirable since HIWAY is used by the regulatory agencies in their decision-making process.

REFERENCES

Benson, P.E., "CALINE 3 - A Versatile Dispersion Model for Predicting Air Pollutant Levels Near Highways and Arterial Streets", FHWA/CA/TL-79/23 (1979).

Cadle S.H., Chock D.P., Monson P.R. and Heuss J.M., "Results of the General Motors Sulfate Dispersion Experiments", General Motors Research publication, GMR-2107 (1976).

Carpenter W.A. and Clemaña G.G., "Analysis and Comparative Evaluation of AIRPOL-4", Virginia Highway and Transportation Research Council Report, VHTRC 75-R55 (1975).

Chock D.P., "A Simple Line - Source Model for Dispersion Near Roadways", Atmos. Environ., 12: 823 (1978).

Chock D.P., "General Motors Sulfate Dispersion Experiment: An Overview of the Wind, Temperature and Concentration Fields", Atmos. Environ., 11: 553 (1977).

Chock D.P., "General Motors Sulfate Dispersion Experiment: Assessment of the EPA-HIWAY Model", J. Air Poll. Cont. Assoc., 27: 39 (1977).

Danard M.B., "Numerical Modeling of Carbon Monoxide Concentrations Near a Highway, J.Appl. Met., 11: 947 (1972).

Draxler R.R., "Determination of Atmospheric Diffusion Parameters", Atmos. Environ., 10: 99 (1976).

Dufort E.C. and Frankel S.P., "Stability Conditions in the Numerical Treatment of Parabolic Differential Equations", Mathematical Tables and Other Aids to Computations, 7: 135 (1953).

Eskridge R.E. and Hunt J.C.R., "Highway Modeling: Part I - Prediction of Velocity and Turbulence Fields in the Wake of Vehicles", J. Appl. Met., 36: 387 (1979).

Eskridge R.E., Binkowski F.S., Hunt J.C.R., Clark T.L. and Demerjian K.E., Highway Modeling: Part II - Advection and Diffusion of SF_6 Tracer Gas", J. Appl. Met., 36: 401 (1979).

Golder D., "Relations Among Stability Parameters in the Surface Layer", Boundary Layer Met., 3:47 (1972).

Kirsch J.W. and Mason B.F., "Mathematical Models for Air Pollution Studies Involving the Oregon I-205 Highway Project", Systems, Science and Software report, SSS-R-76-2744 (1975).

Noll K.E., Miller T.L. and Claggett M., "A Comparison of Three Highway Line Source Models", Atmos. Environ., 12: 1323 (1978).

Petersen W.B., "A Pilot Study on Dispersion Near Roadways", EPA - 600/4-78-044 (1978).

Pitter R.L., "User's Manual ROADS, PSMOG, VIS1", Oregon Graduate Center Report, Beaverton, Oregon (1976).

Rao S.T. and Ketchum C.B., "Spectral Characteristics of Baroclinic Annulus Waves", J. Atmos. Science, 32: 698 (1975).

Rao S.T., Chen M., Keenan M.T., Sistla G., Peddada R., Wotzak G., and Kolak N., "Dispersion of Pollutants Near Highways: Experimental Design and Data Acquisition Procedures", EPA-600/4-78-037 (1978).

Rao S.T., Keenan M.T., Sistla G. and Samson P.J., "Dispersion of Pollutants Near Highways: Data Analysis and Model Evaluation", EPA-600/4-79-011 (1979).

Rao S.T., Sedefian L. and Czapski U.H., "Characteristics of Internal Oscillations in Lake Ontario," J. Geophy. Res., 82: 1725 (1977).

Rao S.T., Sedefian L. and Czapski U.H., "Characteristics of Turbulence and Dispersion of Pollutants Near Major Roadway", J. Appl. Met. 36: 283 (1979).

Rao S.T. and Keenan M.T., "Suggestions for the Improvement of the EPA-HIWAY Model", J. Air Poll. Cont. Assoc., 30: 247 (1980).

Rao S.T., Sistla G., Keenan M.T. and Wilson J.S., "An Evaulation of Some Commonly Used Highway Dispersion Models", J. Air Poll. Cont. Assoc., 30: 239 (1980).

Rao S.T., Samson P.J. and Eskridge R.E., "Traffic-Induced Turbulence Near Roadways", in preparation, 1980.

Sistla G., Samson P.J., Keenan M.T. and Rao S.T., "A Study of Pollutant Dispersion Near Highways", Atmos. Environ., 13: 669 (1979).

Turner D.B., "A Diffusion Model for an Urban Area", J. Appl. Met., 3: 38 (1964).

Turner D.B., "Workbook of Atmospheric Dispersion Estimates", USEPA, Research Triangle Park, NC, (1970).

Wandel C.F. and Kofoed-Hansen O., "On the Eulerian-Lagrangian Transform in the Statistical Theory of Turbulence", J. Geophys. Res., 67: 3089.

Ward C.E., Ranzieri A.J., and Shirley E.C., "CALINE 2 - An Improved Microscale Model for the Dispersion of Air Pollutants from a Line Source", FHWA report, FHWA-RD-77-74 (1977).

Zimmerman J.R. and Thompson R.S.", User's Guide for HIWAY, A Highway Air Pollution Model", EPA-650/4-74-008 (1975).